MODELLING OF HEAT AND MASS TRANSPORT IN COMPOSITE MATERIALS

BY

NILINDU UMAYANGIKA MUTHUMINI MUTHUBANDARA

B.Sc. (Hons.), Materials Engineering (University of Moratuwa, Sri Lanka)
Diploma in Computer System Design (National Institute of Business Management, Sri Lanka)

A Thesis submitted for the
Degree of Master of Philosophy

School of Engineering
Faculty of Engineering & Built Environment
The University of Newcastle
Australia

June 2008

"I hereby certified that the work embodied in this Thesis is the result of original research and has not been submitted for a higher degree to any other University or Institution"

(signed) _____

Acknowledgements

I would like to express my most sincere thanks and gratitude to my supervisors Prof. Irina Belova and Prof. Graeme Murch for the guidance, complete support and provision of financial assistance during this research. I am indebted to Prof. Graeme Murch for his limitless assistance towards reading and polishing my English skills in this Thesis.

Special thanks to Prof. Andreas Öchsner from Technical University, Malaysia for his collaboration and work that extended the data of this thesis.

I gratefully acknowledge the financial assistance received being a recipient of Endeavour International Postgraduate Research Scholarship (EIPRS) and University of Newcastle Research Scholarship (UNRSC).

My special thanks to my colleagues and postgraduate students at the Discipline of Mechanical Engineering for providing a warm and a friendly environment.

Finally, I would like to thank my husband Punsara for his endless support, love and encouragement throughout the period of my studies. Last but not least I owe the greatest debt of gratitude for my parents for their unlimited love, continuous encouragement and patience extended during my studies in overseas.

Contents

Figures

Tables

Abstract

Thermal conduction properties are of major concern for those metal/ceramic composite materials having applications in semiconductor devices and electronic packaging materials. A higher thermal conductivity to coefficient of thermal expansion ratio is an advantage for such materials employed in electronic devices due to the subjective high thermal loads. It is well known that the shape, size and distribution of the insulating phase have an effect on the overall thermal conductivity properties. But the details are lacking and well deserving of study.

Metal/ceramic oxide interfaces are important in the strengthening mechanisms of dispersion strengthened materials. Accordingly, considerable attention has been given to recent investigations of oxygen diffusion characteristics and the bonding mechanisms at such interfaces. Susceptibility to oxidation can be studied by analysing several thicknesses of material. As an example, studying a thin film and a semi-infinite material subjected to a high oxygen partial pressure environment and a vacuum condition would help to determine the oxidation (in-diffusion) and de-oxidation (out-diffusion) processes respectively. Since metal/ceramic internal interfaces play a very important role in controlling the mechanical, thermal and electrical properties, it is timely to consider these diffusion processes for detailed study.

In this Thesis, the two areas mentioned above were selected for detailed investigation. The Thesis also addresses the further development of a method for solving complex phenomenological diffusion problems. This method makes use of lattice-based random walks of virtual particles, directed according to the Monte Carlo method (the Lattice Monte Carlo method) which is then used to address various mass and thermal diffusion processes. Chapter 2 is concerned with using this method to determine the thermal conductivity of model composites. In that chapter, the Lattice Monte Carlo method is used to calculate the effective thermal conductivity of several models of a composite, where inclusions are arranged in square planar and cubic arrangements with periodic boundary conditions. Excellent agreement is found of the effective thermal conductivity with the century-old Maxwell-Garnett Equation. Chapter 3 is concerned with a phenomenological representation of oxygen diffusion and segregation in a model composite based on Ag/MgO. The Lattice Monte Carlo method is employed to address mass diffusion in this composite. Square and randomly distributed multiple inclusions were considered as shapes of the MgO inclusion phase. The time-dependence of oxygen concentration depth profiles and contour maps were determined. First, oxygen in-diffusion is

considered from a constant surface source solely into the Ag metal matrix: oxygen depth profiles were in excellent agreement with exact results. Next, oxygen in-diffusion/segregation is simulated in the composite by permitting and restricting the mobility of oxygen in different scenarios involving the Ag-MgO interface. The (higher temperature) out-diffusion of oxygen from the composite was also simulated and corresponding results obtained for the oxygen depth profiles. In both cases, very good agreement was found between the results from the Lattice Monte Carlo method and analytical expressions.

Notation

All symbols and notations are used in this Thesis are defined where they are first appear in the text. For convenience, most frequently used variables are given below.

t	Time
λ, K	Thermal conductivity and thermal diffusivity
T	Temperature
x, h	Distance
D, D^0	Diffusion coefficient
D_0	Pre-exponential factor, frequency factor
ΔH	Activation enthalpy
R	Ideal gas constant
f	Correlation factor
ν^0	Attempt frequency
a	Lattice parameter, jump distance (s.c. lattice)
ΔS	Entropy of activation
ΔG	Gibbs free energy of activation
Γ_{ij}	Inter-site transition jump rate/jump frequency
N	Avogadro's number
η	Medium viscosity
r	Radius
R'	Gas constant
$< \Delta R^2 >$	Mean square displacement
$< \Delta R >$	Mean displacement
N, n	Number of particles
d	Dimension
J	Flux
C	Concentration (particles per unit volume)
V	Electric potential
I	Current intensity
σ	Electrical conductivity
E	Electric field

M	Diffusant amount per unit area
LMC	Lattice Monte Carlo
$\overline{K}$	Conductivity matrix
F	Nodal vector
D_{Eff}	Effective diffusivity
g	Fraction of grain boundaries
D_b	Diffusivity in grain boundaries
D_l	Lattice, grain or bulk diffusivity
s , s'	Segregation factor
n	Number of lattice sites along the source
P_i	Probability of a particle reaching the sink
ρ	Density
C_p	Specific heat
ϕ	Fraction of inclusions, grains
E_s	Segregation energy
Π	Boundaries in the lattice
Ω_i	Regions in the lattice
∇^2	Laplacian operator
∇	Del operator
SL	Single Lattice
VP	Virtual plane
erf	Error function
erfc	Complementary error function

Chapter 1

1. Introduction

1.1 Heat and Mass Transport in Solids

Mass transport, also known as atomic migration and mass diffusion, refers to the flux of matter driven by a chemical potential gradient. Mass transport plays an important role in almost all processes occurring in everyday life and is also regarded as a fundamental topic in the science of materials. Mass diffusion processes play a key role in the kinetic reactions occurring in the microstructure of solid materials such as metals, ceramics, alloys, polymers, glasses and semiconductors. Nucleation of new phases, phase transformation by diffusion, precipitation, recrystallization, high-temperature creep and thermal oxidation are just a few examples. Mass diffusion is widely applied in present technological applications as diffusion doping during the fabrication of microelectronic devices, solid electrolytes for battery and fuel cells, surface hardening of steel through carburization or nitriding, diffusion-bonding and sintering [1]. Fick's diffusion laws and the Einstein equation for random motion are fundamental in describing mass diffusion processes in solids. Not only the chemical potential but also gradients in temperature affect the atomic migration process. Experimental analysis of mass diffusion is best obtained by using the tracer method, which is regarded as the most direct and accurate technique for the determination of diffusion coefficients in solids [2]. Other comprehensive experimental methods for the determination of mass diffusion coefficient in solids are well described in the literature [3 -5].

Crystalline solids exhibit several structurally different paths for atomic transport to take place. Lattice diffusion and grain boundary diffusion are examples of such paths. Lattice diffusion, also known as bulk diffusion, occurs mainly by point defects such as vacancies or interstitials. A detailed description of the vacancy and interstitial mechanisms is given in section 1.1.3. Grain boundaries and dislocations are also associated with mass transport in solids. In metals and ceramics, the diffusivity rates of atoms along grain boundaries or dislocations are very much higher compared with through the lattice. In effect, dislocations and grain boundaries provide short circuit paths for mass transport. In nanocrystalline materials, the grain boundary regions are unrelaxed and loosely packed. Furthermore, a large number of atoms in such materials

reside in these regions. Hence the diffusion flux through such regions is much higher than in the corresponding microcrystalline materials. This inevitably has a major impact on the physical properties of nanocrystalline materials.

Similar to mass transport, heat transport is very important in many applications. The main heat transfer method in solids is by conduction. In conduction mechanism, heat transfer occurs through the substance of the body itself. Conduction is initiated when different parts of the solid substance are at different temperatures and heat flows from hot regions to cold regions. In solids, heat energy can be transmitted through the crystal via the motion of phonons (quantised lattice vibrations), photons, free electrons (or free holes) and electron-hole pairs. Free electrons are the most prominent mechanism of conduction in metals. In semiconductors electron-hole pairs contribute to heat conduction, whereas in non-metals thermal conduction occurs by lattice vibrations except at higher temperatures where photons may become dominant.

Experimental methods for determining the thermal conductivity in solids include various steady state methods for poor thermal conductors and metals, steady state electrical methods for metals, periodic heating methods and variable state methods [6]. Since thermal conduction and mass diffusion have a very close mathematical relationship, they both are expressed commonly under the heading of 'Diffusion' in the next chapter.

1.1.1 Dependence of Mass Diffusion on Temperature

Diffusion is affected by thermodynamic parameters such as temperature, pressure and composition. The rate of diffusion in solids is very largely affected by temperature, being low at low temperatures and high at high temperatures. The temperature dependence of the diffusion coefficient D generally follows an Arrhenius relationship:

$$D = D_0 \exp\left(-\frac{\Delta H}{RT}\right) \tag{1.1}$$

where in D_0 denotes the pre-exponential factor or frequency factor, ΔH the activation enthalpy of diffusion, T is the absolute temperature and R is the ideal gas constant.

The pre-exponential factor is given by:

$$D_0 = gfv^0 a^2 \exp\left(\frac{\Delta S}{R}\right) \tag{1.2}$$

where ΔS is the activation entropy, g is a geometrical factor, f is the correlation factor, ν^0 is the attempt frequency and a is the lattice parameter.

Combining Equation (1.1) and (1.2) we have that:

$$D = gfv^0 a^2 \exp\left(-\frac{\Delta G}{RT}\right) \tag{1.3}$$

where ΔG is the Gibbs free energy of activation.

ΔH and f_0 are affected by the type of diffusion mechanism and the lattice geometry. Pronounced deviations from Arrhenius behaviour are generally due to effects associated with impurities or short circuit paths such as grain boundaries or dislocations.

1.1.2 Diffusion Mechanisms

Solid state diffusion makes use of the defects in the structure. Examples are point defects such as vacancies or interstitials or extended defects such as dislocations, grain and inter-phase boundaries. The latter defects provide short circuit paths in crystalline solids since the mobility of atoms along such extended defects is usually much higher than in the crystalline lattice. The diffusion coefficient is determined by jump rates and jump distances. The diffusion process also depends on various other factors as crystal structure, size and the chemical nature of the diffusing atom in addition to the defects. In a few situations, the directions of a given atom are completely random but in general, correlations in the jump directions occur. These correlations are embodied in the correlation factor f. The following diffusion mechanisms in the lattice itself are relevant to the present study [7].

1.1.2.1 Interstitial Mechanism

The interstitial mechanism is typically used by atoms (e.g. H, C, N and O), which are considerably smaller than the solvent or host lattice atoms. These atoms reside at the interstitial

sites of the host thus forming an interstitial solid solution. Such interstitial sites are formed according to the geometry of the host lattice. These interstitial atoms can migrate from one such site to the next interstitial site by what is termed the direct interstitial mechanism. Generally, interstitial solutes occupy octahedral or tetrahedral sites of the lattice and require no defects to mediate direct interstitial jumps. Hence, higher diffusion coefficients are observed with the direct interstitial mechanisms. Figure 1.1 illustrates the interstitial mechanism.

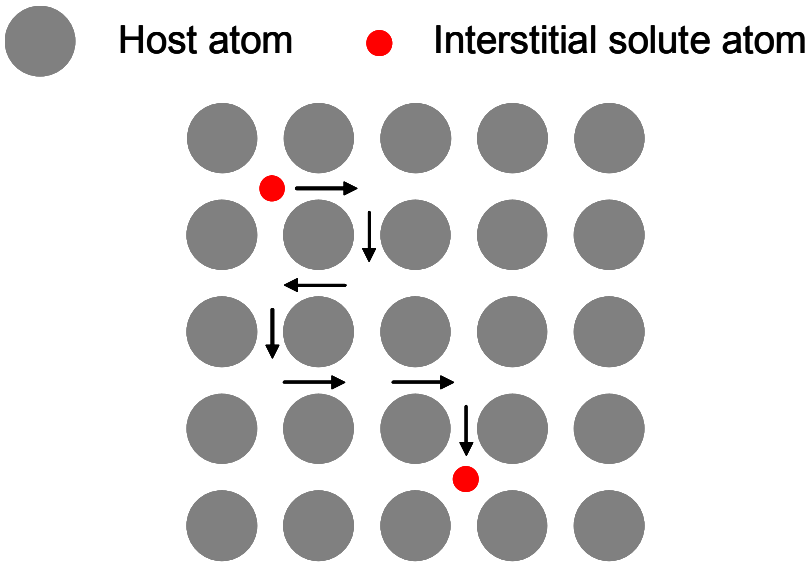

Figure 1.1 Direct Interstitial Mechanism of Diffusion

1.1.2.2 Vacancy Mechanism

Vacancies are formed thermally in metals, alloys and ionic crystals, by radiation damage and by nonstoichiometry in ionic crystals and some intermetallics. The vacancy mechanism is regarded as the dominant mechanism for lattice and substitutional atoms in most metals and alloys and ionic crystals. The vacancy mechanism is simply the exchange of an atom with a neighbouring vacancy. Overall atomic diffusion occurs by a series of such atom movements with vacancies. Figure 1.2 illustrates the vacancy mechanism.

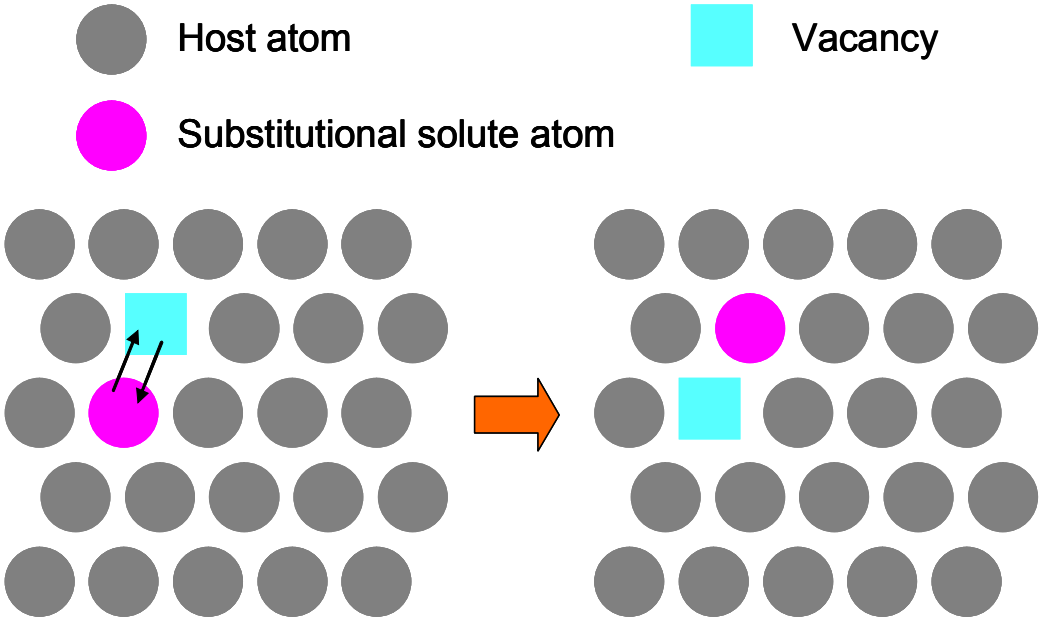

Figure 1.2 Schematic representation of the Vacancy Mechanism

1.2 Analytical Solutions for Mass Transport in Materials

The Einstein and Fick equations provide the basis for experiments to determine diffusion coefficients in solids. The Einstein and Fick equations also provide the basis for the simulations in the present study.

1.2.1 Einstein Equation

Einstein showed how the erratic Brownian movement of molecules or particles in a liquid could be quantitatively described. Brownian motion had previously been seen by the Scottish botanist Robert Brown and named after him. Einstein demonstrated how Brownian motion offered experimentalists the possibility to prove that molecules existed despite the fact that molecules themselves were too small to be seen directly [12]. By analysing Brownian motion, Einstein obtained a quantitative measure of the size of the atom.

Shvindlerman [11] recently discussed the development of Einstein's theory of Brownian motion. He noted that in his PhD thesis Einstein considered the expression (Equation 1.4) for the diffusion coefficient D for a system of suspended particles:

$$D = \frac{RT}{N}\frac{1}{6\pi\eta r} \tag{1.4}$$

where N is Avogadro's number, η is the medium viscosity and a is the radius of the hard-sphere molecules, R is the ideal gas constant and T is the absolute temperature. Equation 1.4 further illustrates that the diffusion coefficient of the suspended substance depends only on the coefficient of viscosity of the liquid and size of the suspended particles [12].

The Einstein equation for Brownian motion (see Equation 1.5 below) contradicted the ideas current at that time by formulating the relationship between the mean square displacement ($<\Delta R^2(t)>$) of the particles in time t and the diffusion coefficient already known from the Fick equations. Einstein stressed that it is the *mean square displacement* which is the meaningful quantity in describing a diffusion process and not a quantity such as the mean displacement. In fact, the mean displacement or first moment $<\Delta R(t)>$ of a large number of particles is zero for the situation of a truly random walk [13]. The Einstein equation is only valid when the system is at equilibrium with randomly walking particles in d dimensions (d = 1, 2, 3):

$$D = \frac{\left\langle \Delta R^2 \right\rangle}{2dt} \tag{1.5}$$

Later Jean Perrin [12] verified the Einstein Equation for Brownian motion having checked that the particle displacement exactly follow random laws. He combined Einstein's relation with Stokes's law and ended up with Equation 1.6, successfully determining Avogadro's number.

$$\left\langle \Delta R^2 \right\rangle = \frac{RT}{3\pi Na\eta}t \tag{1.6}$$

The Einstein Equation remains valid for long diffusion times even when the material has different diffusivities in different regions of the material, provided that the material remains isotropic in its diffusion properties overall.

1.2.2 Fick's Law

Fick's laws were introduced at a period where mass, heat and charge transfer were considered as examples of flows taking place under the influence of forces occurring in the medium

considered. These forces are generally gradients of concentration, temperature or electric potential. The analogy between heat flow and mass flow was first noted by Berthollet [15] in his paper discussing the mechanism of dissolution of a salt crystal in water. In the situation of heat conduction, Fourier [16] pioneered the idea of heat flow being a linear function of the temperature gradient. Ohm showed some five years later that the electric current flowing in a conductor has a linear relationship with the potential difference between the ends of the conductor. In effect, Fick [17] rediscovered Berthollet's analogy between heat conduction and diffusion by assuming the force responsible for mass transport in a binary mixture was the gradient of concentration. He formulated the relationships now known as Fick's First and Second Laws of diffusion, the first of which is identical to that formulated by Fourier in heat transfer problems by replacing the temperature gradient by the concentration gradient.

If $\partial T / \partial x$ refers to the temperature gradient, $\partial C / \partial x$ is the concentration gradient, $\partial V / \partial x$ is the electric potential gradient then the phenomenological relationships for mass, heat and electrical current flow can be written as:

$$J = -D\frac{\partial C}{\partial x} \qquad \text{(Fick's First Law)} \qquad (1.7)$$

where D is called the diffusion coefficient or diffusivity.

$$J_q = -\lambda\frac{\partial T}{\partial x} \qquad \text{(Fourier's Law)} \qquad (1.8)$$

where λ is the thermal conductivity and J_q is the flux of heat.

$$I = \sigma E = -\sigma\frac{\partial V}{\partial x} \qquad \text{(Ohm's Law)} \qquad (1.9)$$

where I is the current density and σ is the electrical conductivity.

By themselves, equations 1.7-1.9 are probably most conveniently employed experimentally under steady-state conditions, i.e. when the flux is independent of time.

In the following, the author will focus on mass diffusion and Fick's Laws only. In the steady state regime, the flux defined in Fick's first law, when the concentration is independent of *t* is a constant. In the non-steady state or the time-dependent case, where the flux at every point varies with time, the Equation of Continuity:

$$\frac{\partial J}{\partial x} = -\frac{\partial C}{\partial t} \tag{1.10}$$

can be introduced and usefully combined with Fick's First Law to remove the flux term and thus to give Fick's second law (written here for a diffusion coefficient independent of concentration):

$$\frac{\partial C}{\partial t} = D\frac{\partial^2 C}{\partial x^2} \tag{1.11}$$

Well-known solutions of Fick's second law for specific geometries are the 'thin-film solution' and the 'error function solution' [11]. The thin-film solution will be discussed further in section 1.4.1 and the error function discussed in section 1.4.2.

1.3 Brief Historical Review of the Monte Carlo Method

The Monte Carlo method was first developed at Los Alamos during World War II as part of the Manhattan Project [18]. The purpose was to model neutron trajectories during fission. Since the Manhattan Project, the Monte Carlo method has undergone extremely numerous and extensive development and has become very popular with the development of faster computers. In the Monte Carlo method, a carefully selected statistical sample is used to predict the behaviour or characteristics of a large group. In the Monte Carlo method, algorithms which involve large numbers of random numbers are used as a method of repeated random sampling. For this reason, the Monte Carlo method is most suited to calculation by a very high speed computer. Monte Carlo methods have been popular for addressing both mass and heat transport problems in materials. Examples for mass transport problems solved by Monte Carlo are atomistic problems in crystalline solids which now are usually described generically as the 'Kinetic Monte Carlo' (KMC) method [19, 20]. A recently developed Monte Carlo method for dealing with phenomenological problems is the 'Lattice Monte Carlo' (LMC) method which forms the principal method used in the present study. The LMC method is described in section 1.4. For many years, various other variants of the Monte Carlo method have been widely used for addressing transient heat conduction problems in homogeneous solids [21].

1.4 Initiation of the Lattice Monte Carlo (LMC) Method

The basic idea of simulating a problem with the LMC method is to map the problem onto a lattice which is then conveniently analysed using lattice-based random walks that are directed by the Monte Carlo method. The lattice model can be designed in such a way by rescaling the jump distance according to atomic dimensions and the spatial distribution of the diffusivities of the phases given in the problem. Accordingly, the lattice model is suited to address any phenomenological diffusion problem at any length scale [24]. The method uses computer-generated random numbers to select which particles move and in which directions they move according to the jump probabilities scaled with actual diffusivity values. Because multiple occupancy of a site by particles is allowed here, no correlation effects arise. This means that the jump direction of particles does not depend on the previous jump of the particle. *Atomistic* simulations, which very often focus on correlation effects, are generally referred to as Kinetic Monte Carlo calculations [19].

The LMC method has its basis in an early lattice model proposed by Benoist et al. [22, 23]. This was conceived as a very primitive model for describing the *atomic* motion around grain boundaries.

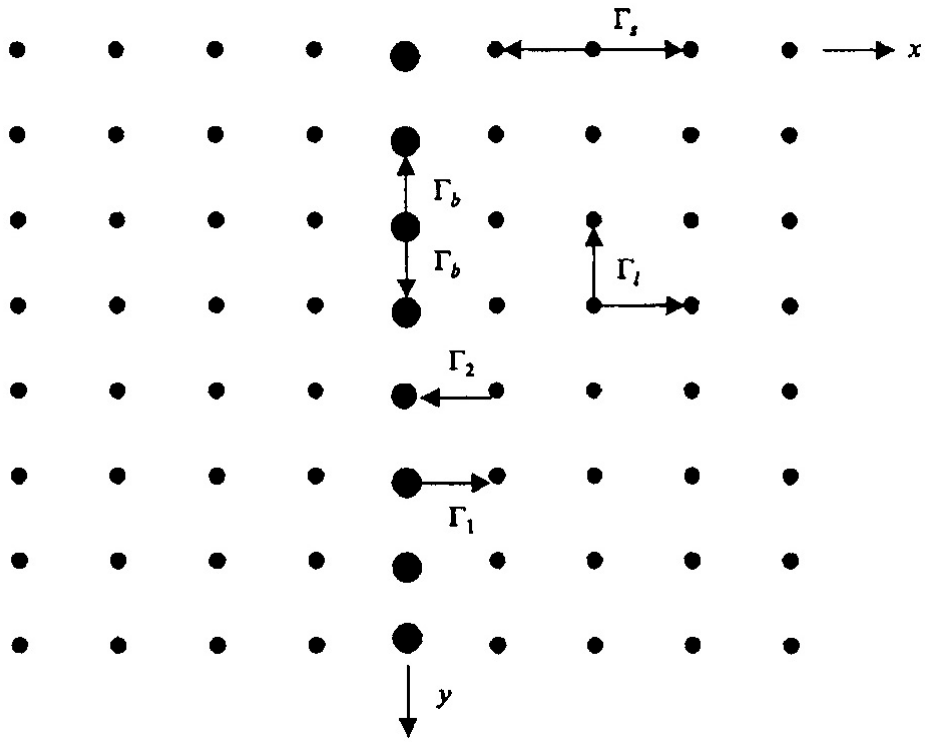

Figure 1.3 A schematic representation of the basic lattice model, shown here in 2D form [24].

Benoist and colleagues examined grain boundary diffusion in a bicrystal, which was represented by a discrete set of points. These points also represent a simple cubic lattice where each site is specified by three coordinates *x, y, z*, enabling 6 diffusion directions for a diffusant at each site. Here, the grain boundary itself is represented by a single plane of sites where the grain boundary diffusion coefficient of the diffusing substance is associated with a single atomic jump frequency Γ_b. Diffusion in the surrounding grains is represented by having an atomic jump frequency Γ_l. Moreover, two other jump frequencies Γ_1 and Γ_2 are also defined to describe jumps to and from the grain boundary. This formally allows the addressing of segregation of diffusant in the grain boundary region. There is also a further jump frequency Γ_s shown in Figure 1.3 to describe a different mobility on the surface.

The big conceptual step was to recognize that the atoms can in fact be exploring 'particles' representing a diffusing species. The jump distances and the jump frequencies can be rescaled so that this basic lattice model can be used to address any conceivable phenomenological diffusion problem at *any* length scale. Although the use of Einstein equation itself is of very limited direct use in experiments, it is the platform for much of the random walk theory describing the diffusion of atoms in the solid state and can be very usefully employed in the LMC method. This is possible because the diffusion coefficient (D) can be partitioned as essentially a product of a jump frequency (Γ) and a jump distance (a) squared in d dimensions (d =1, 2 and 3) as:

$$D = \frac{\Gamma a^2}{2d} \tag{1.12}$$

Although it is not actually considered formally as a lattice model, Brandt [25] used a floating random walk model with a variable step length and angle to simulate tracer diffusion in the presence of bulk, grain boundary and surface diffusion. The floating random walk model was first suggested by Brown [26] and was widely used to simulate heat conduction problems by Haji-Sheik and Sparrow [21, 27]. The variable step length comes from the random walk and the magnitude of this step equals the shortest distance between momentary positions of the particle and the external surface. The angle or the direction is chosen with the help of two random numbers and two functions of Eulerian angles such that all directions in space are selected with equal probability. The finding and the suggestions made by Brandt was improved by later calculations using the lattice model because the lattice model has always seemed to be much the simpler way of simulating such systems. Murch [28] pioneered the development of the first formal LMC calculation to address a phenomenological-based diffusion problem. Murch described a Monte Carlo procedure which led to the solution of tracer diffusion from a thin-film

source in the presence of dislocation pipes and was able to compare the results with analytical solutions provided by Le Claire and Rabonovitch [29, 30]. The method not only addressed an isolated dislocation but it was general enough to solve the problem for a situation of regularly or randomly spaced dislocations and also the impurity segregation problem. Murch's idea was significantly used by others in their calculations [31].

The principal outputs of LMC calculations are generally twofold: time-dependent concentration profiles and effective diffusivities. The concentration profiles are constructed by determining the number of particles that have reached a given plane from the particle source after some time t. 2D or 3D concentration profile maps can also be established in a similar way by simply counting the number of particles that have reached a given site. A comprehensive explanation of determining concentration profiles can be found in section 2.1.3.3. of Chapter 2. The effective diffusivity of a material can be calculated in the long-time limit. The effective diffusivity can either be calculated from a concentration depth profile or by using the Einstein equation. A detailed description can be found in section 2.1.3.1 of Chapter 2 and in section 3.3.1.1 of Chapter 3.

1.4.1 Instantaneous Source Condition (The Thin-Film Solution)

The most commonly used examples of diffusion experiments [32] refer to instantaneous tracer sources, where a fixed number of tracer atoms diffuse for a predetermined time (the anneal time). In other words, the source is modelled in such a way that the diffusion substance is deposited within a certain restricted region initially and left to diffuse throughout the surrounding medium. Then the instantaneous source acts as a boundary condition when a fixed number of particles diffuse, each for the same time *t*. The thin-film solution for Fick's Second Law for diffusion into a semi-infinite solid is given by:

$$C(x,t) = \frac{M}{\sqrt{\pi Dt}} \exp\left(-\frac{x^2}{4Dt}\right) \tag{1.13}$$

where a thin film of diffusant (of amount M per unit area) is localised at $x = 0$ of a semi-infinite sample. The quantity $\sqrt{6Dt}$ is a typical diffusion length, which is a characteristic distance for (3D) diffusion problems. The thin-film solution is also sometimes described as the Gaussian solution in the literature.

1.4.2 Constant Source Condition (The Error Function Solution)

The constant source condition was implemented in LMC modelling only very recently. Differing from the instantaneous source condition the diffusant concentration at the source plane or the boundary is kept constant at all times during the diffusion experiment. This means that when a particle leaves the source, the concentration is 'topped up' and when a particle returns and therefore exceeds the allowable concentration then any particle at the source is annihilated. In modelling generally the tracer source is arranged in a 'sandwich configuration' to avoid any artefacts or 'edge effects' caused by having a formal surface. A detailed description of the construction of the constant source will be discussed in Chapter 3 and the 'error function solution' for Fick's Second Law is given by Equation 3.34 in section 3.3.1.1.

1.4.2.1 Boundary Conditions

In the following, we discuss in detail the boundary conditions when the continuous source is modelled as a 'sandwich configuration', whilst leaving the source plane in the middle. LMC modelling of a continuous source is implemented in Chapter 3 while simulating in-diffusion and out-diffusion processes, wherein periodic boundary conditions are applied to both sides of the lattice. However, in both infinite and semi infinite materials we modelled edges in the y direction to be periodic. In this periodic boundary condition, when a particle reaches the first plane or the last plane of the lattice, and if the next jump is generated in such a way that it would go outside the lattice, then the particle is simply plugged back into the beginning or end plane of the lattice. In effect, with the periodic boundary condition at all four edges, the original lattice is now surrounded with periodic images or replicas of itself. In using periodic boundary conditions we can avoid surface effects completely. However, the lattice must not be too small or historical effects may arise in some diffusion problems as particles leave one side and enter the opposite side of a lattice which has not significantly changed.

1.5 Random Numbers in the LMC Method

The Monte Carlo method requires the generation of many random numbers. Random numbers r are floating numbers typically generated uniformly on the interval $0 \leq r < 1$. The LMC method requires random numbers in numerous situations such as in the selection of which particle moves, the allocation of a jump direction, the evaluation of local jump rates etc. The most important thing when generating random numbers is that the numbers should be uniformly

distributed over the above interval. This can be tested using various statistical testing methods [33]. These tests require generating large numbers of random numbers and subjecting them to standard statistical tests to check the uniformity [34]. In some cases, the LMC calculation can be run for a diffusion situation where there is a known exact solution. This provides a most useful test of the method and the degree of randomness of the generated random numbers. In principle, random numbers can be obtained from radioactive decay data or white noise but such methods tend to be slower than generation by the very efficient algorithms presently available.

1.6 References

[1] H. Mehrer and F. Wenwer: Diffusion in Metals, in Diffusion in Condensed Matter, ed. by Jörg Kärger, Paul Heitjans and Reinhold Haberlandt, Vieweg, Germany , 1998, p. 1

[2] S.J. Rothmann, The Measurement of Tracer Diffusion Coefficients in Solids, in Diffusion in Crystalline Solids, ed. by G.E. Murch and A.S. Nowick, Academic Press, 1964, p. 1

[3] J. Philibert, Diffusion Fundamentals, Proceedings of Diffusion Fundamentals I Conference (Leipzig 2005), 2005, p. 8

[4] Th. Heumann, Diffusion in Metallen, Springer, Berlin, 1992

[5] Landolt-Börnstein, Numerical Data and Functional Relationships in Science and Technology, New Series ed. by H. Mehrer, New Series Vol. **III/26**, Springer Verlag, 1990

[6] H.S. Carlslaw and J.C. Jaeger, Conduction of Heat in Solids, Second Edition, Oxford University Press New York, 1959

[7] H. Mehrer, Diffusion in Solids - Fundamentals, Methods, Materials, Diffusion-Controlled Processes, Springer Berlin Heidelberg New York, 2007

[8] E.O. Kirkendall, Trans. AIME, **Vol. 147**, 1942, p. 104

[9] A.D. Smigelskas and E.O. Kirkendall, Trans. AIME, **Vol. 171**, 1947, p.130

[10] A.W. Imre, S. Voss, H. Staesche, M.D. Ingram, K. Funke and H. Mehrer, J. Phys. Chem. B, **Vol. 111**, 2007, p. 5301

[11] L.S. Shvindlerman, Defect Diffus. Forum, **Vol. 249**, 2006, p. 7

[12] A. Einstein, Investigations on the theory of the Brownian movement, Dover Publication, Inc. New York, 1956

[13] H.J.V. Tyrell, Diffusion and Heat Flow in Liquids, Butterworths London, 1961

[14] J. Philibert: Atom Movements Diffusion and Mass Transport in Solids, Les Éditions de Physique France, 1991

[15] C. L. Berthollet, Éssai de Statique Chimique, Paris, 1803

[16] J.B.J. Fourier, Théorie Analytique de la Chaleur, Paris, 1822

[17] A. Fick, Pogg. Ann., **Vol. 94**, 1855, p. 59

[18] G.W. King, Ind. Eng. Chem., **Vol. 43**, 1951, p. 2975

[19] G.E. Murch, Diffusion in Crystalline Solids, Academic Press, Orlando, Florida, 1984, p. 379

[20] Y. Mishin, I.V. Belova and G.E. Murch, Defect Diffus. Forum, **Vol. 237-240**, 2005, p. 271

[21] A. Haji-Sheik and E.M. Sparrow, J. Heat Transfer, **Vol. 89**, 1967, p. 121

[22] P. Benosit and G. Martin, Thin Solid Films, **Vol. 25**, 1975, p. 181

[23] P. Bensoit and G. Martin, J. de Physique, Colloqu., **Vol. 36**, 1975, p. C4-213

[24] I.V. Belova and G.E. Murch, Sol. St. Phen., **Vol. 129**, 2007, p. 1

[25] W.W. Bandt, J. Chem. Phys., **Vol. 59**, 1973, p. 5562

[26] G.M. Brown, in: Modern Mathematics for the Engineer, edited by E.F. Breckenbach, McGraw-Hill New York, 1956, Chap. 12

[27] A. Haji-Sheik, J. Soc. Ind. Appl. Math., **Vol. 14**, 1966, p. 370

[28] G.E. Murch, Diffusion and Defect Data, **Vol. 32**, 1983, p. 1

[29] A.D. Le Claire and A. Rabonovitch, J. Phys., **Vol. 14**, 1981, p. 3863

[30] A.D. Le Claire and A. Rabonovitch, J. Phys., **Vol. 15**, 1982, p. 3455

[31] N.L. Peterson, Intl. Metals Reviews, **Vol. 28**, 1983, p. 65

[32] S. J. Rothman, Diffusion in Crystalline Solids, Academic press, Orlando, 1981, p. 1

[33] D.E. Knuth, The art of computer programming, **Vol. 2**, Semi-numerical Algorithms, Addison-Wesley, Reading, MA, 1969

[34] A. Proykova, Comput. Phys. Commun., **Vol. 124**, 2000, p. 125

Chapter 2

2. Calculation of the Effective Thermal Conductivity in Composite Materials

2.1 Introduction

2.1.1 The Importance of Thermal Conductivity and its Applications

In designing new materials it is a crucial to be able to predict the thermal conductivity in advance. By knowing the thermal conductivity, it assists in being able to predict the temperature fields and understand the extent to which the material can withstand allowable temperature limits. Recently, metal matrix composites have been used in electronic packaging materials due to the high thermal conductivity to coefficient of thermal expansion ratio [1, 2]. When discussing heat and mass transfer properties of composite materials, the effective properties play a vital role. The effective properties are an 'unknown' average of the individual properties of the phases associated with the composite material. That means effective properties are affected by the individual properties of the constituent phases. Because of the importance of this, numerous studies have been carried out to determine the effective thermal conductivity. The effective thermal conductivity depends on the geometry and thermal conductivities of individual phases, their distribution in the host material and the interface properties. In this Chapter, we study how the geometry and thermal conductivities of individual phases affect the effective conductivity of a model composite material.

The determination of the effective thermal conductivity in simple models of composite materials has been described for various situations by Torquato et al. [3]. He described the fact that the geometrical arrangements and shapes of the inclusions have an impact on the effective thermal conductivity of composite materials. For simulation models, various ordered and random packing arrangements of impermeable spheres were used. Ordered distributions were formed by arrangement of inclusions in f.c.c, b.c.c and s.c arrangements, whereas random distributions were formed by the dense random packing of spheres.

Recently, the finite element method has been used to calculate effective thermal conductivity in various models of composites [4]. The finite element solution is formed by solving the principal finite element for thermal conductivity problems:

$$\overline{K}.T = F \tag{2.1}$$

where $\overline{K}$ is the conductivity matrix, T is the vector of the unknown nodal temperatures and F is the nodal load vector. Generally, in the finite element method, the solution is formed by decomposing the complex structure into geometrically simple shapes which are also identified as elements. These single elements are associated with differential equations. The way of assembling such single element solutions and giving boundary conditions to obtain the complete system solution will balance equations at the nodes of the elements.

2.1.2 Historical Review of Effective Thermal Conductivity/Mass Diffusivity Studies

In this section, a brief summary of most of the published results on determining the effective diffusivity is given for composite and porous materials. It is observed that most of the results are published in the form of effective mass diffusivities. However, later in the present chapter (section 2.1.4), we show that the thermal conductivity in a phase *i* of the composite material can be equated to the thermal diffusivity in that phase by simply requiring that the values of density and specific heat be unity everywhere in the calculation. This in-turn makes the effective thermal diffusivity simply equal to the effective thermal conductivity. Therefore, in the following section (section 2.1.2.1) we consider that the calculation of the effective mass diffusivity applies the same meaning to the calculation of the effective thermal conductivity. Conversely, the results of models that are discussed from the point of view of the thermal conductivity in the present chapter would also apply equally to the effective mass diffusivity.

2.1.2.1 Effective Mass Diffusivity

The effective mass diffusivity represents the mass diffusivity in a composite material taken at chemical equilibrium. Experimentally, the effective diffusivity is measured by means of a tracer diffusion experiment in a polycrystalline material in the so-called Harrison Type-A kinetics

regime. In this regime, the effective diffusivity is expressed by some weighted average of the lattice or bulk diffusivity of the diffusant and its grain boundary diffusivity. Other examples are measuring effective ionic conductivity of a composite solid electrolyte and the effective diffusivity of a diffusant in a two-phase material.

Heat conduction and mass diffusion, both of which are random processes, can be simulated by a LMC method that simulates the random walk of particles. These particles can be atoms, molecules, colloidal particles or unicellular organisms in mass diffusion and heat particles in heat conduction problems. The effective diffusivity/conductivity can be calculated by means of the Einstein equation. In principal, the effective diffusivity or effective thermal conductivity can also be calculated in a LMC calculation by processing the concentration depth profile in the region adjacent to the source at very long times [5].

2.1.2.2 Effective Diffusivity Obtained by Analytical Methods for Two Phase Materials

There have been several theoretical attempts to calculate the effective diffusivity. The first was made by Hart [6] who considered the effective diffusivity of a microcrystalline material. His expression, now usually called the Hart equation, is:

$$D_{Eff} = gD_b + (1-g)D_l \tag{2.2}$$

where g is the volume fraction of grain boundaries, D_b is the diffusivity in the grain boundaries and the D_l is the lattice or the grain diffusivity. It was assumed that the grain boundary slabs are parallel to diffusion direction. In fact, the Hart equation is exact for this situation. Later, the Hart equation was extended by Mortlock [7] by adding the segregation factor (s) which takes into account the possibility of segregation of solute to the grain boundaries. This expression is commonly called the Hart-Mortlock Equation:

$$D_{Eff} = sgD_b + (1-sg)D_l \tag{2.3}$$

Here the segregation factor is considered as the ratio of the equilibrium concentration C_b of solute in the grain boundaries to the concentration C_g of diffusant in the grains. A problem arises when calculating the effective diffusivity in nanocrystalline materials which can have

very high g values, sometimes as high as 0.5 [8]. Equation 2.3 is not correct in such situations even for parallel grain boundary slabs. This was corrected by Kaur et al. [9] who determined the exact equation for the effective diffusivity of the solute for parallel boundary slabs in the diffusion direction as follows:

$$D_{Eff} = \frac{sgD_b + (1-g)D_l}{1-g+sg} \tag{2.4}$$

For the situation of alternating grain boundaries and grains in the diffusion direction, the effective diffusivity of the solute is given by:

$$D_{Eff} = \frac{sD_bD_l}{gD_l + s(1-g)D_b} \tag{2.5}$$

Equation 2.5 is exact for this geometry.

If a diffusing atom crosses a grain boundary in the diffusion direction (this will generally be the case) Equation 2.4 is violated. Equations 2.4 and 2.5 are only used as exact solutions for the two geometries described. There have been a large number of expressions for the effective diffusivity for various geometries but of all of them, the Maxwell-Garnett equation [10, 11] is found to be surprisingly accurate for the description of the effective diffusivity:

$$D_{Eff} = \frac{D_b[(g+d-gd)D_l + gD_b(d-1)]}{D_b(d-g)+gD_l} \tag{2.6}$$

where d is the dimension (1, 2, or 3). However, the original Maxwell-Garnett equation was actually derived to determine the effective electrical conductivity in porous media. The expression 2.6 was found by substituting electric conductivity with the diffusivity assuming that the numbers of charge carriers per unit volume in each phase are equal. The Maxwell-Garnett Equation was further generalized by Kalnins et al. [12] by using a concentric sphere model and incorporating the segregation factor:

$$D_{Eff} = \frac{sD_b[(g+d-gd)D_l + sgD_b(d-1)]}{[1-g+sg](sD_b(d-g)+gD_l)} \tag{2.7}$$

Later Belova and Murch [13] derived a 'composite equation' by dividing the diffusion paths into two parallel types. One path corresponds to grain boundaries arranged in the diffusion direction, while the other path refers to those grain boundaries oriented normal to the diffusion direction and the grains which is similar to the alternate configuration. The composite equation can be expressed with the segregation factor as:

$$D_{Eff} = \frac{sD_b((1-\varepsilon+\varepsilon^2)D_l + \varepsilon(1-\varepsilon)sD_b)}{(1-g-sg)(\varepsilon D_l + (1-\varepsilon)sD_b)} \tag{2.8}$$

where $g = 2\varepsilon - \varepsilon^2$. The advantage of Equation 2.8 is that it directly provides the effective diffusivity for the actual arrangement of cubes and gives a superior fit to the Monte Carlo data compared to the Maxwell-Garnett equation at large values of g [14].

2.1.2.3 Effective Diffusivity Obtained by Analytical Methods for Three Phase Materials

Brailsford and Major [15] derived a general expression for the thermal conductivity in a model of a three-phase material. Later, this expression was generalized by Belova and Murch [16] and extended to calculate the effective diffusion coefficient of a three phase material including segregation factors. The modified expression is as follows;

$$\frac{D_{Eff}}{D_c} = \frac{1 - 2g_A\frac{D_C - s_A D_A}{2D_C + s_A D_A} - 2g_B\frac{D_C - s_B D_B}{2D_C + s_B D_B}}{(1+(s_A-1)g_A + (s_B-1)g_B)\left[1 + g_A\frac{D_C - s_A D_A}{2D_C + s_A D_A} + g_B\frac{Dc - s_B D_B}{2D_C + s_B D_B}\right]} \tag{2.9}$$

where A and B refers to two phases with diffusivities D_A and D_B and volume fractions g_A and g_B separated by inter-phase boundaries phase C having a diffusivity D_C, s_A and s_B are segregation factors for phases A and B. LMC results [16] showed that the effective diffusivity of the composite is roughly described by Equation (2.9).

Let us consider the situation in composite electrolytes. Generally these materials are formed by embedding insulating phases (phase B) in an ionically conducting matrix (phase C) [17, 18]. An interesting phenomenon occurs here when the phase having a higher electrical conductivity (e.g. phase A) immediately surrounds the insulating phase. This situation will give rise to two

percolation thresholds, one where the high conductivity regions overlap and the other where the insulating regions are overlap. Belova and Murch [19] modified the Maxwell Equation appropriate for the above discussed situation for two geometric models (2D models of coated cubic and spherical particles).

$$\frac{D_{Eff}}{D_C} = \frac{1-2(g_A+g_B)\dfrac{D_C - D_{AB}s_{AB}}{2D_C + D_{AB}s_{AB}}}{(1+(s_A-1)g_A+(s_B-1)g_B)\left(1+(g_A+g_B)\dfrac{D_C - D_{AB}s_{AB}}{2D_C + D_{AB}s_{AB}}\right)} \tag{2.10}$$

where;

$$s_{AB} = \frac{s_A g_A + s_B g_B}{g_A + g_B}$$

and

$$\frac{D_{AB}}{D_A} = \frac{g_A + g_B - 2g_B\dfrac{D_A s_A - D_B s_B}{2D_A s_A + D_B s_B}}{\left(g_A + \dfrac{s_B g_B}{s_A}\right)\left[g_A + g_B + g_B\dfrac{D_A s_A - D_B s_B}{2D_A s_A + D_B s_B}\right]}$$

They calculated the effective conductivity/diffusivity using Equation 2.10 and compared with LMC results.

2.1.3 Effective Diffusivity by the LMC Approach

The first LMC calculation of the effective diffusivity was conducted to determine the effective diffusivity in the void space of randomly packed arrangements of spheres (f.c.c., b.c.c and s.c) [20]. These arrangements were obtained by collapsing loose arrangements of spheres using a Lennard-Jones pair potential between the spheres. It was assumed that the diffusivity within the spheres to be zero when comparing ordered and random arrangements of spheres with analytical expressions.

The next LMC study examined the effective diffusivity of a model with cubic grains [21]. Grains were modelled in a simple cubic arrangement whilst keeping the diffusivity in the grain boundaries much greater than in the grains. Results were compared with the Maxwell-Garnett Equation. Later, a model with spherical inclusion models with f.cc., b.c.c and s.c arrangements were examined [22]. Data were acquired in two different simulations, one having the diffusivity

of the inclusions less than the grain boundaries, the other with diffusivity in the grains greater than that in the grain boundaries. They compared their LMC data with the Maxwell-Garnett Equation and concluded that the Maxwell-Garnet Equation generally does well except near the percolation threshold where spherical inclusions are touching. Another detailed study of the effective diffusivity for square planar and brickwork arrangement of 2D square inclusions was conducted when the diffusivity of inclusions are about three orders of magnitude less than grain boundaries [23].

Two different strategies can be used to calculate the effective diffusivity with the LMC method namely the Einstein Equation method and the Fick's First and Second Law Method. Each one will be discussed below in some detail.

2.1.3.1 The Einstein Equation Method

The LMC method of computation for the direct calculation of the effective diffusivity starts with the Einstein Equation. The Einstein method is much more convenient to use compared with the other two methods. The Einstein equation describes the self-diffusivity D of migrating random particles in d dimensions (d =1, 2 and 3) as:

$$D = \frac{< \Delta R^2 >}{2dt} \tag{2.11}$$

(ΔR is the mean displacement of a given particle over a long time (t) and the Dirac brackets refer to an average over a large number (N) of particles.)

The Einstein equation can only be employed at systems in equilibrium. In a mass diffusion context, the Einstein Equation refers only to the determination of the diffusivity of individual particles that can be followed or traced in a system that is already at chemical equilibrium, i.e. with no concentration gradient acting or external fields acting. In other words, each particle needs to be followed for some longer time t in order to determine its displacement ΔR. In a real experiment, there are rather few examples where this has been possible to achieve. One well known experimental method traced the migration of surface rhodium atoms on various faces of a f.c.c. rhodium crystal using a field ion microscope. After a long diffusion time, the surface diffusivity of rhodium atoms can be expressed by Equation 2.11. The Einstein Equation

provides a highly useful means for calculating in models the effective thermal diffusivity or conductivity from random walks of virtual particles using the Monte Carlo method.

The Einstein Equation has been extremely useful, especially for providing the basis for much of the theory that describes diffusion of atoms in the solid state, where it is commonly assumed that atoms jump from site to site on a lattice with very long residence times on each site between jumps and an assumed flight time between sites of zero. This is sometimes referred to as the 'hopping model'. The atoms, individually and also their centre of mass, undertake random walks on a lattice. In a period extending over half a century, a vast literature has been built up that has been especially concerned with describing memories or correlations between individual jumps of the random walk of primarily tracer atoms [24]. Since about the early 1970s, much of this literature has made use of the Monte Carlo method [25]. For random walks with correlations on the simple cubic lattice the diffusivity can be partitioned from Equation 2.11as [24]:

$$D = \frac{\Gamma f a^2}{2dt} \tag{2.12}$$

where f is termed the correlation factor. This quantity expresses any correlations in the direction of jumps. When each jump in the walk is completely independent or uncorrelated with all previous ones, then $f = 1$. On the other hand, for a hypothetical walk where every jump of the particles is immediately reversed, then $f = 0$. As an aside, it is worth noting that for many solid state diffusion mechanisms, such as the vacancy mechanism, there are considerable correlations in the directions of successive jumps of the atoms because of the continued proximity of the vacancy to a tracer atom. For the vacancy diffusion mechanism the correlation factor is given approximately by:

$$f \approx 1 - \frac{2}{z} \tag{2.13}$$

where z is the local coordination number. It is very important to recognize that the Einstein Equation (Equation 2.11) is still valid over long times even when the material has different hopping rates in different regions of the material (for example in a composite), *provided* that the material remains isotropic in its diffusion properties overall. The implication also is that each tracer particle 'explores' a sufficiently large portion of the structure to be representative of the composite structure. (By allowing multiple occupancy of sites by particles then the correlation

factor f = 1.) The diffusivity represented in the Einstein Equation is then the *effective* diffusivity of the structure. If the material is anisotropic in its diffusion properties, one can still nonetheless define diffusivities in the three principal directions simply by using:

$$D_x = \frac{<\Delta X^2>}{2t}; \quad D_y = \frac{<\Delta Y^2>}{2t}; \quad D_z = \frac{<\Delta Z^2>}{2t} \tag{2.14}$$

where ΔX , ΔY , and ΔZ are the displacements of a particle in time t in the x , y and z directions respectively.

Since the first diffusion application of Monte Carlo method in the immediate post WWII period, the Einstein Equation itself does not seem to have been used until almost twenty years later and then only indirectly. A possible reason for this is the difficulty in dealing with time. In fact, in contrast to the other principal diffusion kinetics simulation method of molecular dynamics, the simulation of real time is not possible in a Monte Carlo kinetics calculation. What one actually does is to use a discrete quantity that is proportional to actual time. This quantity is the number of jump *attempts* per particles. Using the Einstein Equation with this quantity acting as 'time', one can then calculate a *relative* diffusivity, i.e. a diffusivity that is relative to one of the specified diffusivities (usually the highest) in the system.

2.1.3.2 Fick's First law method

The Fick's first law method is an alternative for calculating the effective diffusivity from the Einstein equation method. Fick's first law is written as:

$$J = -D\frac{\partial C}{\partial x} \tag{2.15}$$

where J is the particle flux and $\partial C/\partial x$ is its concentration gradient. In a LMC calculation Equation 2.15 is most conveniently used under steady-state conditions by introducing a source plane, at which particles can be created at a random position and released one at a time, and a sink plane, at which the particles are annihilated as soon as they arrive. This of course gives an apparent particle concentration 1/n, where n is the number of sites on the source plane and a zero concentration for the sink plane, providing a uniform concentration gradient $\partial C/\partial x$. This gradient can also be adjusted by changing the length of the lattice or by adjusting the probability

for the particle to be annihilated at the sink plane. For example, if a particle arrives at the sink plane and annihilated with a probability of P_i (appropriately evaluated on the spot using a new random number), the effective concentration of particles on that plane is then simply given by $(1-P_i)/n$ and the concentration gradient in the problem is thus reduced. Let us consider in a 2D lattice of dimensions 100×100 where the source and sink are separated by 50 planes in the +x direction and by the same number of planes via the periodic boundary in the –x direction. A particle released from the source plane and is permitted to diffuse to the sink, thereby providing, in effect a well-defined uniform concentration gradient. The flux *J* is simply calculated as the net number of particles crossed between two neighbouring planes in the x-direction as calculated over a long time t in between source and sink planes, during which time some 10^5 particles are released from the source and annihilated at the sink. Inclusions are introduced in exactly the same way as the Einstein equation method and diffusion is simulated in the same way. However, it should be noted a particle may 'see' in effect only one isolated inclusion in its lifetime in going from source to sink and possibly give an incorrect result for the effective diffusivity. For this reason, periodic arrangements of inclusions would require at least two inclusions between the source plane and the sink plane of particles. Overall, the Einstein equation method is considerably more convenient to use compared with the Fick's first law method and more flexible in its application.

2.1.3.3 Concentration profile method (Fick's First law method)

As the name implies, the method uses the concentration profile of the diffusant modelled by the LMC method to determine the diffusion coefficient. The concentration profile method is similar to solving the Diffusion Equation (Fick's Second Law) once the initial and boundary conditions are specified. However, to apply this method, the diffusivity should preferably be the same throughout the material to be considered. This method can be applied in two situations. One is described as the 'thin-film' or an 'instantaneous source' condition and the other is called the 'constant source' condition.

In the instantaneous source condition a thin layer of diffusant is deposited at the surface at time $t = 0$. The modelling of a concentration profile in the presence of an instantaneous source by the LMC method is described below. A source plane of particles is established in the centre of a large periodic square planar or simple cubic lattice in order to avoid edge effects in the calculation. Particles are generated at random positions on this source plane and released from the plane either sequentially or all at once. Assuming the latter for convenience here, we allow

the particles to diffuse independently of one another for the entire time Nt, at which time the final position of each particle is recorded. The final positions of all particles are then simply assembled from the individual final positions to form a concentration penetration profile. If the lattice is large in the diffusion direction, at relatively short times, the profile is the familiar Gaussian profile as appropriate for diffusion from a thin source into a 'semi-infinite' solid.

In the modelling of a constant source, it is required that a constant concentration of particles is maintained at the 'surface' for all diffusion times. The basic idea is simply to keep the total number of particles at the source plane constant at all diffusion times. This is achieved in the following simple way. All particles are released at the same time. As a particle makes a jump from the source plane it is immediately replaced by a new one, which is again generated at a random position on this plane in order to maintain the required number. On the other hand, whenever a particle returns to the source plane, thereby exceeding the number designated for the source, then any particle at the source is permanently removed from the system. Over a period of time, the number of particles within the system naturally increases as more particles diffuse away from the source than return to it. Accordingly, the diffusion time t must be constantly re-scaled since the time is required to be proportional to the number of attempts *per particle*. At longer times, the two profiles emanating from each side of the source start of course to meet up via the periodic boundary. However, if the particle source is now conceived as two 'separated surfaces', then the profile represents diffusion from two opposing surfaces into a material of finite width.

In principle, it is possible to determine the effective mass diffusivity of a model material by analysing the simulated concentration profiles. This would assume that there has been averaging of the profile over all possible locations of the second phase in the matrix phase. The profile would then need to be processed to give the effective mass diffusivity in much the same way as an experimental diffusant concentration depth profile by using the appropriate solution to the Diffusion Equation. In practice, it is far easier to calculate the effective diffusivity of the model material in a separate calculation using the Einstein equation.

2.1.4 Calculation of the Effective Thermal Conductivity by LMC Method

Thermal diffusion process is also a random process which can be represented by the random walks of particles. Here we consider particles as virtual heat particles. Since thermal diffusion

process is a random process it can also be described by the Einstein Equation. The thermal diffusivity K is in d dimensions ($d = 1,2,3$):

$$K = \frac{< \Delta R^2 >}{2dt} \tag{2.16}$$

where ΔR is the vector displacement of a given particle after a long time t. It is averaged over a very large number of particles (N) and represented by the Dirac brackets. The thermal conductivity λ_i of phase i is related to the thermal diffusivity K_i in a phase by;

$$K_i = \frac{\lambda_i}{\rho_i C^i{}_P} \tag{2.17}$$

where ρ_i is the density of phase i and $C^i{}_p$ is the specific heat of phase i. Then we can change Equation 2.16 by assigning densities and specific heats to be equal to unity in the phases considered. This equals $\lambda_{Eff} / \lambda_i$ ($\lambda_i = \lambda_1$, if $\lambda_1 > \lambda_0$ and $\lambda_i = \lambda_0$, if $\lambda_0 > \lambda_1$) to the relative effective thermal diffusivity K_{Eff} / K_i. This means that this situation can be usefully modelled by Monte Carlo simulations in calculating the relative effective thermal conductivity.

For the lattice hopping model the Einstein equation can be further expanded to Equation 2.18 for the purposes of Monte Carlo modelling as:

$$K = \frac{\Gamma a^2}{2d} \tag{2.18}$$

where Γ is the hypothetical inter-site transition jump rate or jump frequency of a thermal particle at the particular site considered and a is the jump distance in the lattice.
When $i = 2$, we can approximate the effective diffusivity/conductivity in such a composite, by writing the effective diffusivity as a simple linear combination of the individual diffusivities as:

$$K_{Eff} = \phi K_2 + (1 - \phi) K_1 \tag{2.19}$$

where ϕ is the area/volume fraction of the inclusion phase and Equation 2.19 is commonly referred to as the Hart Equation (see also Equation 2.2).

2.2 Methodology

2.2.1 Effective Thermal Conductivity/Diffusivity in a Single Phase Material

In calculating the thermal conductivity of a homogeneous material or calculating effective thermal conductivity in a composite material, the particles that explore the lattice are no longer considered to represent individual entities as heat particles but are considered as virtual particles that represent the macroscopic thermal conductivities in each region. Since different particles can occupy the same site there are no diffusion correlation effects in conducting this simulation.

In the very first case, we considered a single phase material with the same thermal conductivity everywhere. For convenience, the effective diffusivity is addressed in terms of the effective conductivity in the following.

We modelled a homogeneous single phase material in a 2D lattice of dimensions 50×50, having 2500 lattice sites. There are 4 jump directions for each jump of a particle, i.e. $z = 4$. Periodic boundary conditions are given on all four faces of the lattice. This very common type of boundary condition specifies that when a particle reaches an edge or face of the lattice, if the next jump would take it outside of the lattice, then the particle is simply plugged back into the edge of the face of the lattice directly on the opposite side of the lattice. In effect, with the imposition of periodic boundaries, the original lattice is now surrounded by periodic images or replicas of itself. The use of periodic boundaries thus enables surface effects to be avoided completely. However, this lattice is a small system, and, if too small, historical effects may be perpetuated in some diffusion problems as a particle leaves one side and enters on the opposite side into what is, in effect, essentially the same environment that it has just left. In a problem such as diffusion in a thin film, a formal surface(s) is of course necessary and is retained in the calculation.

There are two methods for calculating the diffusion coefficient. One releases all the particles at the same time at randomly chosen sites and then commences the movement by choosing them randomly to jump. Here the particles are capable of moving independently of each other over the lattice for the entire time considered in the simulation. The second method releases particles one at a time wherein all the particles are capable of having exactly the same time for exploring the lattice. However, at long times, both of these procedures become completely equivalent and would take about the same computational time. We preferred the latter method for convenience.

In our calculation here, a particle is created at some randomly chosen site where random numbers are used to generate the x and y coordinates for this site. The direction to jump is also chosen at random from the four available directions where the square planar lattice is used. We released N particles one at a time at randomly chosen sites in the lattice and then started the simulation allowing each of them to randomly explore the lattice for exactly the same time t. Provided that we permit multiple occupancy of a given site, the particles would diffuse independently of each other for the entire time Nt. Whilst the random walk of the particle is being directed by computer-generated random numbers, step-by-step contributions to the vector displacement of the particle ΔR are also being accumulated. It was found that it is best to do this by assuming that each particle starts from its own origin (0, 0). It should be especially noted that if the particle crosses a periodic boundary and is therefore plugged into the opposite side of the lattice, this process is completely ignored in the calculation of the displacement ΔR. The process of directing the random walk of the particle continues for 10^6 jump attempts. The entire process is then repeated with further particles until a total of $N = 50000$ particles have been released, all having had 10^6 jump attempts in their walks. Here every attempt to jump is permitted to be successful ($\Gamma = 1$). The jump distance here $a = 1$ is the lattice spacing. From Equation 2.18, when $d = 2$, it is evident that K should equal 1/4 and also carries the units: lattice spacings squared per jump attempt. A calculation of K directly from the Monte Carlo calculation using the Einstein equation (Equation 2.16), verifies this perfectly. The value here of $1/4$ taken by K then must be scaled to the actual thermal diffusivity of the material.

2.2.2 Effective Thermal Conductivity/Diffusivity in a Two Phase Material

2.2.2.1 Models

Figure 2.1 represents the basic 2D models used for the simulation. For 2D simulations square, circular and elliptical inclusions are considered. The 3D models, which are not displayed, are cubic and spherical inclusions within a simple cubic lattice. It is considered that the dispersed phase or inclusions, which are embedded in the matrix phase, are themselves arranged for convenience in a square planar arrangement for 2D simulations or a simple cubic arrangement for 3D simulations. Generally, the host material represents the metal matrix and an inclusion represents the insulating phase. The thermal conductivity in the inclusions themselves is λ_2 and the thermal conductivity in the matrix is λ_1.

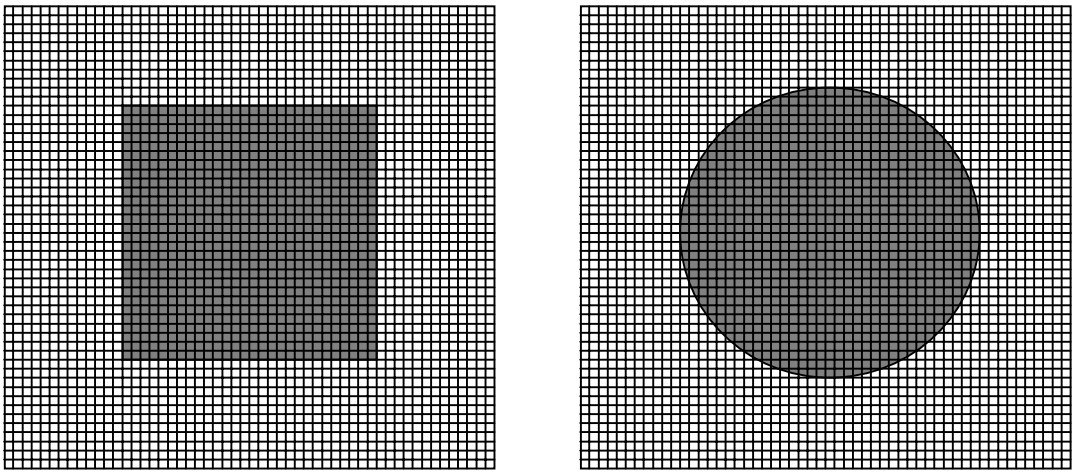

(a) (b)

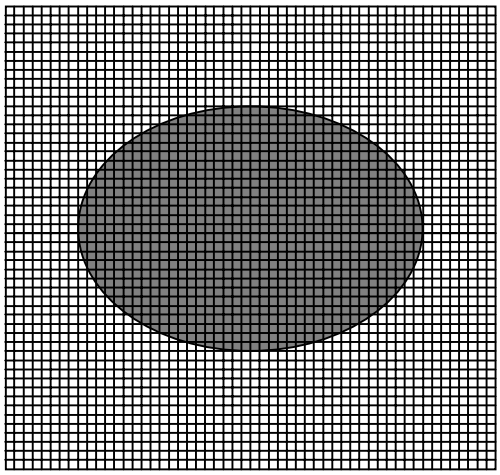

(c)

Figure 2.1 Schematic representation of a 2D model of Ag/MgO composite. (a) square inclusions (b) spherical inclusions (c) elliptical inclusions in a simple cubic arrangement overlaid by a simple cubic lattice

2.2.2.2 Method

The Monte Carlo simulation method containing differently shaped inclusions for 2D and 3D models is described as follows. A fine grained square planar lattice (151×151) was considered for the 2D simulations and a cubic lattice (151×151×151) was considered for the 3D simulations. The fine grained lattice is overlaid on the system, so that the inclusions are within the 2D and 3D lattices. The requirement here of course is that the lattice is sufficiently fine grained that it can adequately capture the shape of inclusions. The area/volume fraction of inclusions ϕ is simply the number of lattice sites in the inclusion(s) divided by the total number of sites (there is usually a small correction that depends on the choice of the jump frequencies between the two phases and will be discussed below). The lattice also has periodic boundaries which are implemented exactly as for the homogeneous system described above. Since there are periodic boundaries, it does not actually matter in this particular example if the inclusion is in the centre of the lattice because the arrangement of the inclusions itself is also simple cubic for 3D simulations and square planar for 2D simulations. This in turn results in the lattice being surrounded by images itself. However, for more complicated arrangements of the inclusions in the lattice, which effectively acts like a unit cell of the structure of the chosen arrangement, the inclusions would need to be located with care.

As for the homogeneous system described above, each particle is created and released from a randomly chosen site in the lattice. As before, no correlation effects need to be considered here since the particles diffuse completely independently of one another. The two conductivities λ_1 and λ_2 are now simply individually represented by two different jump probabilities (per unit time) Γ_1 and Γ_2. It is best to scale the higher Γ to unity for computational efficiency. The jump rate of the particle now varies according to position within the lattice. Thus if the particle is currently on a site known to be within the inclusions, it has a jump rate Γ_1, whereas if the particle is currently on a site known to be within the metal matrix, then it has a jump rate of Γ_2. We modelled for a range of values of λ_1 / λ_2, as an example for a range of values from 0.1 (Γ_1 = 0.1 and Γ_2 = 1) to 10 (Γ_1 = 1.0 and Γ_2 = 0.1). Let us consider Γ_1 = 1 and Γ_2 = 0.1, where the ratio of conductivities $\lambda_1 / \lambda_2 = 10$. Thus when a particle is on an inclusion site, another random number r needs to be generated to determine the outcome of the jump attempt. If r is less than or equal to Γ_2 then the jump attempt is said to have been successful and the particle is permitted to move. A small difficulty occurs at the boundary between the phases. When a particle is just about to cross a boundary, a consistent choice must be made about the jump rate to use. If the jump is from matrix to inclusion and Γ_1 is used, then the reverse jump (from inclusion to matrix)

must also use Γ_1. Otherwise, the principle of local detailed balance would be violated and there is an implication that there is some kind of segregation of the particles in the boundary between the two regions. It is to be noted that for thermal conductivity calculations, the term 'segregation' has no meaning, however, for the mass diffusion calculations, this is not the case of course. Segregation related simulations are discussed in Chapter 3. Now let us return to the jump frequencies at the boundary in the thermal conductivity problem again. Similarly, if the jump between inclusions and matrix used Γ_2 then Γ_2 must also be used for the reverse jump. In practice, the choice made here of Γ has almost no effect on the calculated results of the effective thermal conductivity. The correction is actually to the apparent fraction of inclusions (ϕ). This will arise as a result of this procedure because of the following reason. Obviously, a path of the particle jump with jump rate Γ_i should belong to the phase i. Because we introduce the fraction of sites (exactly $1/z$, where z is the coordination number) being taken from one phase and added to the other phase according to the method of handling the jump at the boundary between the phases it was introduced above. The correction is usually very small and can be shown to be inversely proportional to the number of sites representing an inclusion of a different type.

Similar to the homogeneous material, after a large number of particles have been released, say $N = 50000$ and allocating 10^6 jump attempts per each, then the effective thermal conductivity for the composite can be formed directly from the Einstein equation.

2.3 Results & Discussion

There have been many attempts to describe the relative effective conductivity in composite material in the past [3]. Recent simulations [4, 19, 29] have shown that treatments based on the Maxwell-Garnett treatment [11] invariably provide superior agreement over other treatments that are often far more sophisticated. For two dimensions, the Maxwell-Garnett equation is:

$$\frac{\lambda_{Eff}}{\lambda_i} = \frac{\lambda_1}{\lambda_i} \frac{(1+\phi)\lambda_0 + (1-\phi)\lambda_1}{(1+\phi)\lambda_1 + (1-\phi)\lambda_0} \tag{2.20}$$

where $\lambda_i = \lambda_1$ if $\lambda_1 > \lambda_0$ and $\lambda_i = \lambda_0$ if $\lambda_1 < \lambda_0$. An equation describing the effective conductivity for the case of square inclusions in a square planar arrangement has been derived

especially for very high values of ϕ [19]. This was found to be in excellent agreement with simulation results in the region of interest. That equation reads:

$$\frac{\lambda_{Eff}}{\lambda_i} = \frac{\lambda_1}{\lambda_i} \frac{(1-\sqrt{\phi}+\phi)\lambda_0 + (\sqrt{\phi}-\phi)\lambda_1}{\sqrt{\phi}\lambda_1 + (1-\sqrt{\phi})\lambda_0} \tag{2.21}$$

where $\lambda_i = \lambda_1$ if $\lambda_1 > \lambda_0$ and $\lambda_i = \lambda_0$ if $\lambda_1 < \lambda_0$.

For the three dimension situation, the Maxwell-Garnett equation is:

$$\lambda_{Eff} = \lambda_1 \left\{ 1 + \frac{3\phi(\lambda_0 - \lambda_1)}{\lambda_0 + 2\lambda_1 - \phi(\lambda_0 - \lambda_1)} \right\} \tag{2.22}$$

For all values of λ_1 and λ_0.

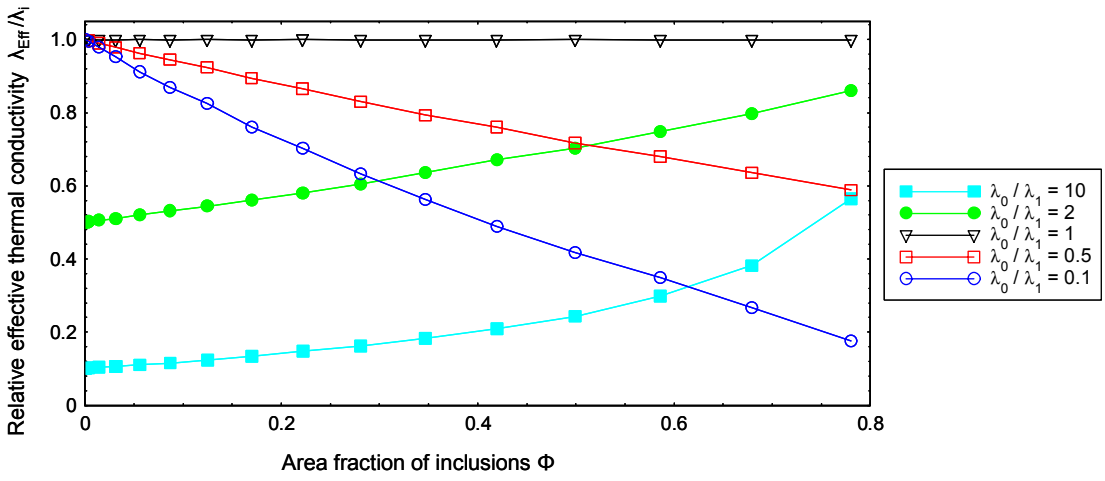

(a)

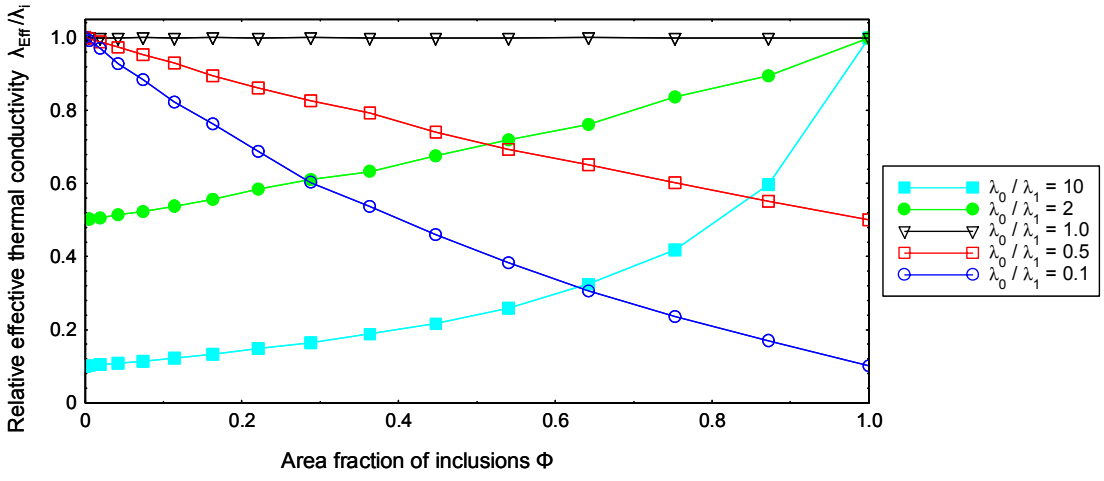

(b)

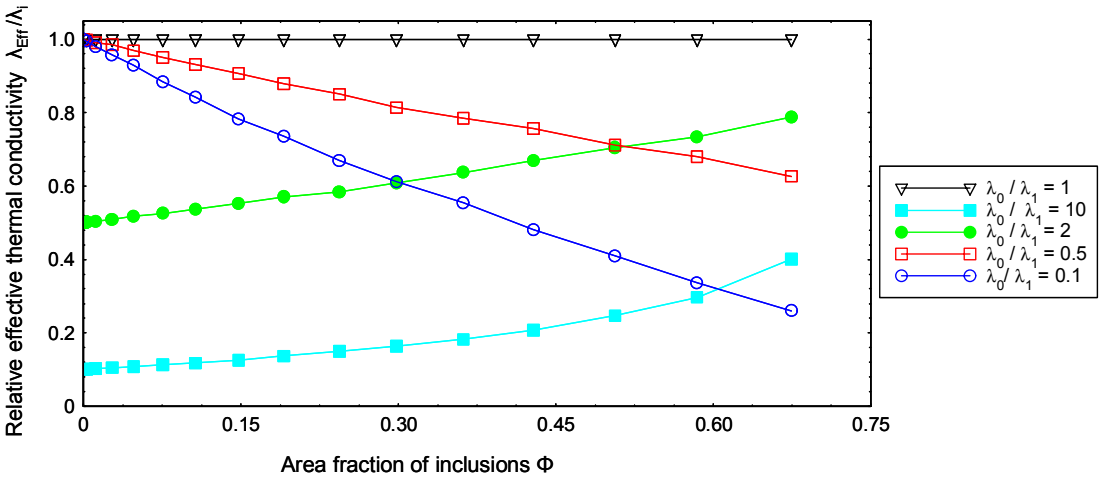

(c)

Figure 2.2 Relative effective thermal conductivity of a composite with (a) circular inclusions (b) square inclusions (c) elliptical inclusions where inclusions referred to as 0 and matrix as 1 in a square planar arrangement as a function of area fraction of inclusions for several values of the matrix and dispersed phase thermal conductivities.

In Figure 2.2 we give LMC results by the Einstein equation method for the relative effective thermal conductivity as a function of area fraction ϕ of circular, square and ellipse inclusions as in 2D simulations for a range of values of the matrix and inclusion conductivities within an order of magnitude. In Figure 2.3 we give the same results for spherical and cubic inclusions and compared with an analytical solution. It is to be noted that in Figure 2.2 (c) the given relative effective thermal conductivity values are equivalent to a randomly oriented elliptical inclusion system.

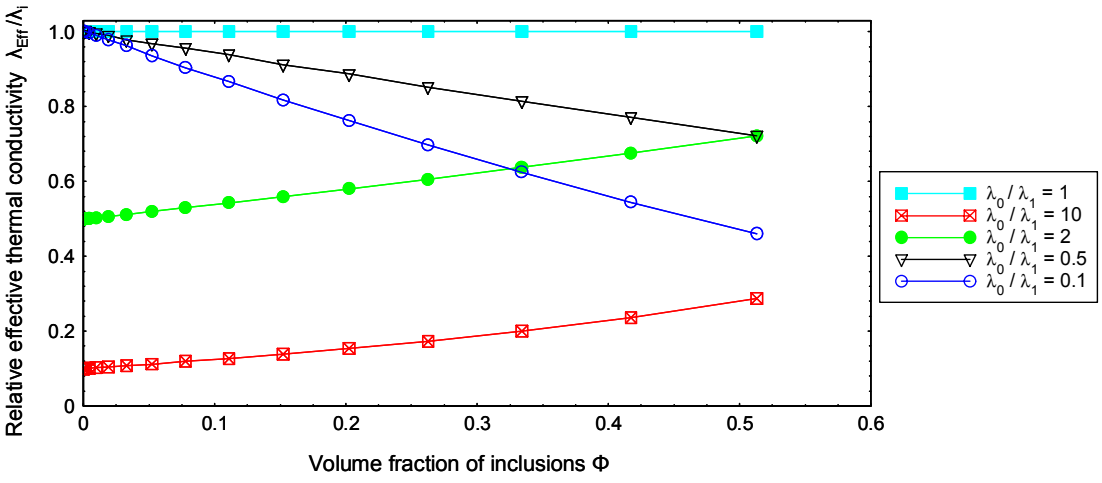

(a)

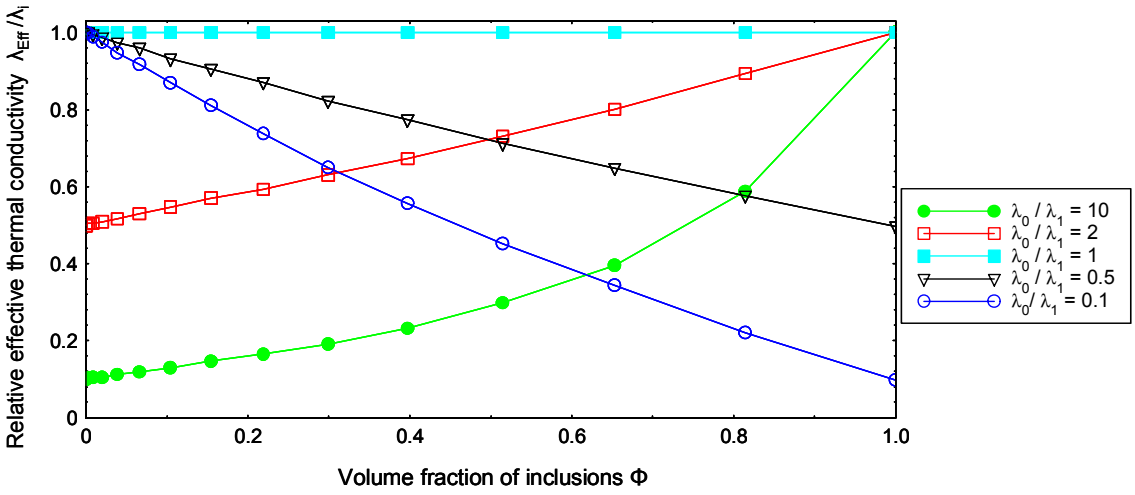

(b)

Figure 2.3 Relative effective thermal conductivity of a composite with (a) spherical inclusions (b) cubic inclusions where inclusions referred to as 0 and matrix as 1 in a cubic arrangement as a function of volume fraction of inclusions for several values of the matrix and dispersed phase thermal conductivities.

The ellipse is modelled in such a way that the distance between the center to the foci is set to be half from the distance of the centre to the vertex. The resulting eccentricity then equals one half, where the semi-minor axis equals √3 /2 of the semi-major axis of the ellipse we considered. It is to be noted that the conductivity values are described only up to 0.7854 for circular inclusions, due to the touching of inclusions beyond those values. However, there is no such limitation for square inclusions (in a square arrangement) to be considered because by the time inclusions are touching; the whole matrix becomes completely filled with inclusions. In such a situation,

Figure 2.2 represents some interesting results. Let us consider the situation where the conductivity ratios (λ_0 / λ_1) equals 0.5 and 2 for the square inclusion composite. For $\lambda_0 / \lambda_1 = 0.5$, when the matrix is entirely full of inclusions the relative effective thermal conductivity reaches a value 0.5, which is equivalent to that of the curve where $\lambda_0 / \lambda_1 = 2$, when the matrix is completely empty of inclusions. This observation can be further extended to $\lambda_0 / \lambda_1 = 0.1$ and $\lambda_0 / \lambda_1 = 10$. Similarly when the matrix is entirely filled with inclusions for $\lambda_0 / \lambda_1 = 2$ and $\lambda_0 / \lambda_1 = 10$, the relative effective thermal conductivity reaches unity, which is obvious. However, when the conductivity ratio equals unity, the relative effective thermal conductivity is kept unchanged irrespective of the inclusion fraction. A similar situation when $\lambda_0 / \lambda_1 = 10$ is observed for circular and elliptical inclusions as well. It is noted that in Figure 2.2 (a) and (c), when $\lambda_0 / \lambda_1 = 2$ and $\lambda_0 / \lambda_1 = 10$ the highest relative effective thermal conductivity for circular inclusions is comparatively higher than for the elliptical inclusions. This is also obvious since the area fraction of the inclusion phase is higher in circular inclusions compared to elliptical inclusions. The observations discussed above for the square inclusion composite in Figure 2.2 (b) are shown to be quite similarly connected with Figure 2.3 (b) for the cubic inclusion composite. The maximum volume fraction of spherical inclusions is limited to 0.5133, the point where a percolation threshold exists in Figure 2.3 (a).

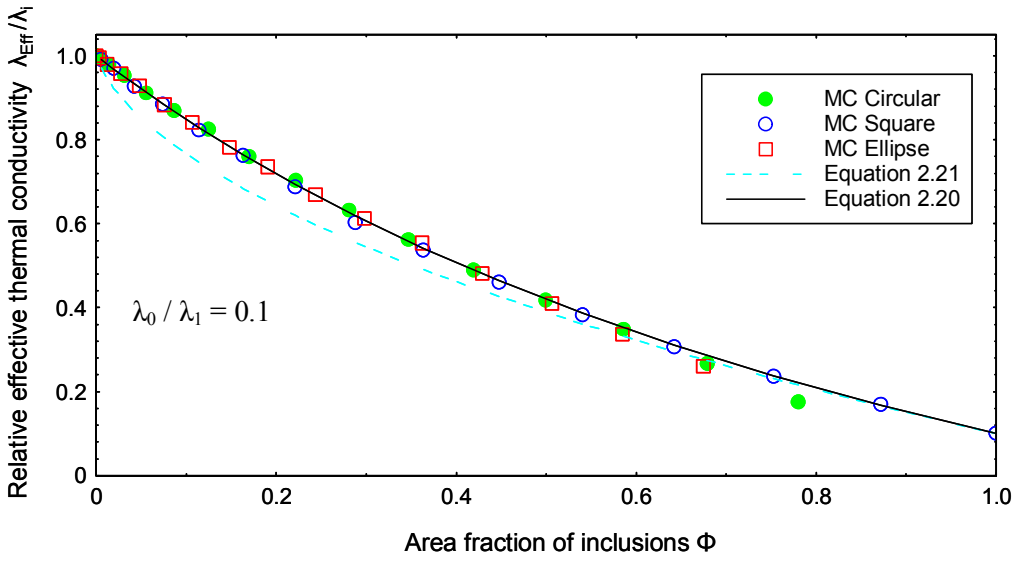

(a)

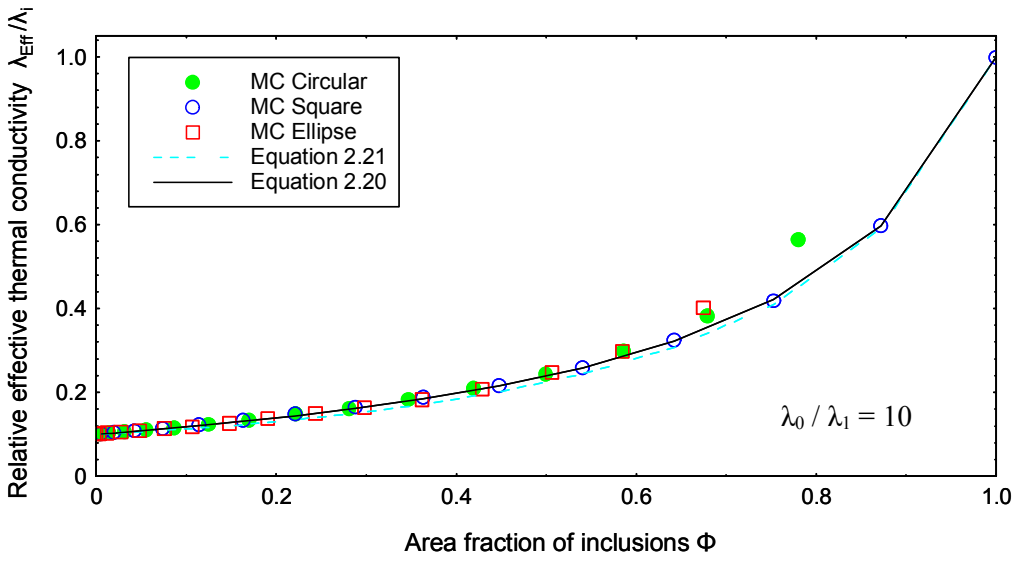

(b)

Figure 2.4 Comparison of numerical and analytical approaches for 2D simulations

Figure 2.4 (a) and (b) represents a comparison between the analytical Maxwell-Garnett equation (Equation 2.20 and 2.21) and computed LMC results for circular, square and ellipse inclusions for conductivity ratios 0.1 and 10. Here, the results are presented for the cases where the thermal conductivity of the inclusions differs from that of the matrix by an order of magnitude. It is clear that Equation 2.20 does very well with all three types of the above inclusion but, along with Equation 2.20, can not of course describe the change of the conductivity when circular inclusions are close to touching ($\phi = 0.7854$). Equation 2.21 does very well for high values of ϕ for square inclusions (for which it was derived) but less well at low values of ϕ.

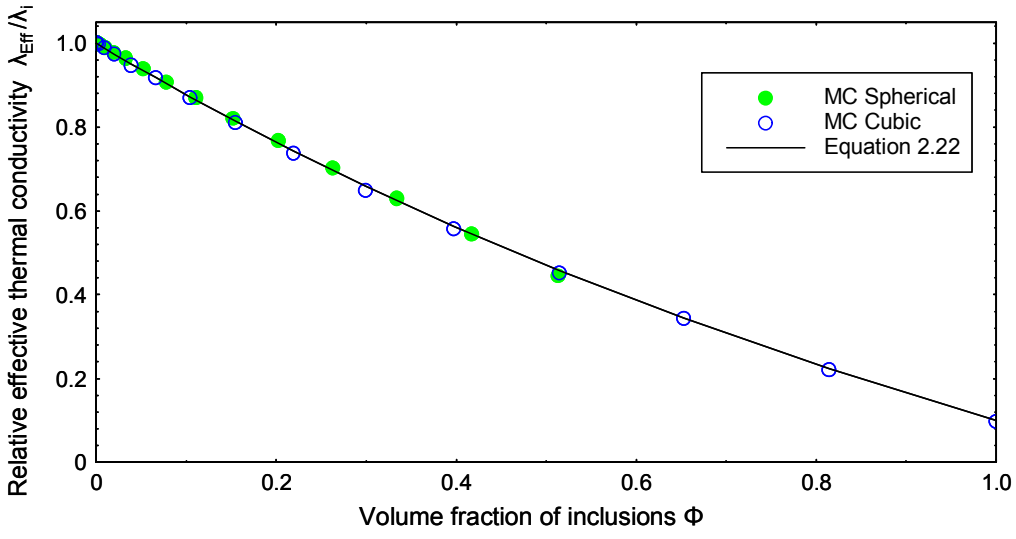

(a)

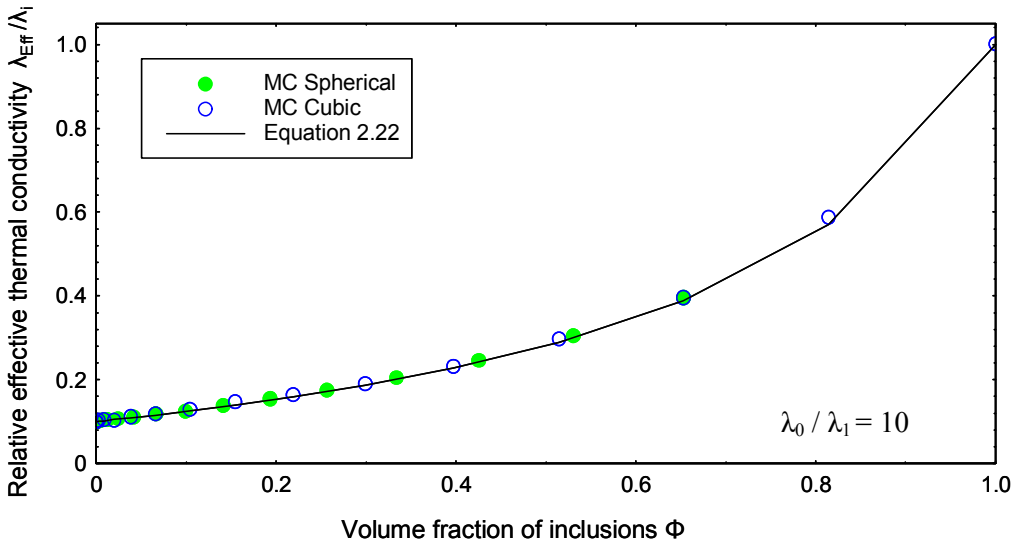

(b)

Figure 2.5 Comparison of numerical and analytical approaches for 3D simulations

Figure 2.5 (a) and (b) also represents a comparison between analytical Maxwell Equation (Equation 2.21) and computed Monte Carlo results for spherical and cubic inclusions for conductivity ratios 0.1 and 10. Similar to the 2D simulation we present results where the thermal conductivity of the inclusions differs from that of the matrix by only an order of magnitude. It can be observed that there is excellent agreement of the computed results for Monte Carlo data for spherical and cubic inclusions with the analytical Maxwell Equation. Therefore it is evident from the results that relative effective thermal conductivities with increasing volume fraction of spherical and cubic inclusions are best described by Equation 2.21.

The principal difficulty in the LMC method for determining the effective diffusivity/conductivity is ensuring that the number of jump attempts is sufficiently large to ensure that the long-time effective diffusivity/conductivity of the composite is accurately determined. At very short diffusion times for each particle (one or two jumps), as might expected, the effective diffusivity/conductivity is simply given by the approximate Equation 2.19 because this would in effect also be the *instantaneous* effective diffusivity/conductivity. At very long diffusion times, after each particle has adequately explored the structure, the correct long-time limit effective diffusivity of the composite is obtained. As a good estimate for what would be a sufficiently long time for a given calculation, it is better to first form the effective diffusivity/conductivity according to the approximate Equation 2.19 and then use this via a calculation of the 'diffusion length', $\left(2dK_{Eff}t\right)^{1/2}$ to determine the number of jump attempts (t) appropriate for the problem. Roughly, the diffusion length should be at least half the length of

the lattice, or the unit cell of the ordered arrangement of inclusions. As noted above, the highest jump rate is scaled to unity for efficiency. When one of the diffusivities is very small, the LMC method with the basic algorithm described above frequently runs into difficulties arising from rather large computational inefficiency (most attempts to jump are rejected in that region) and a slight non randomness in the random number generation and subsequent inhomogeneity of the random numbers generated over the range of zero to unity. This will be magnified for the diffusion in a low diffusivity region. These difficulties can be avoided or at least minimized by making use of straightforward residence time algorithms [26-28]. Such algorithms can be very useful when diffusivities vary by many orders of magnitude. A popular choice makes use of an algorithm that guarantees a jump on every attempt [28] wherein the particle's site residence time (the reciprocal of the jump rate) is simply added to the elapsed time at each move. In principle, this can lead to overshooting of the specified time though this is unlikely to be serious problem at very long diffusion times. There is, of course a significant computational overhead with such algorithms that may offset at least some of the efficiency gains.

2.4 References

[1] K. Yoshida and H. Morigami, Microelectron. Reliab., **Vol. 44**, 2004, p. 303

[2] D. Duschlbauer, H.J. Böhm and H.E. Petetermann, Mater. Sci. Tech. Ser., **Vol. 19**, 2003, p. 1107

[3] S. Torquato: Random Heterogeneous Materials (Springer-Verlag, New York 2002)

[4] T. Fiedler, E. Pesetskaya, A. Öchsner and J. Grácio: Mater. Sci. Forum, **Vol. 514 – 516**, 2006, p. 754

[5] G.E. Murch and I.V. Belova, Interf. Sci., **Vol. 11**, 2003, p. 91

[6] E.W. Hart, Acta Metallogr.,**Vol. 8**, 1957, p. 597

[7] A.J. Mortlock, Acta Metallogr, **Vol. 8**, 1960, p. 132

[8] R. Birringer, U. Herr, H. Gleiter, Suppl. Trans. Jpn. Inst. Metals, **Vol. 27**, 1986, p. 43.

[9] I. Kaur, Y. Mishin, W. Gust, Fundamentals of Grain and Interphase Boundary Diffusion, Wiley, Chichester, 1995

[10] J.C. Maxwell, Treatise on Electricity and Magnetism, 3rd Edition, Clarendom Press, Oxford, 1904

[11] J.C. Maxwell-Garnett, Philos. Trans. Royal Soc. London, **Vol. 203**, 1904, p. 385

[12] J.R. Kalnin, E.A. Kotomin and J. Maier, J. Phys. Chem. Solids, **Vol. 63**, 2002, p. 449

[13] I.V. Belova and G.E. Murch, J. Phys. Chem. Solids, **Vol. 64**, 2003, p. 873

[14] I.V. Belova and G.E. Murch: J. Metastable and Nanocrystalline Materials, **Vol. 19**, 2004, p. 25

[15] A.D. Brailsford and K.G. Major, Br. J. Appl. Phys., **Vol. 15**, 1964, p. 313

[16] I.V. Belova and G.E. Murch, Phil. Mag., **Vol. 84**, 2004, p. 17

[17] P. Knauth, J. Electroceram., **Vol. 5**, 2000, p. 111

[18] P. Heitjans and S. Indris, J. Phys-Condens Matt., **Vol. 15**, 2003, p. R1257

[19] I.V. Belova and G.E. Murch, J. Phys. Chem. Solids, **Vol. 66**, 2005, p. 722

[20] D.P. Riley, I.V. Belova and G.E. Murch, Proc. Mat. Res. Soc. Symp., **Vol. 677**, 2001, AA7.11.1 (e-published)

[21] I.V. Belova and G.E. Murch, Mass and Charge Transport in Inorganic Materials II, Techna, Faenza, Italy, 2002, p. 225

[22] I.V. Belova and G.E. Murch, Defect Diffus. Forum, **218/220**, 2003, p.79

[23] I.V. Belova and G.E. Murch, Phil. Mag., **Vol. 84**, 2004, p.17

[24] A.D. Le Claire, Correlation effects in diffusion in solids, in: Physical Chemistry: An advanced treatise, Vol. 10, Academic Press, New York, 1970, p. 261.

[25] G.E. Murch, Simulation of Diffusion Kinetics with Monte Carlo Method, in: Diffusion in Crystalline Solids, Academic press, Orlando, 1984, p. 379.

[26] J.P. Lavine and D.L. Losee, J. Appl. Phys., **Vol. 59**, 1984, p. 924

[27] J.P. Lavine, Simulation of Semiconductor Devices and Processes, Pineridge Press, 1984

[28] P. Metsch, F.H.M. Spit and H. Bakker, Phys. Stat. Sol. A, **Vol. 93**, 1986, p. 543

[29] I.V. Belova and G.E. Murch: J. Mat. Proc. Tech., **Vols. 153 – 154**, 2004, p. 973.

Chapter 3

3. Modelling of Oxygen Diffusion and Segregation at Interfaces in Ag/MgO Composites

3.1 Introduction

3.1.1 Metal/Ceramic Composites and Applications

Internal interfaces play an important role in controlling the mechanical, thermal and electrical properties of many advanced materials. This has motivated numerous studies to investigate such interfaces. Currently metal/ceramic composites are employed in such diverse applications as thin solid films, anti-corrosion coatings, electronic packaging, gas sensors and combustion engines [1, 2]. Therefore, it can be expected that an understanding of the properties of the interfaces of such composites will help to improve their mechanical, thermal and electrical properties. In metal/ceramic oxide composites the oxide and metal components are chemically very different materials. Metals show metallic bonding which is characterized by the delocalization of electrons. Oxides generally have mixed ionic-covalent bonding because of the high electro-negativity of oxygen. The bond that forms between the ceramic and the metal components is due to the Coulombic attraction between the ions of the ceramic and the screening charge density in the metal [3].

To investigate experimentally the metal/ceramic interfaces, spatially resolved EDX [4], surface spectroscopy [5], high resolution electron microscopy (HREM) [6, 7] and field-ion microscopy with atom-probe (FIP-AP) [8] have so far been used. Electron energy loss spectroscopy (EELS) is also important in determining the bonding states of chemical elements at interfaces that are in the nanometre scale by analysing their near edge fine structure (ELNES) of an EELS spectrum [9]. In addition to the above mentioned experimental techniques, so far, there have been two types of computational approaches conducted for theoretical interface investigations namely: *ab initio* calculations [10, 11] and atomistic simulations [12, 13]. However, what is needed is a

higher level simulation method that can address interface and inclusion configurations at a larger distance scale.

3.1.2 Studies of the Ag/MgO Interface

The bonding of a ceramic to a transition metal has been well described by Schönberger et al. [10]. They determined that strong covalent pd-bonds could be formed across the interface between oxygen and the transitions atoms as the adhesion correlates with the free energy of oxide formation for the transition metal, increasing in the order of Ag < Cu < Ni < Fe … That study concluded that atomically sharp transition metal-ceramic interfaces can exist without inter-diffusion and the formation of a transition-metal oxide layer. Schönberger et al. investigated the bonding state of the Ti/MgO interface and the Ag/MgO interface by *ab initio* density-functional calculations. In the first case, they found that the Ti-O bonding is predominantly covalent with the Ti oxidation state less than + 1 whereas in the second case the Ag-bonding is predominantly ionic as in the oxide Ag_2O with the Ag oxidation state being close to +1. They used the interfaces with $(001)_{Ag} \| (001)_{MgO}$ and $[100]_{Ag} \| [100]_{MgO}$. Ag was replaced with Ti for the comparison.

Experimentally, a Ag/MgO composite is formed by starting with a Ag-Mg alloy that is then gently internally oxidized by heating the sample in an oxygen atmosphere [14, 15]. The oxygen diffuses into the alloy from the surface and, if the temperature is high enough so that Mg atoms can also diffuse, the oxygen and Mg atoms are able to react and form a highly dispersed oxide second phase of MgO since oxygen preferentially reacts with Mg. The MgO is very insoluble in the metallic Ag alloy and there is thus a very sharp discontinuity between the metallic phase and the oxide precipitates. In this sense, the MgO precipitates are present as internally produced 'inclusions' within the metallic phase. The boundaries between the MgO and the metallic phase are thus formally interphase boundaries. It is known that very substantial amounts of oxygen segregate to these boundaries [16-18]. This oxygen probably relieves any local strain that might have developed at the boundaries between Ag and MgO by providing the possibility of new Ag-O bonds. It also has the effect of greatly weakening the adhesion between the oxide phase and the metallic alloy with consequent loss of functional mechanical properties of the composite. Some of this oxygen probably originates from the initial treatment of the alloy in the oxygen atmosphere. But most comes from in-service conditions when the composite becomes hot and allows significant oxygen to diffuse into the sample. In principle, this segregated oxygen can be removed and the composite's properties restored by heating the sample in a vacuum at a higher

temperature so that the oxygen is desorbed. Both the absorption and desorption oxygen processes are limited by oxygen diffusion and the degree of segregation. These factors are addressed in the present study.

It is well-known in the literature that in general materials terms, segregation to grain boundaries can lead to fracture along grain boundaries as a result of temper brittleness, creep embrittlement, stress relief cracking of weldments, hydrogen embrittlement when exposed to uncontrolled atmospheres, environmentally assisted fatigue, grain boundary corrosion and inter-granular stress corrosion cracking [19]. This will change the physical properties of the interface ultimately adversely affecting the bulk properties of the composite. A good example describing segregation phenomena occurring at Ag/MgO and Pd/MgO interfaces was described by Gegner et al. [14]. They analysed the interface using a structural model, purposely allowing vacancies in the terminating (111)-plane of MgO. It was concluded from their results that segregation would be unavoidable to such vacancies, leading to the formation of Ag_2O at the Ag/MgO interface.

Later, Pippel et al. [15] made a thorough experimental investigation of the Ag/MgO interface. They found that the bonding state of oxygen at the interface remains the same after annealing an Ag/MgO specimen in vacuum. It was concluded that the oxygen presence at the interface solely belongs to the stoichiometry of MgO. However, after annealing in an oxygen atmosphere, the precipitation of Ag_2O was shown by having close values between the average free enthalpy of segregation (-70 kT/mol) and free reaction enthalpy (-78 kJ/mol) for oxygen. The bonding state of Ag_2O and MgO was further explained by the bonding energies. For example, from the lower bonding energy (ΔE = -0.24 eV) for Ag_2O compared with the much higher bonding energy for MgO (ΔE = -5.90 eV) it was concluded that oxygen is loosely bound in Ag_2O. These experimental findings were further illustrated by a structural vacancy model of the segregation of oxygen at Ag/MgO interface. This model represents the Ag/MgO interface during annealing in vacuum and with high oxygen partial pressures and can be generalized into describing numerous metal/oxide phase boundaries. Both Gegner and Pippel and colleagues discussed the occurrence of hydrogen embrittlement and the formation of H_2O at the Ag/MgO interface at high oxygen pressures. Therefore, it is important to establish the means for predicting the time-dependence of the concentration of oxygen that can segregate at the various internal interfaces of the material under selected atmospheric conditions.

Recently, the time-dependence of the diffusion of oxygen into an Ag/MgO composite and the subsequent segregation of oxygen in interfaces has been studied theoretically by one-dimensional finite difference models [20]. The principal input parameters to these calculations are the diffusivity of oxygen in the Ag matrix and an estimate of the segregation factor [21] of

oxygen at the Ag/MgO interfaces. The influence of effects such as the kinetic order or non-homogeneity of the ceramic oxide inclusions were investigated by solving the relevant partial differential equations with a one-dimensional finite difference scheme. Later, more sophisticated geometries and particle distributions were investigated with a two-dimensional finite element scheme making use of commercial code that had been extended with special user-subroutines [22]. This numerical approach allowed for the consideration of somewhat more general boundary conditions, specimen sizes and time or concentration-dependent material and material process parameters.

3.1.3 Segregation Effect in Mass Diffusion at the Internal Crystal Interfaces

The segregation effect can be explained using the terminology of grain boundary self and impurity diffusion processes. During self-diffusion in pure elements, the following equation is valid at the interface between the grain boundary and the adjacent crystal where the interface is considered [21]:

$$C_b = C_g \tag{3.1}$$

where C_b is the concentration of the diffusant in the boundary and C_g is the concentration of the diffusant in the grains. However, in the situation of hetero-diffusion in the Ag/MgO composite, equilibrium solute segregation of oxygen will occur. At the Ag/MgO interface the segregation factor *s* is defined by:

$$s = \frac{C_b}{C_g} = \exp\left(-\frac{E_s}{RT}\right) \tag{3.2}$$

Equation 3.2 describes the equilibrium adsorption and desorption of oxygen at the interface according to the Henry Law segregation isotherm. Here, C_b is the concentration of diffusant at the interface, C_g is the concentration of diffusant in the Ag matrix, *R* is the ideal gas constant, E_s is the segregation energy of the diffusant at the interface of the dispersed phase and the bulk and *T* is the absolute temperature.

In a situation where the solute concentration in the boundary or interface is low, Kaur et al. [21] have shown that the experimental segregation obeys Henry's Law. However, in systems with a high level of segregation, i.e. where a high concentration of oxygen is found at the interface at relatively low temperatures, C_b and C_g can no longer be considered to depend linearly on s due to the saturation by solute atoms. In such situations, the equilibrium distribution of oxygen is rather better described by the McLean segregation isotherm:

$$s' = \frac{C_b(1-C_g)}{C_g(1-C_b)} = \exp\left(-\frac{E_s}{RT}\right) \tag{3.3}$$

3.1.4 Out-Diffusion (Diffusion-Limited Evaporation)

Out-diffusion or diffusion-limited evaporation occurs when one or more components selectively evaporate from the material. It is most prominent when the diffusion rate of the evaporating species to the surface is much slower compared with other surface processes and the evaporation rate itself into vacuum. Out-diffusion is well-known in the preparation of alloys [23, 24], polar liquid films [25], catalysis [26], molten glass systems [27, 28] and in semiconductor systems [29-33]. Recent experimental developments are mostly in the semiconductor industry. Few analytical solutions [34] are available. No literature has been located regarding the study of out-diffusion in metal/ceramic composites. It is important because out-diffusion represents perhaps the only way for a composite containing oxygen segregated at the interfaces to be, in effect, regenerated. By taking the composite to a high temperature in vacuum the oxygen can diffuse out. High temperature diffusion processes, especially out-diffusion ones, occur in electronic components leading to premature failure of such components unless careful consideration is made. This is because physical and mechanical properties are affected by the out-diffusion process. Therefore, a simulation means to investigate out-diffusion is important to develop.

3.1.5 Monte Carlo Approach for In-Diffusion and Out-Diffusion

Although there are quite a number of experimental and theoretical methods to address diffusion problems in composites, as the problem becomes more and more complex, the setting up of the phenomenological diffusion equations and obtaining analytical solutions becomes more and

more difficult. Numerical methods such as finite element and finite difference methods can be used to find a fair solution. However, due to meshing difficulties, finite element methods are restricted to quite simple particle distributions and boundary conditions. An alternative general approach to the problem is the Monte Carlo method. This method adopted here is based on a lattice model and hence termed the Lattice Monte Carlo (LMC) method. Recently, the LMC method has been used to address phenomenological diffusion problems by using virtual random walking particles [35, 36]. The LMC methods can be regarded as a simulation form of a finite-difference method which can cope with multi-scale modelling in both space and time in a very convenient way. Accordingly, the LMC method had potential to represent the time-dependent oxygen in/out diffusion and segregation in Ag/MgO composite material and will be discussed in this chapter. The first use of the LMC method was to simulate concentration depth profiles in the presence of dislocation pipes parallel to the diffusion direction [34]. The method has been used since for such problems as diffusion in the presence of grain boundaries, diffusion-limited evaporation and diffusion in nanocrystalline material [34, 37-39]. These studies motivated us to study both in-diffusion and out-diffusion processes occurring in the Ag/MgO composite with the LMC method.

3.2 Methodology

3.2.1 Oxygen in-diffusion in a single phase material

3.2.1.1 The model

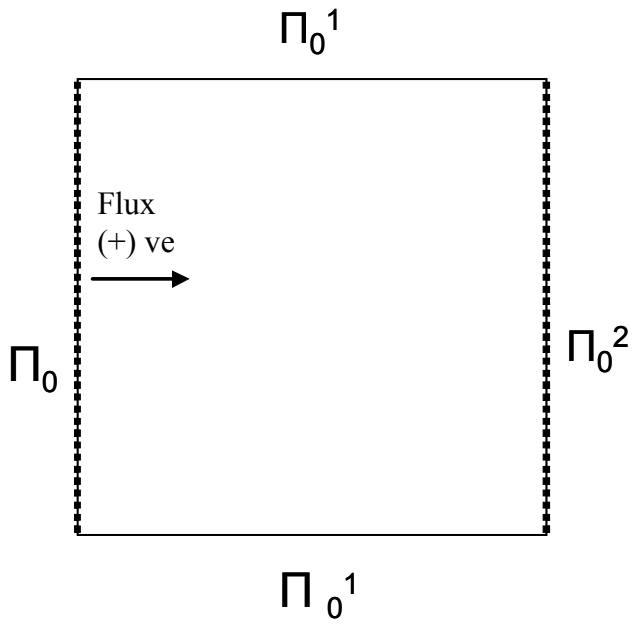

Figure 3.1 Schematic representation of the model for the diffusion of oxygen into a single-phase material

We use Figure 3.1 to represent a 2D model for diffusion in a single-phase material. Here, the outer surface boundary Π_0, is set as the surface plane or the source of oxygen. We modelled the source in a sandwich configuration in order to avoid edge effects. This simply means that there is a mirror image of Figure 3.1 to the left which shares the same boundary Π_0. The Π_0^1 boundary is treated as a periodic boundary: this assumes the model to be periodic in the direction normal to diffusion direction. Depending on the boundary condition at Π_0^2, Figure 3.1 can represent a semi-infinite material or a thin-film material. If a periodic boundary condition is given to Π_0^2, then we can consider it as a thin-film material.

Inside the thin-film bounded by Π_0, the oxygen concentration C_0 is described by:

$$\frac{\partial C_0}{\partial t} = D^0 \nabla^2 C_0 \tag{3.4}$$

where D^0 is the diffusion coefficient of oxygen in the Ag matrix and ∇^2 is the Laplacian operator.

For the boundary conditions at boundary Π_0, a constant concentration for the source is defined by:

$$C_{0|\Pi_0} = const \tag{3.5}$$

for all diffusion times $t \geq t_0$, where t_0 is the initial time.

For the boundary conditions at boundary Π_0^2:

$$C_{0|\Pi_0^2} = 0 \text{ at } t = t_0 \tag{3.6}$$

For the initial conditions $C_0 = 0$ everywhere.

For the purposes of calculation Figure 3.1 is mapped onto a square planar lattice as described below.

3.2.1.2 Method of computation

The Monte Carlo simulation is conducted by mapping Figure 3.1 onto a 101×50 mesh matrix to simulate a thin-film material. The source was placed at the 51st plane and was modelled with a large number of particles (10^5) starting at random locations along the plane. The diffusion process itself was started by releasing particles all at one time (t = 0) from random locations chosen at the source. These particles were permitted to explore the lattice according to a hopping model. Each particle has a coordination of four in this problem. For a jump attempt, a particle was chosen randomly to jump in a random direction at a rate reflected in an inter-site transition rate Γ. This was repeated. These randomly chosen particles move on random walks and explore the structure for a given 'diffusion anneal' time *t* (which is scaled directly to an attempt to jump). In this simulation, this time comprises some 10^5 - 10^{10} jump attempts. This problem is modelled in such a way that multiple occupancy of a site is permitted and thus there are no diffusion correlation effects. The diffusion coefficient (D^0) of oxygen in the Ag matrix is represented by:

$$D^0 = \Gamma_{11} a^2 / 4 \tag{3.7}$$

where Γ_{11} is the inter-site transition rate for the Ag matrix and a is the lattice spacing. The factor 4 comes from the fact that the simulation is in 2D. This factor would be 6 if the simulation were in 3D.

We now describe the constant source condition in a detailed way. When a particle jumps from the source into the lattice the source particle number drops by one particle. A new particle was then immediately implanted at a random location in the source plane thus keeping the number of particles at the source concentration. On the other hand, when a particle returns to the source plane, this would mean that the source concentration would exceed the number designated. Then that particle is removed permanently from the system. Over a period of time, the number of particles in the system naturally increases because particles diffuse away from the source. Therefore, the diffusion time t was rescaled each time with the total number of actual particles in the system at the time when an attempt to jump was made. The diffusion time is proportional to the number of attempts per particle.

An 'infinite' material can be represented by a sufficiently large lattice. This is modelled by mapping a 400×50 lattice onto Figure 3.1, by placing the source on the 201st plane. It is also assumed that the difference between modelling a thin-film and an infinite material is that in the latter case just one source is available unlike the former case where both surfaces are joined onto one source plane. Moreover, in the infinite material the Π_0^2 boundary is assumed to be at zero concentration at all times during simulation. This is only possible if that boundary is kept at an infinite distance from the source.

It is useful to discuss the meaning of 'distance' in the present problem. Let us modify Equation 3.7 to consider diffusion in some characteristic distance d, between the surface and the leading edge of an inclusion. In the simulation, the distance d is represented by 20 lattice spacing. We assume this value at say 0.005 mm. Then the basic mesh size of the lattice in the problem becomes 2.5×10^{-7} m of real distance (x^*).

Now let us consider 'time' in the problem. We considered Equation 3.8:

$$D^0 = \Gamma_{11} (x^*)^2 / 4 \tag{3.8}$$

and $\Gamma_{11} = \dfrac{\Gamma_{11}^*}{t}$

The oxygen diffusion coefficient in the Ag matrix D_0 takes a value of 2.1×10^{-11} $m^2 s^{-1}$ at 773 K [22]. In real time problems the jump frequency Γ_{11} in Equation 3.7 will of course take some value other than unity. For convenience of the numerical simulations, we scaled this value to unity (Γ_{11}^*) in the program and t is the diffusion annealing time in real time (in seconds). While x^* and D^0 are known, t can be calculated as 0.744×10^{-3} s. This is the basic unit of time in the problem. It means that if a particle is selected to jump 1000 times, then real time is advanced by 0.744 s.

3.2.2 Oxygen in-diffusion in a square inclusion composite

3.2.2.1 The model

As with the same conditions in Π_0, Π_0^1 and Π_0^2 boundaries of Figure 3.1, the Ag matrix is represented as the Ω_1 region in Figure 3.2. Each square inclusion of MgO (indicated by Ω_3) is surrounded by a very thin interface region Ω_2 where the oxygen can adsorb and desorb (i.e. segregate). The region Ω_3 is considered impermeable to particles at the temperatures of interest. However, the segregation layer itself is capable of accommodating and allowing the movement of particles within it depending on the scenario to be modelled. The interface boundaries are Π_1, which lies between regions Ω_1 and Ω_2, and Π_2 in between Ω_2 and Ω_3. The square inclusions are arranged in a square planar arrangement. The model is assumed to be periodic in the direction normal to the diffusion direction.

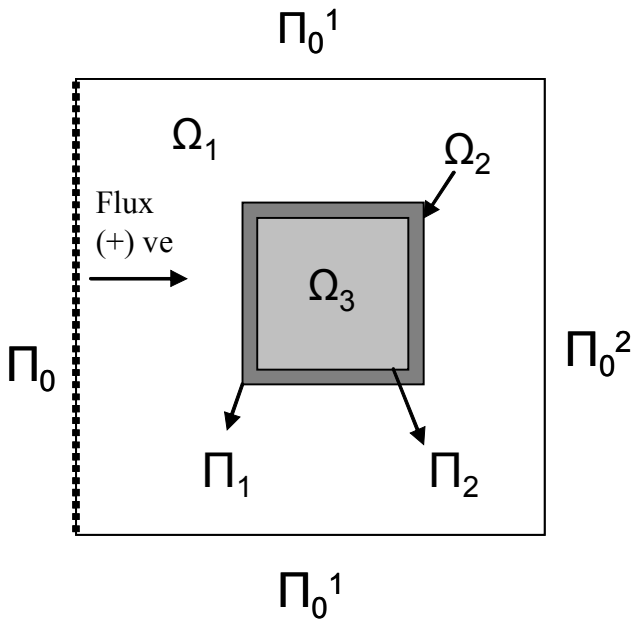

Figure 3.2 Schematic representation of the model for the adsorption/ desorption of oxygen at internal interfaces after diffusion through the matrix from an external surface

I. In region Ω_1 the oxygen concentration C_0^1 is given by:

$$\frac{\partial C_0^1}{\partial t} = D^{0,1}\nabla^2 C_0^1 \tag{3.9}$$

where $D^{0,1}$ is the diffusion coefficient of oxygen in the Ag matrix and ∇^2 is the Laplacian operator.

II. In region Ω_2, the oxygen concentration is assumed equivalent to the coverage. In a real situation, it is the 2D analogue of the 3D concentration C^2_0. We assume our model to display the 1D analogue of 2D concentration C^2_0.

$$\frac{\partial C^2{}_0}{\partial t} = div(D^{0,2}\nabla C^2{}_0) \tag{3.10}$$

In principle, $D^{0,2}$ can take a different value along and perpendicular to Π_1 (Π_2). It can take any (constant) value when oxygen moves along the interface. This has been put equal to zero in the current calculation thus enabling oxygen to adsorb and desorb at the interface but not to move along the interface itself. In the perpendicular direction the quantity is redundant because (by definition) we only have one numerical point across the region.

III. In region Ω_3, since there is no oxygen concentration due to the impenetrable inclusions, we have that $C_0^3 = 0$.

For the boundary conditions at the boundary Π_0, the constant concentration for the source is defined by:

$$C_{0|\Pi_0} = const \tag{3.11}$$

at all times $t \geq t_0$, where t_0 is the initial time.

For the inner boundaries we have the following conditions for the concentrations and fluxes. At the Π_1 boundary:

$$C^1{}_{0|\Pi_1} \neq C^2{}_{0|\Pi_1} \tag{3.12}$$

At steady-state or during longer diffusion times where the interfaces are closer to the surface (source) this will be $sC^1{}_{0|\Pi_1} = C^2{}_{0|\Pi_1}$, where s is the segregation factor and is known before the calculation according to the Henry Law segregation isotherm [21]. In principle, s can be made dependent on $C^2{}_0(C^1{}_0)$ but this factor was modelled here as a constant. This condition can be used as a definition for the segregation factor. The McLean segregation isotherm [21] would be the more appropriate one to describe the segregation factor. However, in the present calculations we have restricted ourselves to the Henry Law conditions.

Then the flux is determined by:

$J^2{}_{0|\Pi_1} = D^{0,1} \frac{\partial C^1{}_0}{\partial \vec{n}_{\Gamma_1}}$, and at steady state:

$$\frac{\partial C^2{}_0}{\partial t} = C^1{}_0 \Gamma_{12} - C^2{}_0 \Gamma_{21} = 0 \tag{3.13}$$

where Γ_{12} , Γ_{21} are the local lattice site to lattice site transition rates which are related to the equilibrium segregation factor s simply as:

$$s = \Gamma_{12} / \Gamma_{21} \tag{3.14}$$

At Π_2 we have that:

$$C^2{}_{0|\Pi_1} = C^2{}_{0|\Pi_2} \tag{3.15}$$

and $$J^2{}_{0|\Pi_2} = 0 \tag{3.16}$$

For the initial conditions $C_0 = 0$ everywhere.

3.2.2.2 Single Lattice (SL) Method

For the purpose of calculation Figure 3.2 is mapped onto a square planar lattice of 400×50 dimensions to model a semi-infinite material. We let eight inclusions of size 9×9 to be contained in the structure whilst maintaining the area fraction of approximately 3%. There is also an interface segregation layer of about 2% area fraction, the size of a mesh point width covering the inclusions. Similar to the simulation for oxygen diffusion in the Ag matrix, the source was located at the 201st plane and equipped with 10^5 particles randomly on the source plane. Once the particles were released they were permitted to explore the structure according to the hopping model. The jump rate depends on the location as reflected by an inter-site transition rate Γ. This means that there are different values for jump rates defined for the metal matrix, interface layer and inclusions. During jumps, multiple occupancy of a site is permitted and thus the diffusion process is considered as having no correlation effects. The diffusion time consisted of 10^5 – 10^{11} jump attempts. We consider three regions to describe the diffusion coefficient.

The diffusion coefficient $D^{0,1}$ of oxygen in the matrix Ω_1 has the same meaning of Equation 3.9 and is given by:

$$D^{0,1} = \Gamma_{11} a^2 / 4 \tag{3.17}$$

We can associate an oxygen diffusion coefficient $D^{0,12}$ locally with the interface by:

$$D^{0,12} = \Gamma_{12} a^2 / 4 \tag{3.18}$$

Similarly the reverse diffusion coefficient $D^{0,21}$ is defined by:

$$D^{0,21} = \Gamma_{21} a^2 / 4 \tag{3.19}$$

where Γ_{12} is the inter-site transition rate from the matrix region Ω_1 to the interface region Ω_2. This can be regarded as an adsorption process of oxygen by diffusion to the interface from the matrix. Γ_{21} is the inter-site transition rate from the interface region Ω_2 to the matrix region Ω_1. This can be regarded as a desorption process of oxygen by diffusion from the interface back into the matrix. As mentioned above, diffusion along the interface in this problem can be suppressed for convenience. Diffusion within the inclusion itself was not permitted. We modelled the highest transition rate as Γ_1, and the rest were scaled accordingly. For example, we set Γ_1 as unity and Γ_{12} also as unity and Γ_{21} at 0.001, whilst keeping the segregation factor equal to 1000. The basic mesh size a in Equations 3.17 and 3.18 was calculated in same way as with single phase material and was 2.5×10^{-7} m. Also the basic time unit in the problem was 0.744×10^{-3} m.

Let us consider the problem of width of the segregation layer. In this preliminary simulation, the interface region was treated as rows of lattice sites within the basic lattice. It is clear from Equations 3.18 and 3.19 that the width of the segregation or interface layer would first appear to be simply the basic lattice spacing $a = 2.5\times10^{-7}$ m. This width is seen to be physically rather too large for an interface layer. A more reasonable value might be in the vicinity of 10^{-8} m or even less. We can achieve this because we have flexibility with the value of the width of this layer simply through a rescaling of Γ_{12} and Γ_{21} that defines the segregation factor s as in Equation 3.14. Thus if we, say multiply both Γ_{12} and Γ_{21} by a factor of 6.25×10^2 then the segregation layer is seen to have a new apparent width of 10^{-8} m.

3.2.2.3 Virtual Plane (VP) Strategy

As an alternative way to address the problem of the width of the segregation layer, one may consider the interface sites as special virtual sites that do not appear formally in the Monte Carlo lattice itself but can be reached only via the lattice sites immediately around the inclusions. In that situation, Equation 29 and 30 then becomes irrelevant and the rates Γ_{12} and Γ_{21} then need to be specified to gain access to and from these special sites. In this way, the width of the segregation layer does not need to be specified. To simulate this phenomenon, we take two identical 2D lattices of size 400×50 described in the SL method above and place them exactly

on top of each other (see Figure 3.3). The VP lattice is placed just above the IP lattice so that all of the sites of the bottom plane and virtual plane coincide. Now the actual segregation layer shifts to the virtual plane and the regions. Although there are two identical lattices, the source was only designed for the IP (refer Figure 3.3). The only possible regions where particles could be located are in the Ag matrix region and the interface region. We consider regions Ω_1 and Ω_2 belonging to the Ag matrix; Ω_4 serves as the segregation layer and Ω_3 as the inclusion in a 50×50 unit size. In this simulation, a particle is allocated a coordination number of 5 everywhere, but depending on the location certain restrictions are given. As an example, a particle in region Ω_1 has one direction blocked and the related transition rate (Γ_{11}) is scaled to unity. A particle in region Ω_2 is free to move in all 5 directions, whereas in region Ω_4 only one direction is possible. The jump transition rates associated with it are jumps from Ω_2 to Ω_1 (Γ_{21}) and vice versa (Γ_{12}), jumps along Ω_2 (Γ_{22}) and jumps into to the segregation layer (Γ_{23}).

A particle in the segregation layer has a coordination of two: a jump directly from region Ω_2 to Ω_4 (Γ_{23}) and vice versa (Γ_{32}). For the sake of the present simulation it is assumed that there is no movement of particles along the segregation layer. This means oxygen can adsorb or desorb but not travel around the interface and settle down at low concentration regions. The simulation was carried out by leaving Γ_{11}, Γ_{12}, Γ_{21}, Γ_{22} and Γ_{23} as equal to unity and Γ_{32} equal to 0.1×10^{-2} by keeping the segregation factor to be 10^3 as follows. As already described, the oxygen source is regarded as a constant source. The particle which leaves the source explores the IP according to a random hopping model. Typically it takes about 10^8 - 10^{11} jump attempts to realize the specified diffusion anneal time. At each jump attempt a particle is selected randomly within the system. Therefore before allowing a particle to move it is checked that there is a particle in that site, if not, another real site is selected. Then the jump attempt counter is increased by one and provides a random direction (out of 5) for the particle to move. These five directions are classified according to transition rates. This means for a jump in + x, - x , + y and - y direction jump frequencies Γ_{11}, Γ_{12}, Γ_{21} and Γ_{22} are specified, whereas for + z, - z jumps the frequencies Γ_{23} and Γ_{32} are specified. The concentration in the source plane is only affected by +x and –x jumps. Therefore, once a particle is removed from the plane another particle is added to a random location along the plane to keep the concentration constant. Conversely, when a particle arrives at the source plane then that particle is regarded as a 'ghost particle' and the total concentration is reduced by one. The total number of real particles in the system is adjusted at each time. If the jump is beyond the source plane then the validity of that jump is checked by the probability of that jump being lesser or equal to the relevant jump frequency. Similarly + y and – y jumps are validated. For a +z jump to occur it is important that the particle should be located in the Ω_2 plane and Ω_4 plane for a -z jump. Now the particle identification arrays are

filled with unwanted 'ghost particles' as well. There needs to be a method to periodically remove the unwanted locations (or 'ghost particles') from the system. This is achieved by rearranging the arrays at regular time intervals (every 10000 attempts). After this it was checked whether the jump attempt counter reached the maximum jump attempts allocated for the program. If it is not, this procedure was repeated until the diffusion time was reached. Once the diffusion part of the calculation was over, the concentration profiles were adjusted.

We also simulated the scenario that allows mobility of particles along the segregation layer itself. This means the possibility of a jump in directions + x, - x, + y and - y in the Ω_4 region. The relevant jump frequency (Γ_{33}) was scaled to unity.

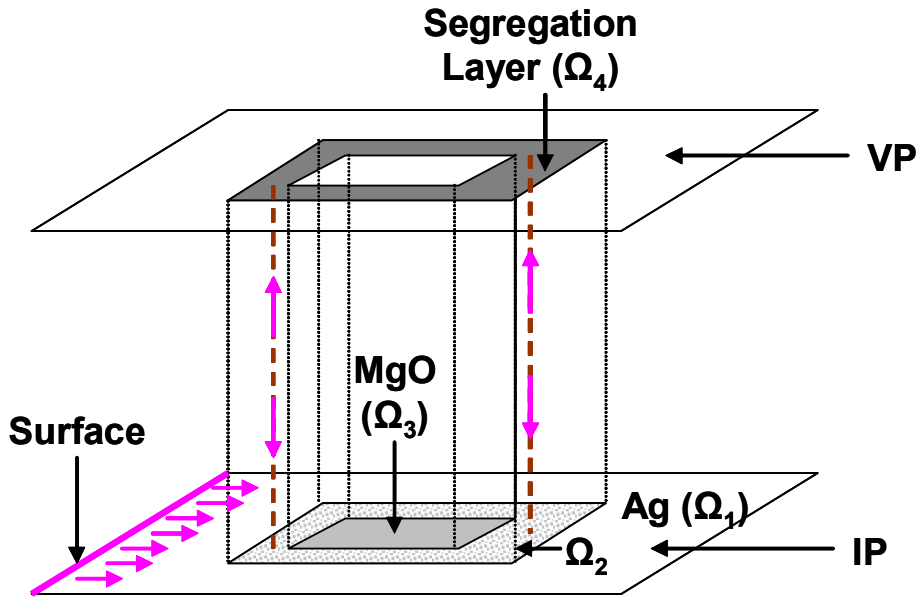

Figure 3.3 Schematic representation of a lattice model to display the Virtual Lattice Plane

3.2.3 Oxygen in-diffusion in a composite containing randomly placed multiple inclusions

Randomly placed multiple inclusions can be modelled by either a SL or a lattice with a VP. Due to the ease of presentation we were interested in the VP presentation. Instead of a square inclusion in Figure 3.3, let us assume a point inclusion without an interface layer. Such a point inclusion contains the interface and inclusion collapsed into one point. The (indirect) implication in such a model is that the mobility around the inclusion is very fast compared with

other processes. We located such inclusions randomly in a 400×50 matrix. The conditions were: the size of an inclusion must always be one lattice point but they were generated in such a way that there are no nearest neighbour inclusions. From a macroscopic point of view this means that there will not be a cluster of inclusions. We took special care to leave no inclusions on the source plane. Also, we maintained a depletion region of two parallel lattice planes next to the source plane. Whilst achieving those conditions we embedded 500 inclusions in each 50×50 repeating units (inclusion fraction of 20%). We mirrored the IP into the VP whilst leaving the sites behind the real inclusions to be part of the Ag matrix but this serves the purpose of entering points to the inclusions. The inclusions themselves serve as sites for segregation but no movement of particles within them can be considered as no inclusions are adjacent. Similar to the square inclusion simulation jump frequencies the following frequencies are considered: Γ_{11} is the jump frequency from matrix site to another matrix site in the IP plane, Γ_{12} is the jump frequency from matrix site to an entry point to the inclusions and Γ_{21} is vice versa, Γ_{23} is the jump frequency from an entry site to inclusions into inclusions in the interface layer and Γ_{32} is vice versa. In the simulation the frequencies Γ_{11}, Γ_{12}, Γ_{21} and Γ_{23} are scaled to unity and Γ_{32} is scaled to 0.001 (a segregation factor of 10^3). The source plane is placed at the 201st plane in the 400×50 lattice and is regarded as a constant source. Depending on the size of lattice and periodic boundary conditions we simulated both semi-infinite and thin-film materials.

3.2.4 Oxygen out-diffusion in a single phase material

To model the out-diffusion process of a semi-infinite medium, we considered a much smaller lattice of size 45×11 and filled the entire lattice with particles randomly leaving a maximum number of particles per site as 1000. This number is regarded as the 'occupancy per site' and affects the statistical nature of the averaged concentration profiles. In other words, a more uniform concentration profile can be obtained via high occupancy levels. We modelled a (surface) sink at the 23rd plane capable of 'attracting' particles towards it and assumed that the sink was always at a zero concentration. In order to obtain 1000 particles per site, except on the sink plane, a total of 484,000 particles must be accommodated in the matrix. Therefore, a much smaller lattice was selected for out-diffusion calculations. The initial concentration inside the material was made according to the following.

The matrix is filled in such a way that a lattice site is selected randomly and then it is checked if occupancy has reached the maximum value (e.g. 1000). If not, a particle will be added to the same location and the coordinates are recorded in corresponding arrays with respect to the

unique particle identification number. If the occupancy is exceeded at that site, a new site will be chosen randomly and this process is repeated until the total numbers of available sites are filled. It is assumed that particles do not 'see' each other, i.e. multiple occupancy of a given site is allowed. As before, this conveniently avoids diffusion correlation effects. Once the matrix is completely filled with oxygen, the out-diffusion process is permitted to commence. After the diffusion process ceases, either satisfying all the jump attempts (i.e. the specified time the diffusion process is running for) or the system is completely empty of oxygen. This phenomenon was modelled as follows. An arbitrary lattice site was chosen randomly to check if a particle exists at that location. If it is an empty site then the total system is scanned to see if any real particles remain to carry on the diffusion process. If there are particles found in the rest of the Ag matrix, then control is transferred to the selected location of another randomly chosen particle. If the matrix is completely empty before the total number of jump attempts is achieved, control will be taken to the end of the program without calculating concentration profiles. In that situation the real time taken to empty the lattice will be displayed in units. If the previously selected particle exists then it is permitted to jump in a random jump direction chosen from 4 (+x, -x, +y and -y). This jump is also validated according to the inter-site transition rate in the matrix. The inter-site transition rate Γ_{11} is scaled to unity. The system is modelled in a way that periodic boundary conditions are specified in the y direction for a semi-infinite material. The diffusion process is continued until either the composite become completely emptied of particles or the specified number of jump attempts ($10^{3\cdots}10^{11}$) is satisfied. Once the specified number of jump attempts is satisfied the concentration profiles for the out-diffusion process were calculated.

3.2.5 Oxygen out-diffusion in a composite with square inclusions

We modelled the composite according to the VP method with the same lattice size of 45×11. Square impenetrable inclusions of size 3×3 were incorporated at the centre of a square unit cell of size 11×11 each. Moreover, an interface layer was also designed covering inclusions of a width of one lattice point. Therefore inclusions take about 7% and the segregation layer takes about 13% of the area fraction from the entire lattice. We let the maximum occupancy for a matrix site to be 10 and the segregation coefficient to be 100. With respect to initial values, inter-site transition jump rates were scaled. To fill the whole model except on the sink plane and on inclusions, 68,840 particles were required. Initial filling of the lattice was carried out in a way similar to that described in the previous section 'without inclusions'. However, a problem arises when filling in the interface layer as how a particle should be filled in the interface layer at the VP and the corresponding sites in the matrix immediately below the segregation layer.

This was resolved as follows. In that situation, a random variable was generated which can take only one of two values: 1 or 2. If the value of the variable equals one then it corresponds to the matrix and if the value is 2 then the corresponding location would be in the VP. It is important that the maximum number of particles that can be accommodated at a site in the segregation layer is 1000. It is a product of maximum occupancy of a site in the matrix just below the interface layer and the segregation factor.

Similar to the in-diffusion process (Section 3.2.2.3), the out-diffusion process also has the same meanings and values for inter-site jump frequencies except Γ_{32}. Here, Γ_{32} was set at 0.01 to be compatible with the segregation factor. We simulated two situations, one by restricting mobility at the interface ($\Gamma_{33} = 0$) and the other by permitting rapid mobility at the interface ($\Gamma_{33} = 1.0$).

3.2.6 Oxygen out-diffusion in a composite containing randomly placed multiple inclusions

Randomly placed multiple inclusions can be modelled in a similar way as in section 2.2.3 (in-diffusion process). We modelled inclusions in the VP for ease of calculation: however it can also be achieved in a single lattice simulation as well. We modelled a 51×25 lattice with a fraction of 3.03 % inclusions to model a semi-infinite material. Similar conditions described as in the in-diffusion process were employed whilst generating inclusions. A segregation factor of 100 was employed. The 26^{th} plane was considered as the surface. 10^4 observations were considered in order to average the different configurations of inclusions in the structure to achieve an average concentration profile.

3.3 Results and Discussion

3.3.1 Oxygen in-Diffusion Process

3.3.1.1 Diffusion in a single phase material

Here, we describe the results for the oxidation process in the Ag metal matrix. Two material geometries were considered depending on the length of the specimen: namely semi-infinite and thin-film materials. As with the oxygen diffusion process, it would be interesting to ascertain some knowledge about the oxygen diffusion coefficients associated with both materials. We used the concentration profile method (Refer Chapter 2) in calculating the effective diffusivity in both systems. This method is equivalent to solving Fick's second law:

$$\frac{\partial C}{\partial t} = D\frac{\partial^2 C}{\partial x^2} \tag{3.20}$$

where D is the diffusion coefficient, C is the concentration and x is the diffusion distance. The analytical solution for Equation 3.20 will not be the same for both materials. At first, let us consider the solution for semi-infinite material. The concentration profile C (x, t) for semi-infinite geometry is given by solving Equation 3.20 [41]:

$$\frac{C - C_1}{C_0 - C_1} = erf\left[\frac{x}{2\sqrt{(Dt)}}\right] \tag{3.21}$$

where *erf*, the error function, is given by:

$$erf\ z = \frac{2}{\sqrt{\pi}}\int_0^z e^{-t^2}\,dt \tag{3.22}$$

where C_0 is the initial distribution given by: $C = C_0$, $0 < x < h$, $C = 0$, $x > h$ and C_1 is the constant concentration maintained at the surface. According to the boundary condition in the previously described simulation $C_0 = 0$ because initially the Ag matrix is completely empty of oxygen before the simulation is started. Therefore, Equation 3.21 reduces to:

$$C = C_1\left(1 - erf\left[\frac{x}{2\sqrt{(Dt)}}\right]\right)$$

$$\text{i.e. } C = C_1\left(erfc\left[\frac{x}{2\sqrt{(Dt)}}\right]\right) \tag{3.23}$$

The concentration profiles should take the form of a complementary error function. According to the concentration profile method, analytical and computational data must be plotted in the same concentration vs. distance graph and compared. For graphing, we considered a 400×50 lattice with a constant source condition on plane 201. In Equation 3.23, x and t are the variables and D is the unknown. t, which is the diffusion time can be calculated in units. If Equation 3.23 is plotted for different time scales according to Table 3.1 below, it can be observed that there is a relationship between the comparable Monte Carlo data. Most importantly, these graphs coincide when the value of D equals 0.25 (see Equation 2.11 in Chapter 2), which comes from the Einstein equation method.

Figure 3.4 represents typical concentration profiles at a comparison of computed results and LMC results for 10^5 – 10^{10} jump attempts in a semi-infinite material. Table 3.1 is related to Figure 3.4.

	Diffusion Time	
Jump attempts	Real Time (Units)	Real Time (s)
10^5	5.1395	0.0038
10^6	25.6326	0.0191
10^7	121.7493	0.0906
10^8	615.1260	0.4576
10^9	2866.2757	2.1325
10^{10}	9310.7425	6.9272

Table 3.1 Typical mappings between diffusion times used in the LMC method for semi-infinite material.

Diffusion Time		
Jump attempts	Real Time (Units)	Real Time (s)
10^5	5.1395	0.0038
10^6	25.6326	0.0191
10^7	121.7493	0.0906
10^8	615.4172	0.4579
10^9	3057.5922	2.2748
10^{10}	22244.0401	16.5496

Table 3.2 Typical mappings between diffusion times used in the LMC method for a thin-film material.

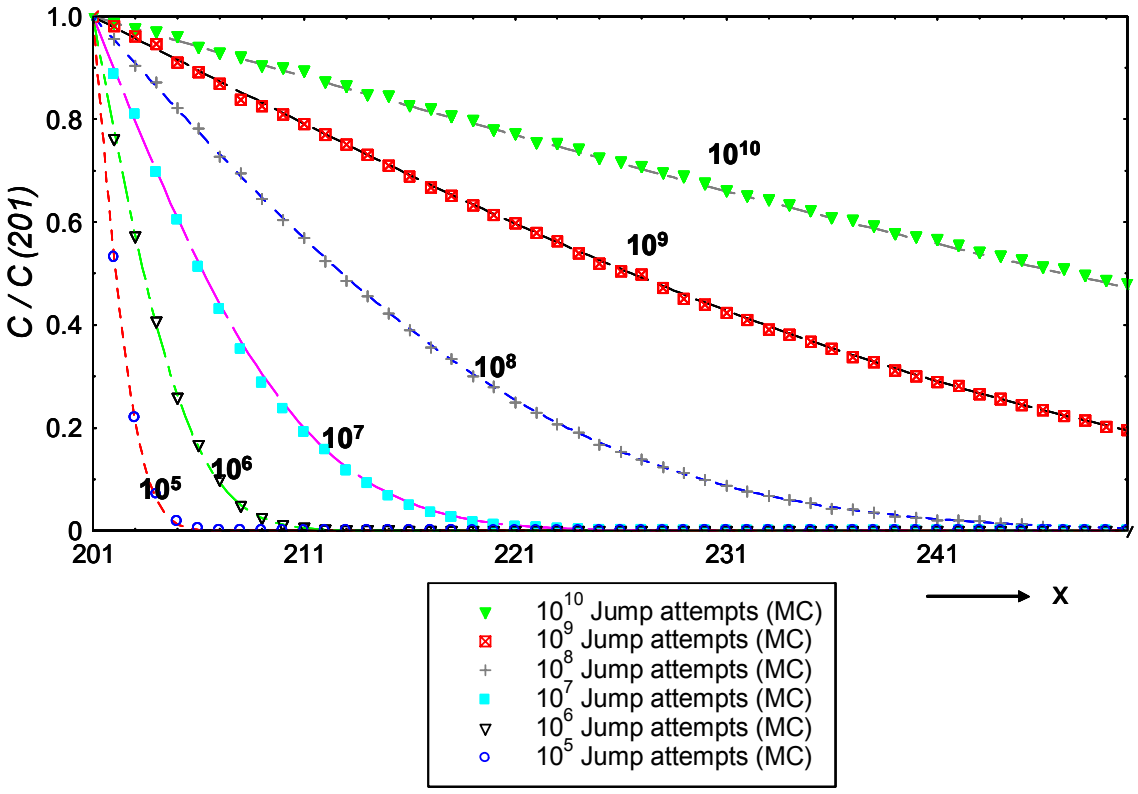

Figure 3.4 Typical concentration profiles averaged in the y-direction (y = 1-50, x-direction is shown as lattice plane number), calculated by the LMC method for diffusion times ranging from 10^5 jump attempts to 10^{10} jump attempts. Markers refer to the LMC solution and dashed lines refer to the complementary error function solution for a semi-infinite material according to Equation 3.23. Diffusion times are related with Table 3.1.

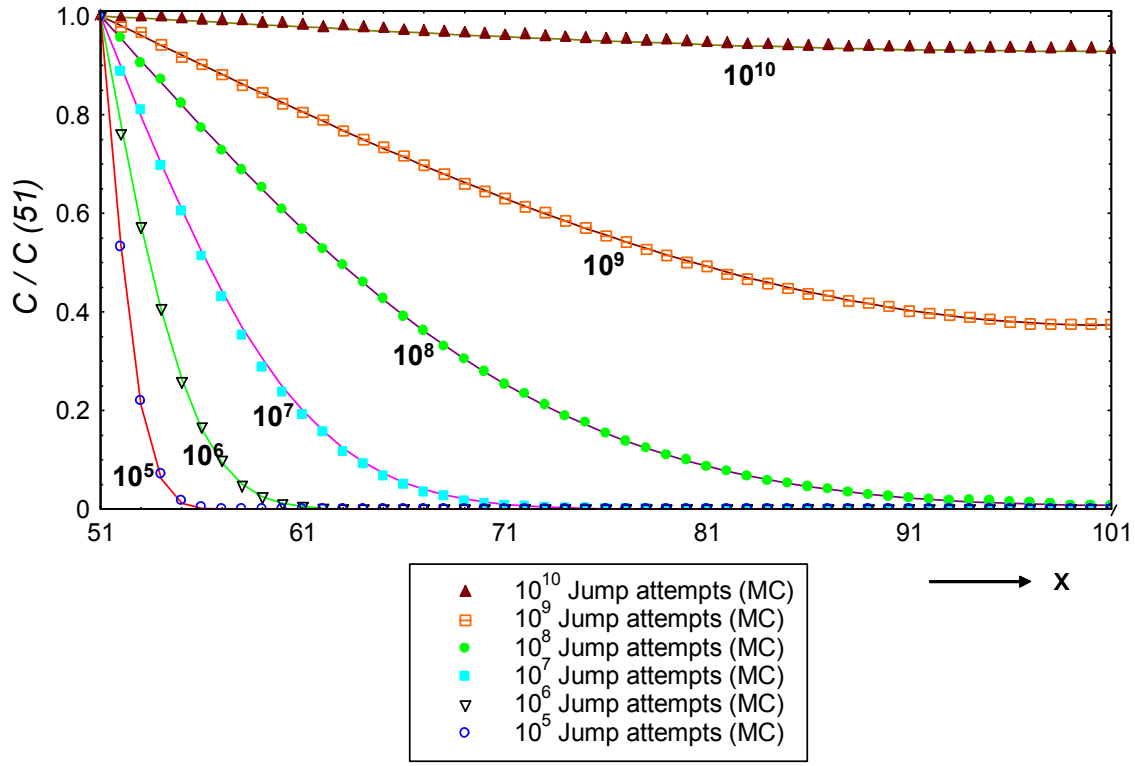

Figure 3.5 Typical concentration profiles averaged in the y-direction (y = 1-50, x-direction is shown as lattice plane number), calculated by the LMC method for diffusion times ranging from 10^5 jump attempts to 10^{10} jump attempts. Markers refer for LMC solution and the dashed line refer for computed results according to Equation 3.28. Diffusion times are related with Table 3.2.

Figure 3.5 shows a typical concentration profile according to the LMC method for different time scales shown in Table 3.2 for a thin-film material. For ease of presentation, Figure 3.5 is considered for representation of only a half of the profile of the thin-film material. The other half takes the form of a mirror image of the profiles in Figure 3.5 showing both source planes in the lattice. This thin-film material was initially mapped to a lattice of size 101×50, placing the source at the 51st plane. Both profiles from left and right from the source are nearly identical and one side of the profile is considered for Figure 3.5. Comparing Table 3.1 and Table 3.2, a similarity is observed between the two tables at early diffusion annealing times (e.g. consider 10^5 – 10^8 jump attempts). This means that during early times, the concentration profiles in a thin film material are similar to those for the semi-infinite material. We compared LMC data with the solution for 1D diffusion in a medium bounded by two parallel planes under non steady-state conditions [40]. The standard solution is in a trigonometric series form for the boundary conditions given below:

$C = C_1, \quad x = 0, \quad t \geq 0$ (3.24)

$C = C_2, \quad x = l, \quad t \geq 0$ (3.25)

$C = f(x), \quad 0 < x < l, \quad t = 0$ (3.26)

$$C = C_1 + (C_2 - C_1)\frac{x}{l} + \frac{2}{\pi}\sum_{n=1}^{\infty} C_1 \frac{(\cos n\pi - 1)}{n} \sin\frac{n\pi x}{l} \exp\left(\frac{-Dn^2\pi^2 t}{l^2}\right) + \frac{2}{\pi}\sum_{1}^{\infty} \sin\frac{n\pi x}{\pi} \exp\left(\frac{-D\pi^2 n^2 t}{l^2}\right) \int_0^l f(x^1) \sin\frac{n\pi x^1}{l} dx^1 \quad (3.27)$$

In our situation, C_1 and C_2 are the same and were scaled to unity. $f(x)$ is zero as there is no initial concentration of oxygen involving at the beginning of the diffusion program. Therefore, Equation 3.27 reduces to Equation 3.28:

$$C = C_1\left[1 + \frac{2}{\pi}\sum_{i=1}^{n} \frac{(\cos i\pi - 1)}{i} \sin\frac{i\pi x}{l} \exp\left(\frac{-Di^2\pi^2 t}{l^2}\right)\right] \quad (3.28)$$

Here, the variables are D, t, n and x. We selected n at 100 because values above 100 give almost the same profiles as with n = 100. The quantity t represents the diffusion time in units and l is the total length of the sample. Similarly with Equation 3.23, D was replaced with 0.25. One half of the calculated data were selected for presentation in Figure 3.5. The calculated profiles are seen to be in excellent agreement with the LMC data. The results show an excellent agreement between the concentration profile method and the Einstein equation method for calculating the effective diffusivity.

3.3.1.2 Diffusion in two phase material with square shape inclusions

In this section, we discuss the oxygen in-diffusion process occurring in the Ag/MgO composite medium. Before moving to the real situation, let us consider a situation with impenetrable inclusions without segregation.

In Figure 3.6 (a) we show an example of an averaged concentration profile for the case where there is no segregation and the inclusions simply are impenetrable to oxygen. Figure 3.6 (b) gives the corresponding 2D concentration profile. The behaviour is as expected with a drop in the profile where the impenetrable inclusion impedes the flux of oxygen atoms. Figure 3.7 (a) is an example of an averaged concentration profile where a segregation factor s of 10^3 has been assumed and in Figure 3.7 (b) the corresponding 2D concentration profile is given. Both graphs were considered by restricting movement of particles along the interface in the SL method. In Figure 3.7 (b), it can be seen that the higher concentration near the source in the segregation layer and the concentration, gradually decrease with distance away from the source. Similarly, Figure 3.7 (c) shows an averaged profile for the same segregation factor and the corresponding 2D concentration profile in Figure 3.7 (d) for the mobility permitted situation along the interface. In Figure 3.7 (d) it is also observed that the higher concentration at the segregation layer near the source and gradual decrease of it with distance away from the surface.

The maxima in the concentration in the four figures correspond to oxygen that has segregated to the interface region. It is noted in Figure 3.7 (b) that the corners of the interface region have a much higher concentration than elsewhere on the interface. This would appear to result from the fact that in the lattice model the corner sites of the interface region have two neighbouring sites that can 'provide' oxygen to them whereas other sites have only one such provider site. However, when mobility is permitted at the interface a corner of an interface site is expected with the highest concentration compared to the other sites in the interface. But Figure 3.7 (d) shows that the higher concentration is still observable. However, due to the rapid movement of particles along the interface, such very high concentrations are not observable. In all four figures we have scaled the inter-site jump rate in the interface layer to be exactly the same as in the Ag matrix. Table 3.3 and Table 3.4 give corresponding diffusion time of simulations carried out at 10^5 – 10^{11} jump attempts. From the two tables it can be seen that there is little difference between real diffusion times taken to satisfy the required number of jump attempts.

It is likely that the maxima seen at the corners is an artefact of the lattice model being used here to model segregation and that a superior way to model segregation is to invoke the local virtual interface sites as in the VP method. In the implementation of this method we effectively added one more coordination direction to all sites to keep the time steps equally spaced. Therefore, Equation 3.27 should be used now with a factor of 5 not 4.

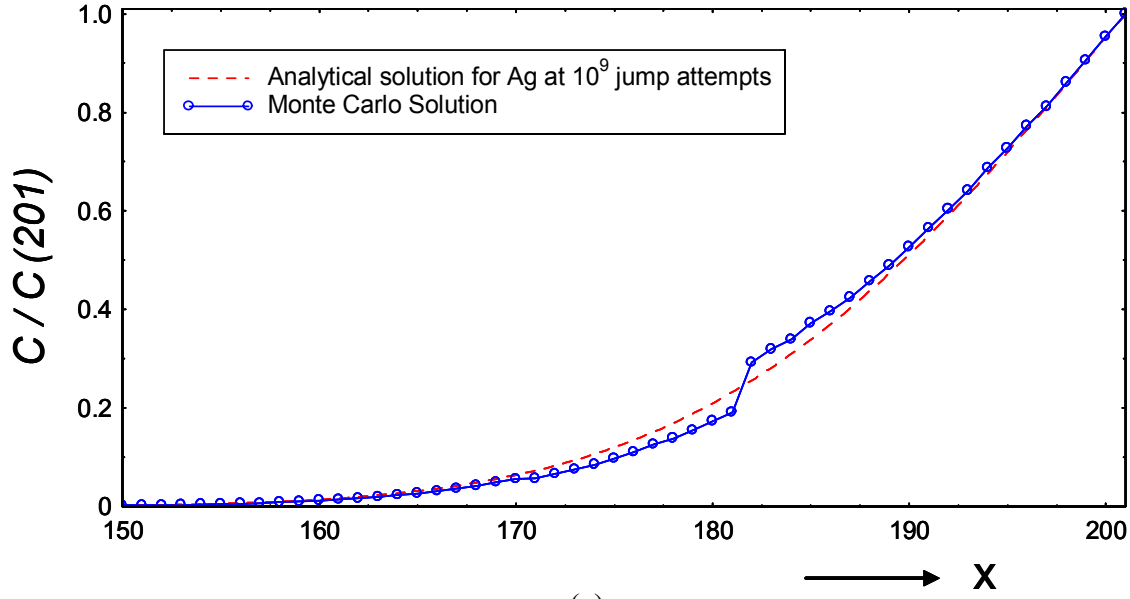

(a)

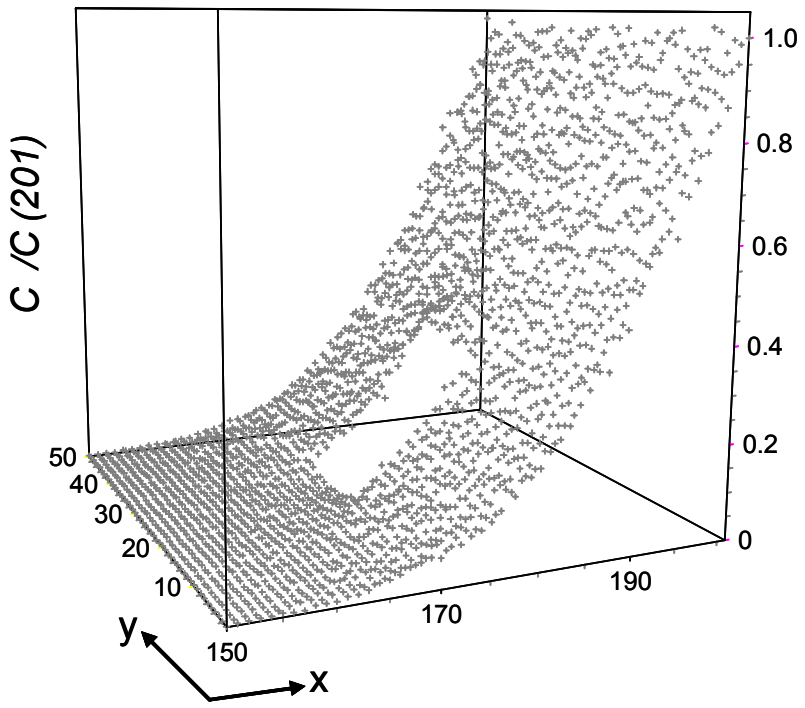

(b)

Figure 3.6 (a) A typical concentration profile calculated by the LMC method and averaged in the y-direction (y = 1-50, x-direction is shown as lattice plane number). No segregation effect (s = 1.0). Total number of jump attempts: 10^9, real time: 0.4166 s, diffusivity in the matrix: 2.1×10^{-11} m^2s^{-1}, inclusion fraction: 0.0324. (b) The 2D concentration profile for the same conditions.

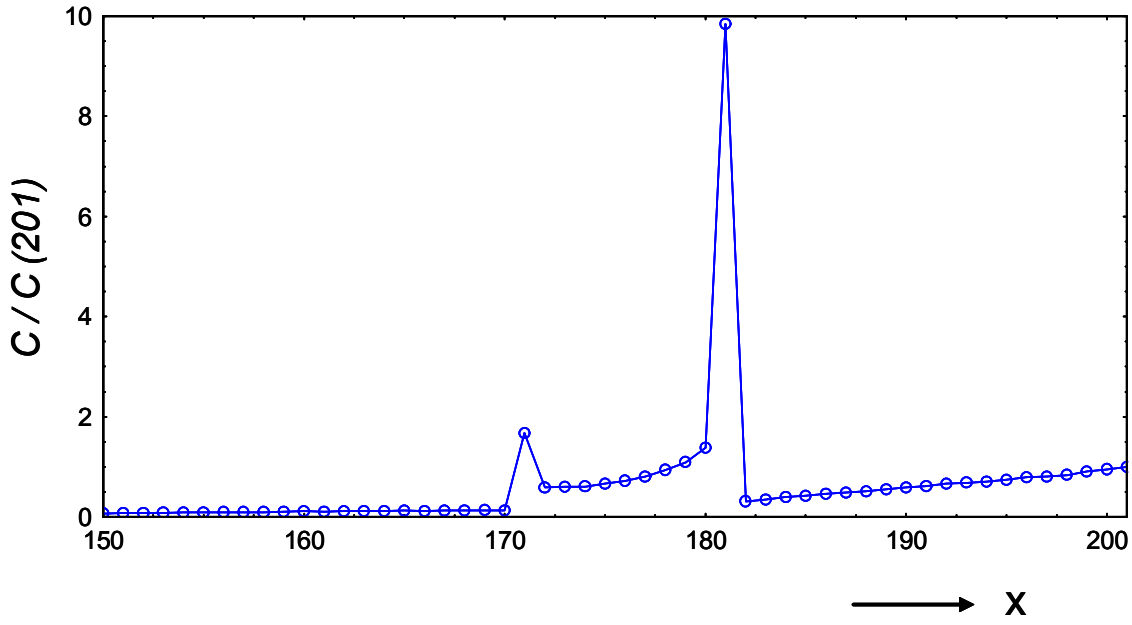
C / C (201)
0
2
4
6
8
10
150
160
170
180
190
200
X

(a)

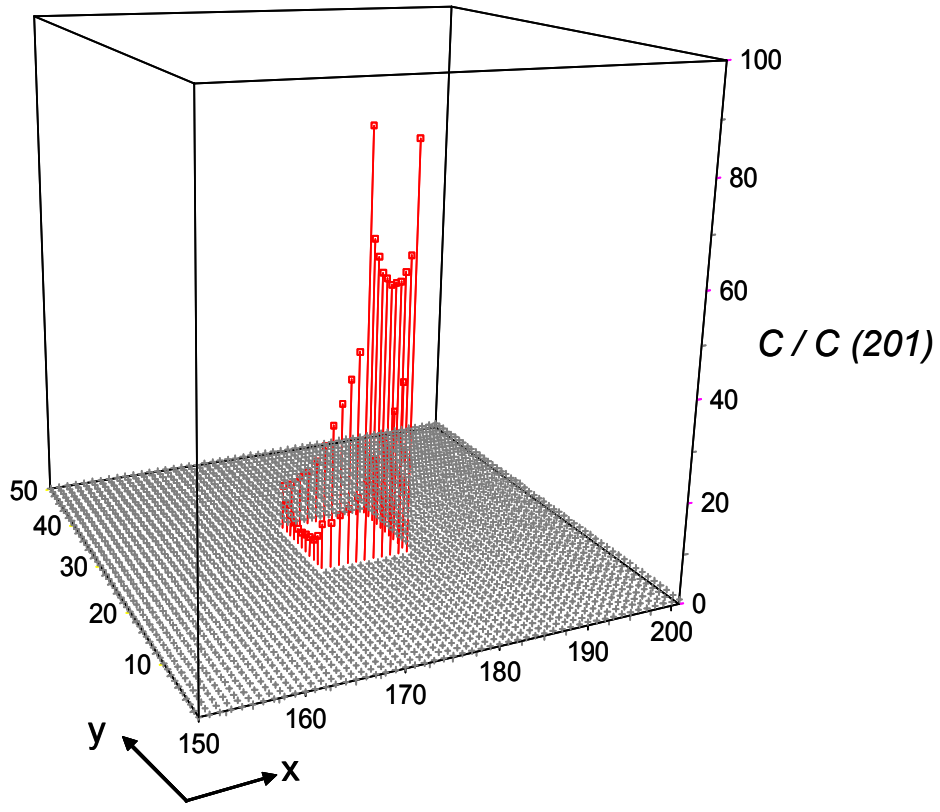
C / C (201)
0
20
40
60
80
100
50
40
30
20
10
y
150
160
170
180
190
200
x

(b)

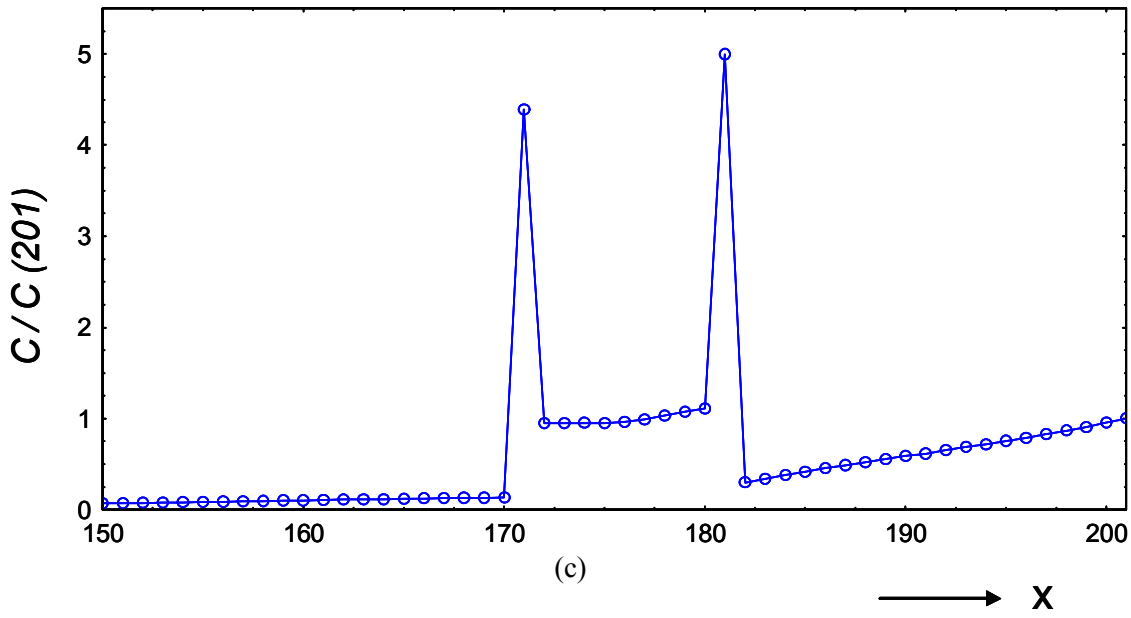

(c)

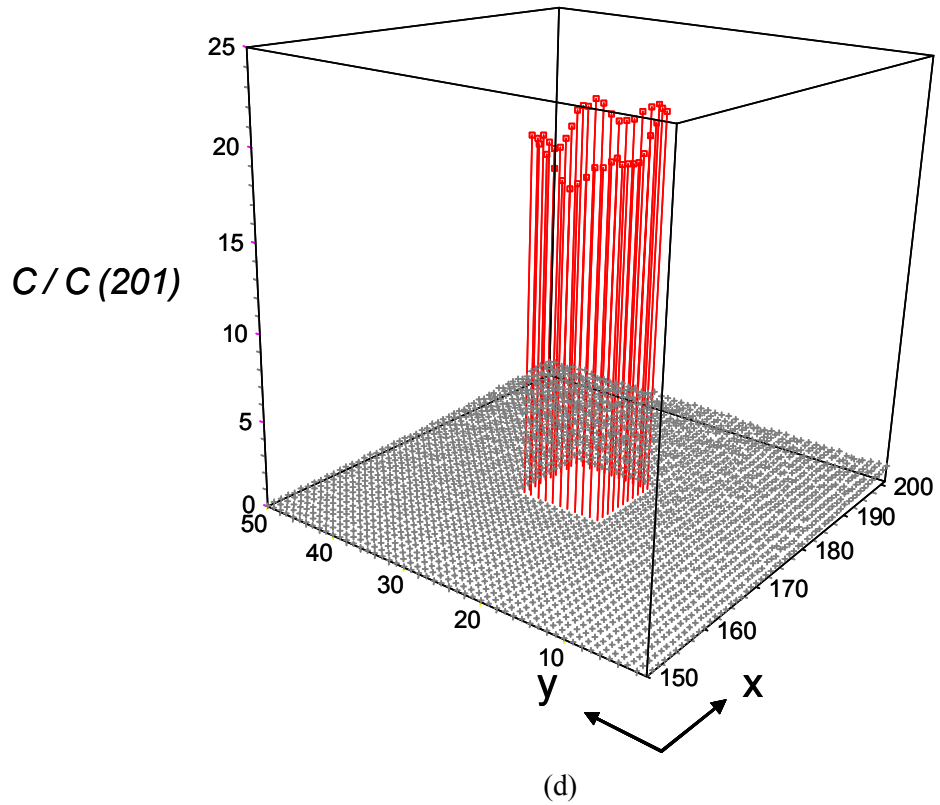

(d)

Figure 3.7 (a) A typical concentration profile calculated by the LMC method and averaged in y-direction (y = 1-50, x-direction is shown as lattice plane number) according to the SL strategy. Movement along the interface is restricted. Segregation factor s = 10^3, total number of jump attempts: 10^9, oxygen diffusivity in the matrix: 2.1×10^{-11} m^2s^{-1}, inclusion fraction: 0.0324. (b) The 2D concentration profile for (a). (c) The averaged concentration profile for the same conditions when the mobility along the interface layer is permitted. Inter-site transition jump rate is kept equal to unity. (d) The 2D concentration profile for (c).

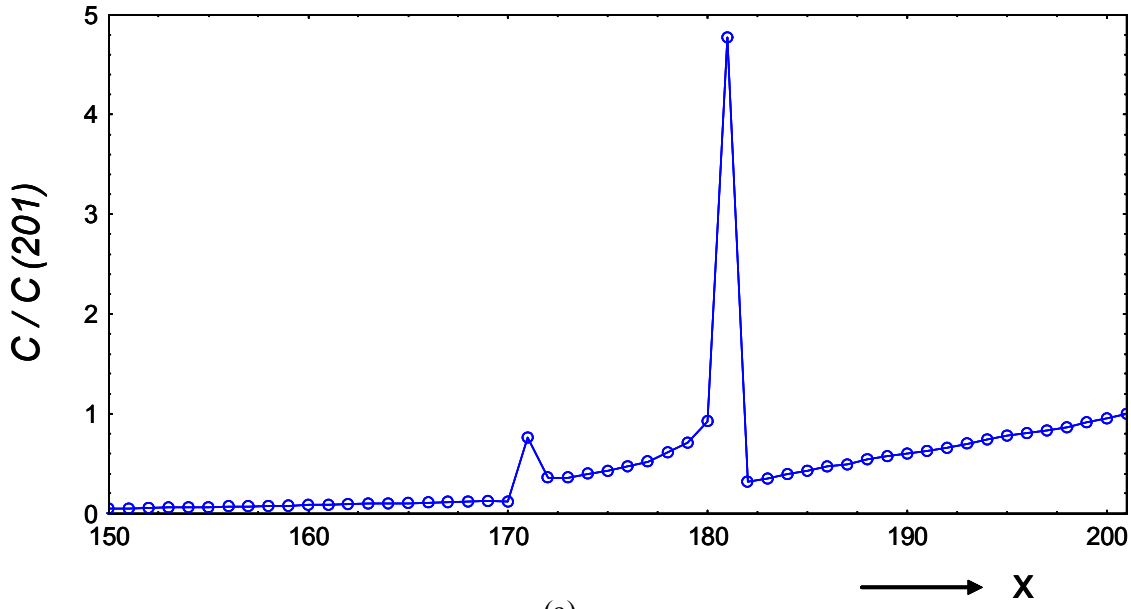
C / C (201)
0
1
2
3
4
5
150
160
170
180
190
200
x

(a)

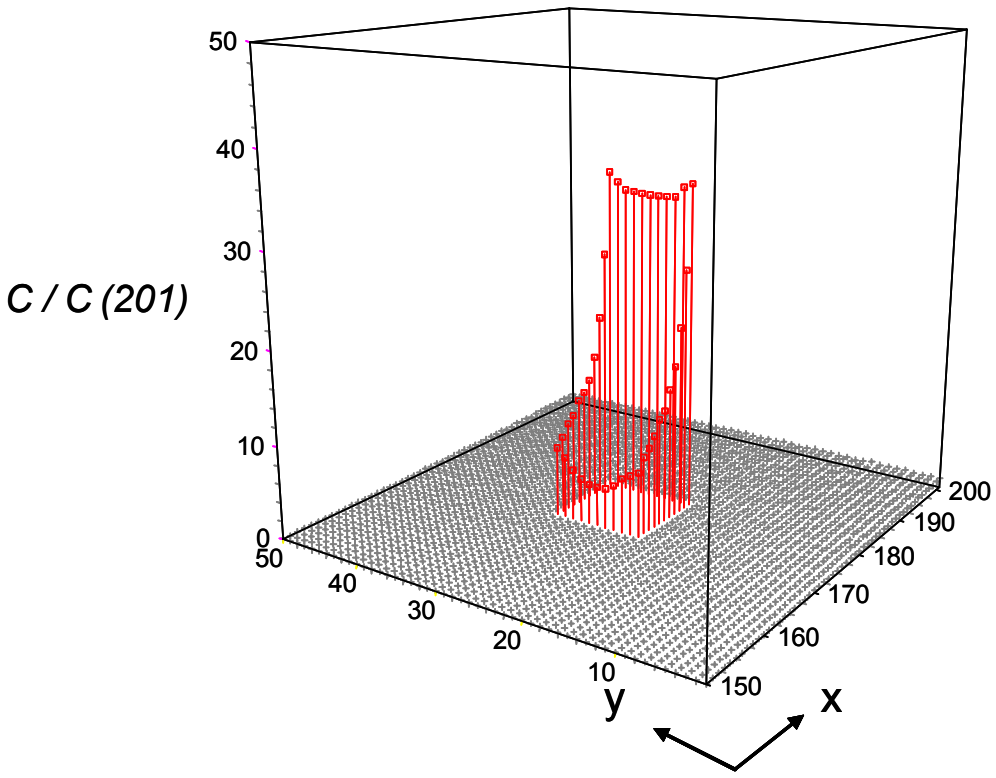
C / C (201)
0
10
20
30
40
50
50
40
30
20
10
y
150
160
170
180
190
200
x

(b)

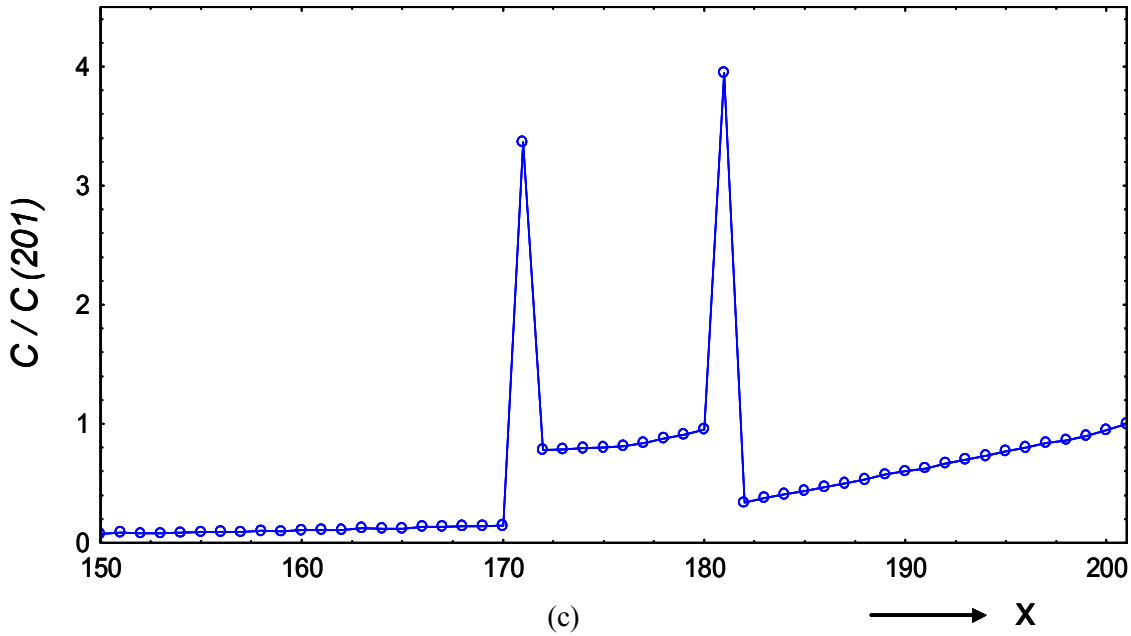

(c)

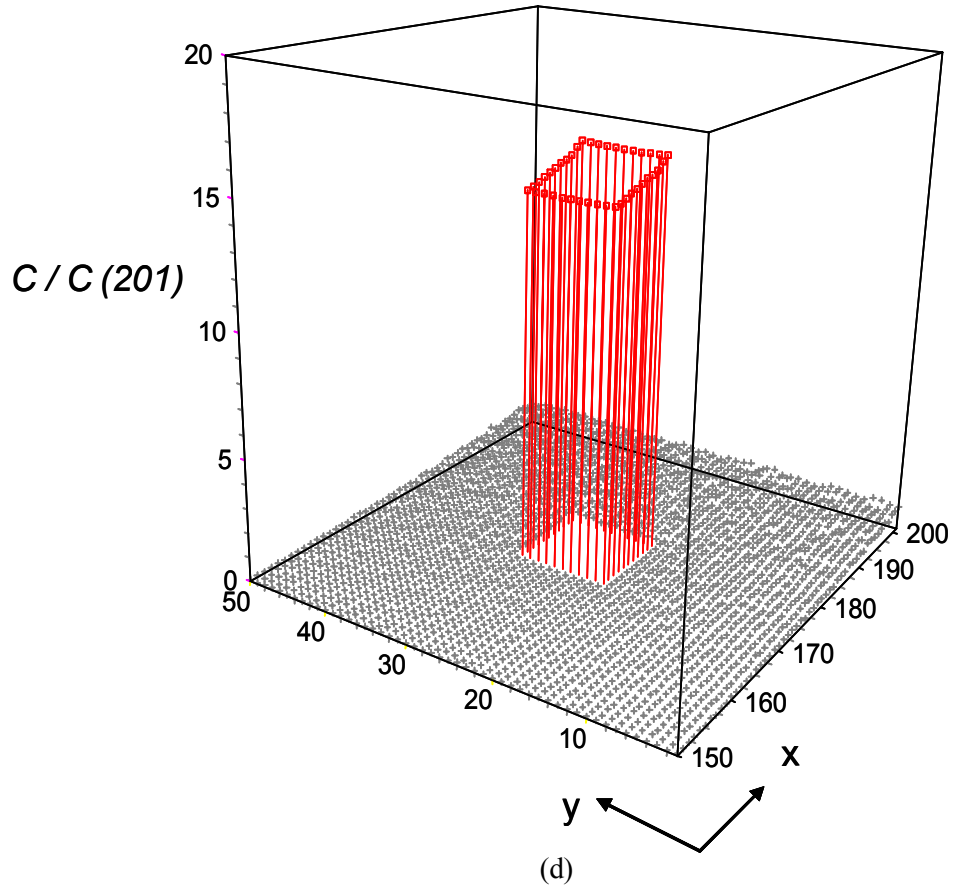

(d)

Figure 3.8 (a) A typical concentration profile calculated by the LMC method and averaged in y-direction (y = 1-50, x-direction is shown as lattice plane number) according to the VP strategy. Movement along the interface is restricted. Segregation factor s = 10^3, total number of jump attempts: 10^9, oxygen diffusivity in the matrix: 2.1×10^{-11} m^2s^{-1}, inclusion fraction: 0.0324. (b) The 2D concentration profile for (b). (c) The averaged concentration profile for the same

conditions when the mobility along the interface layer is permitted. Inter-site transition jump rate is kept equal to unity. (d) The 2D concentration profile for (c).

Figure 3.8 (a) and (b) represents concentration profiles for the restricted particle mobility at the interface and (c) and (d) represents for mobility permitted at the interface. All four figures of Figure 3.8 are modelled according to the VP strategy. As compared with the profiles described in Figure 3.7, similarities are observed in Figure 3.8. However, the total number of particles located in segregation layer of VP strategy seems lower compared to the SL strategy. Moreover, the corners of the segregation layer are observed with a much lower concentration thus removing the artefacts mentioned above. The reason for this phenomenon is as follows. In the SL strategy, the corner sites in the interface layer are prone to take more particles compared to the VP strategy where the corner sites in the interface layer can only gain particles from one site in the matrix. With this scenario, it is possible to explain the drop of concentration in the segregation layer in Figure 3.7 (d) and Figure 3.8 (d). In Figure 3.7 (d) it is observed that the concentration drop between the edge near the source and the farthest edge in the interface layer is having a considerably small drop compared to Figure 3.8 (d). This is due to the rapid movement of an extensive amount of particles located in the interface layer in the SL strategy.

Diffusion Time		
Jump attempts	Real Time (Units)	Real Time (s)
10^5	5.1358	0.0038
10^6	25.5518	0.0190
10^7	120.7536	0.0898
10^8	573.9542	0.4270
10^9	2349.5648	1.7481
10^{10}	5666.5899	4.2159
10^{11}	13275.8234	9.8772

Table 3.3 Typical mappings between diffusion times used in the square inclusion semi-infinite composite mapped with a 400×50 mesh by the SL strategy. Particle mobility along the interface layer is restricted.

Diffusion Time		
Jump attempts	Real Time (Units)	Real Time (s)
10^5	5.1328	0.0038
10^6	25.5518	0.0190
10^7	120.6675	0.0898
10^8	574.6724	0.4275
10^9	2383.0933	1.7730
10^{10}	5999.6779	4.4638
10^{11}	14486.0374	10.7776

Table 3.4 Typical mappings between diffusion times used in the square inclusion semi-infinite composite mapped with a 400×50 mesh by SL strategy. Mobility is permitted along the interface layer.

Diffusion Time		
Jump attempts	Real Time (Units)	Real Time (s)
10^5	5.4729	0.0041
10^6	27.0221	0.0201
10^7	121.8819	0.0907
10^8	524.5297	0.3902
10^9	1860.0709	1.3839
10^{10}	5163.5902	3.8417
10^{11}	13736.2942	10.2198

Table 3.5 Typical mappings between diffusion times used in the square inclusion semi-infinite composite mapped with a 400×50 mesh by the VP strategy. Mobility is restricted along the interface layer.

Diffusion Time		
Jump attempts	Real Time (Units)	Real Time (s)
10^5	5.4585	0.0041
10^6	27.0526	0.0201
10^7	122.1400	0.0909
10^8	524.6795	0.3904
10^9	1904.9428	1.4173
10^{10}	5491.7005	4.0858
10^{11}	14454.1583	10.7538

Table 3.6 Typical mappings between diffusion times used in the square inclusion semi-infinite composite mapped with a 400×50 mesh by VP Method. Mobility is permitted along the interface layer.

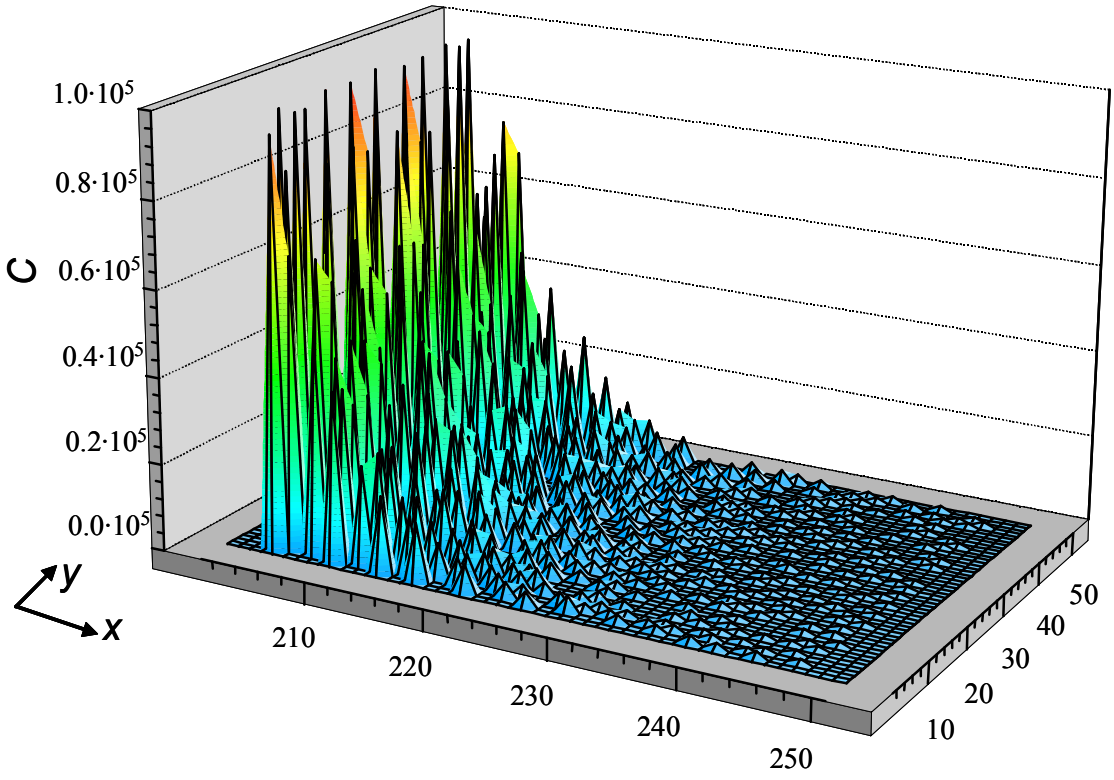

Figure 3.9 The 2D Oxygen concentration distribution profile for a system of randomly arranged multiple inclusion distribution, real time 14211.7952 time units equivalent to 10.5736 s, segregation factor s = 10^3, oxygen diffusivity in the matrix: 2.1×10^{-11} m^2s^{-1} .

We simulated the random inclusions model under the same conditions described in the VP strategy. Figure 3.9 represents the 2D oxygen concentration profile taken at 10^{11} jump attempts. It is possible to observe the gradual decrease of concentration in the interface layer with time.

3.3.2 Oxygen Out-Diffusion Process

Here, let us consider the out-diffusion process in a single phase material. The concentration profile C for a semi-infinite geometry for an out-diffusion process is given by Equation 3.29 as follows [41]:

$$\frac{[C(x,t)-C_0]}{[C_e-C_0]} = erfc(\frac{x}{2\sqrt{Dt}}) - \exp(hx+h^2Dt)erfc\left\{(\frac{x}{2\sqrt{Dt}}) + h\sqrt{Dt}\right\} \tag{3.29}$$

Putting h → ∞, we have that:

$$\frac{[C(x,t)-C_0]}{[C_e-C_0]} = erfc(\frac{x}{2\sqrt{Dt}}) \tag{3.30}$$

$$C(x,t) = erf(\frac{x}{2\sqrt{Dt}}) \tag{3.31}$$

where C_0 is the initial concentration in the semi-infinite medium. C_e is the equilibrium oxygen concentration in the atmosphere and we put this value equal to zero assuming no oxygen concentration at the sink plane. D is the diffusion coefficient of the semi-infinite medium and t is the real time (in units). *erfc* is the complementary error function where $erfc(z) = 1 - erf(z)$. We let $C_0 = 1.0$ and compared Equation 3.31 with the LMC solutions at different time scales. Figure 3.10 was obtained by such a comparison and related timing is displayed in Table 3.7. Results show an excellent agreement of Monte Carlo solution with the analytical solution.

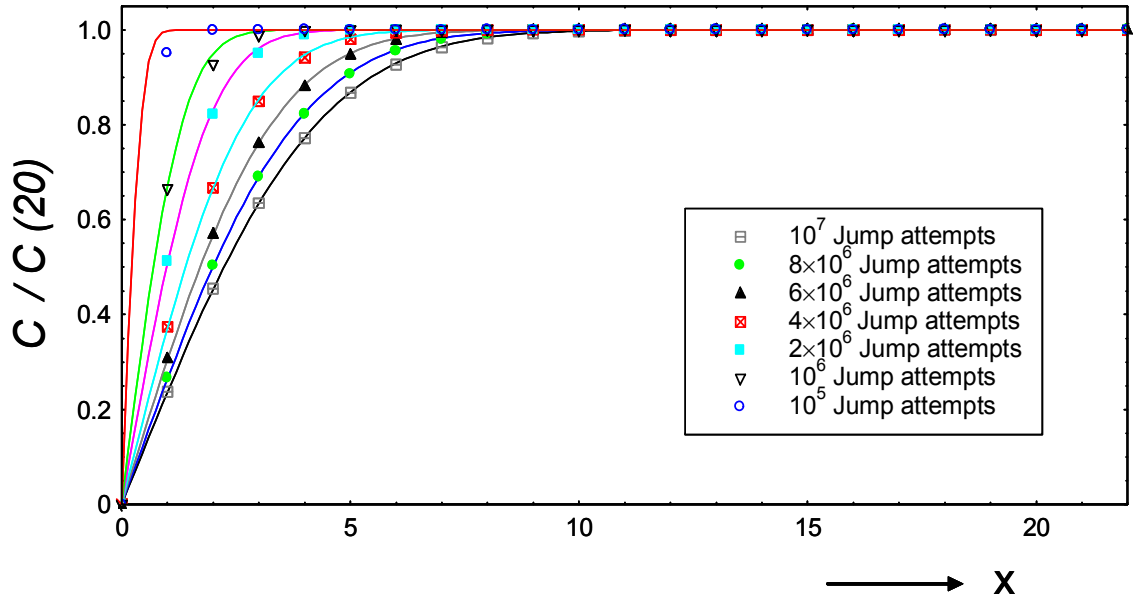

Figure 3.10 Time-dependent concentration profiles resembling the out-diffusion process in a semi-infinite Ag metal matrix. Profiles are averaged in the y-direction (y = 1-11, x-direction is shown as lattice plane number), calculated by the LMC method for diffusion times ranging from 10^5 jump attempts to 10^7 jump attempts. Markers refer to Monte Carlo simulation results and solid lines refer to the analytical solution according to Equation 3.31. Occupancy per site is 103. Size of the mesh 45×11. Total particles in the system 484,000. Diffusion times are related with Table 3.7.

Diffusion Time		
Jump attempts	Real Time (Units)	Real Time (s)
10^5	0.2068	0.0001
10^6	2.0876	0.0015
2×10^6	4.2094	0.0031
4×10^6	8.5323	0.0063
6×10^6	12.9414	0.0096
8×10^6	17.4256	0.0130
10^7	21.9786	0.0163

Table 3.7 Typical mappings between diffusion times for the out-diffusion process by the LMC method. Single phase semi-infinite material was mapped with a 45×11 mesh by the VP strategy.

Figure 3.11 displays concentrations profiles in a material with square impenetrable inclusions in a similar diffusion process at three different times (jump attempts 2×10^6, 4×10^6 and 10^7). The profiles are averaged over 10^5 observations. In an out-diffusion process two major phenomena can be observed. One is the dropping of the interface concentration and the other is the commencement of the out-diffusion process itself from the surface of the composite. These two processes are clearly shown in Figure 3.11. Figure 3.11 (a) and (b) shows the gradual dropping of the concentration in the matrix that is related to the out-diffusion process from the matrix. Figure 3.11 (c) and (d) shows the dropping of the concentration at the interface with time. Both profiles from Figure 3.11 (a) and (b) seem quite similar. Generally a higher concentration is observed near inclusions in both figures. This is due to the desorbing of particles from the interface layer to the metal matrix. It is interesting to note that the drop of concentration in the interface layer of the first inclusion is clearly comparable to the next inclusion. We can observe this situation in both Figure 3.11 (c) and (d). It is important to obtain a clear idea about the diffusion process occurring in the vicinity of the interface layer. We assumed that *s* is consistent with the jump frequencies Γ_{23} and Γ_{32} in the present simulation. Yet, in reality it is not the situation, because the segregation factor (out-diffusion process) depends on jump frequencies, which in turn depend on temperature. This means that changes in jump frequencies involved at the interface layer will affect the segregation factor in high temperature out-diffusion processes.

Now let us explore the details of processes happening at the interface and its impact on the results. Adsorption associated with the jump frequency Γ_{23}, desorption associated with the jump frequency Γ_{32} are the common processes that can occur in Figure 3.11 (c) and (d). Let us consider Figure 3.11 (c). It is noted that the concentration of the interface layer of the 2nd inclusion is only a little higher compared to the right edge of the 1st inclusion's interface layer. Also the left edge of the 1st inclusion's interface layer is observed with decreasing concentration with time. The reason for the dropping of the concentration is due to the out-diffusion process at the surface. This leaves fewer particles available for adsorption into the interface layer and hence gradually there is a decrease in the total concentration of particles in the interface with time. In Figure 3.11 (d), we can observe an even concentration distribution at the interface layer of the 1st inclusion and a considerable drop of concentration in the two inclusions. As mobility of particles along the interface layer is being permitted with the very high jump rate Γ_{33} scaled to a value of unity, it is assumed that the particles travel at a rapid rate along the interface, compared to the desorption process where $\Gamma_{23} = 0.01$. Due to this effect, nearly the same concentration is observed at both edges of the interface layer at the first inclusion. The concentration of the second interface can also be explained by the same reasoning. However, it is also observed that the concentration in the interface gradually decreases with time due to

fewer particles being found in accordance with the out-diffusion process. It is noted that inclusions placed at a considerable distance away from the surface (e.g. 2nd inclusion) in Figure 3.11 (c) and (d) show a higher concentration compared to the other inclusions located closer to the surface. The reason behind the above observation would be not having a considerable concentration gradient in the matrix region in-between the above mentioned inclusions types. This could be more likely due to the availability of more oxygen particles in the matrix from closer inclusions due to desorption process. These particles tend to compensate for the lost particles in the matrix due to surface evaporation. However, once the desorption process at closer inclusions is not capable for compensating for the loss of particles from the matrix, then diffusion of particles occurs from high concentration regions towards the surface.

The analytical equation describing the effective diffusivity in the presence of a random distribution of multiple inclusions (traps) is given as [42]:

$$D_{Eff} = \frac{1}{4}\left(\frac{1}{1-g+sg}\right) \tag{3.32}$$

where g is the fraction of inclusions and s is the segregation factor. The factor 4 comes from the fact that the experiment is modelled as a 2D lattice. We considered the 2D lattice having an inclusion fraction of 3.03 % at segregation coefficient of 100. Hence the effective diffusivity of the system results in 0.25 according to Equation 3.32. Concentration profiles are averaged over 10^4 observations in such a way to get even profiles for ease of comparison. The out-diffusion simulations are explained in Figure 3.12 as below.

In Figure 3.12 (a), a contour concentration plot for an averaged distribution of 10^4 different configurations of randomly arranged multiple inclusions are shown at a segregation factor of 100. Figure 3.12 (b) gives the total concentration profile averaged in the x-direction. The corresponding 2D concentration profile is shown in Figure 3.12 (c). Here, we considered the LMC results and the analytical solution (Equation 3.32) where it is observed that the LMC results show excellent agreement with the analytical solution. It inevitably means that if the randomly arranged point inclusion model was averaged over a large number of configurations then the whole model acts as a pseudo single-phase material.

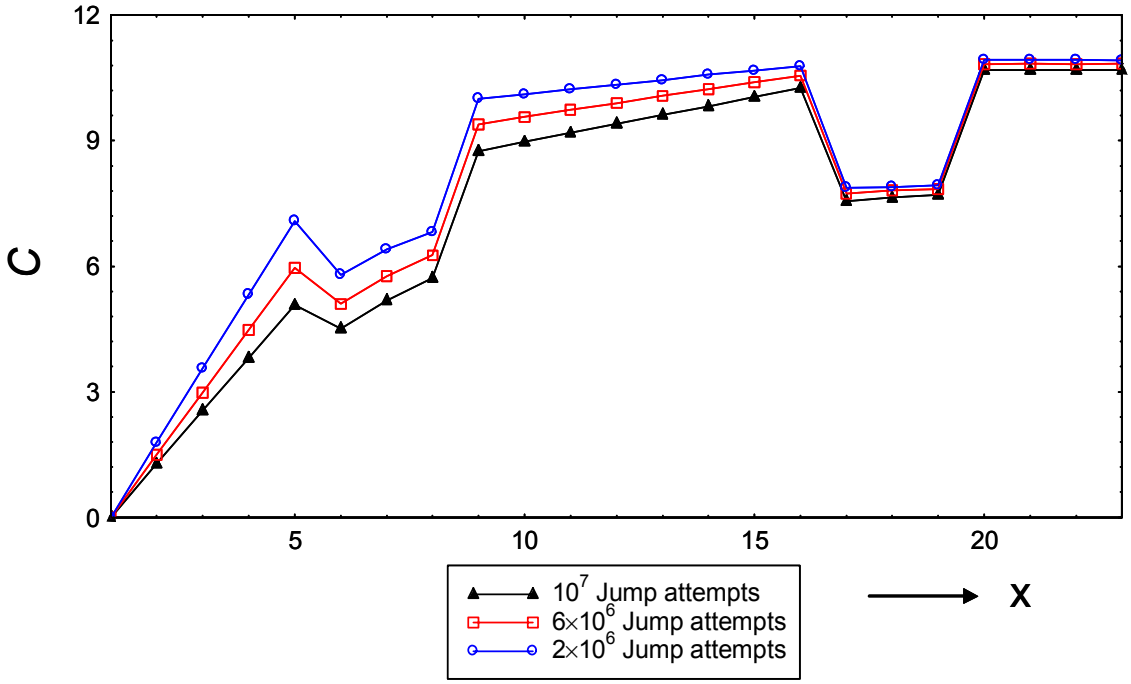
12
9
6
3
0
C
5
10
15
20
X
10^7 Jump attempts
6×10^6 Jump attempts
2×10^6 Jump attempts

(a)

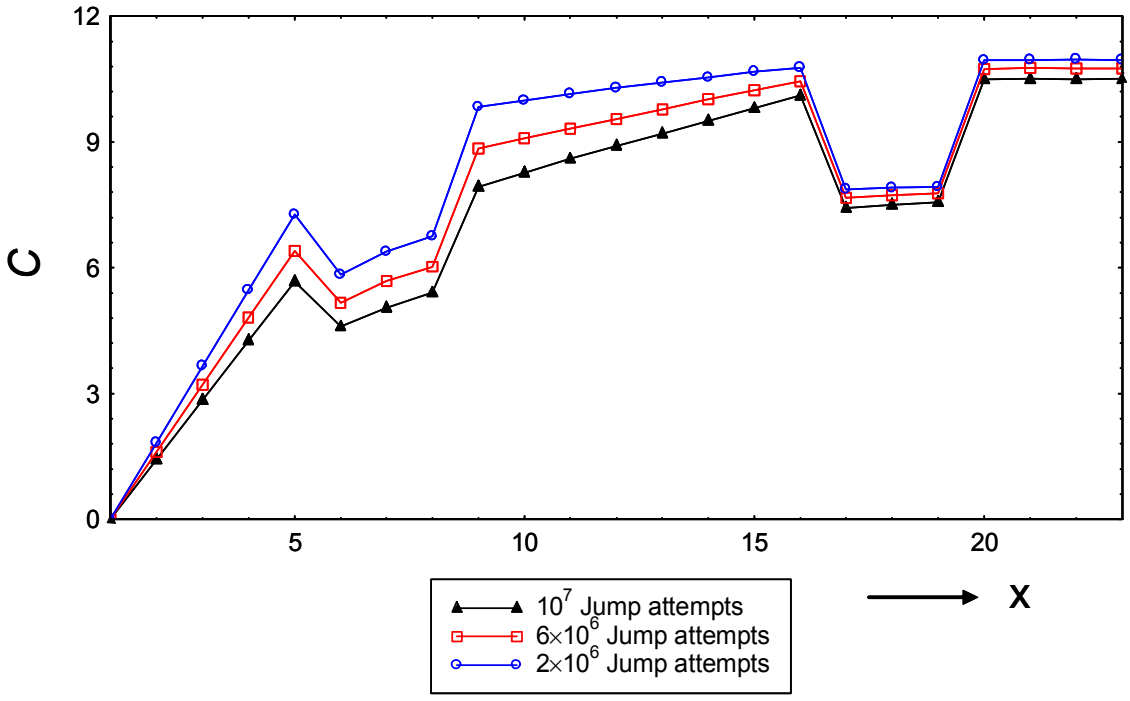
12
9
6
3
0
C
5
10
15
20
X
10^7 Jump attempts
6×10^6 Jump attempts
2×10^6 Jump attempts

(b)

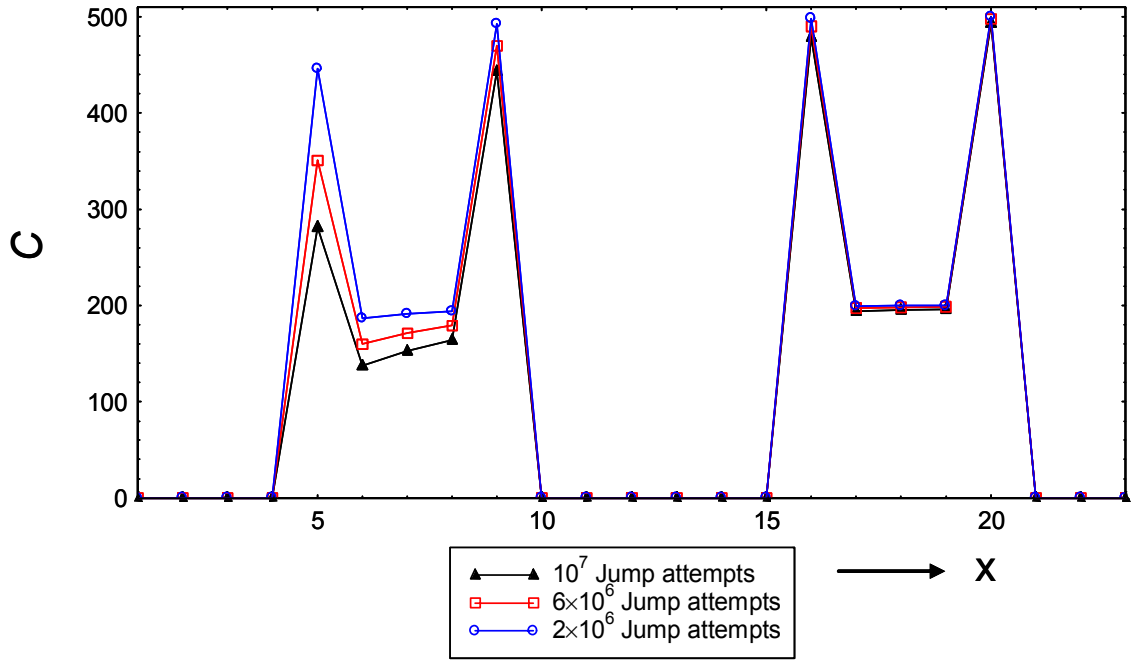

(c)

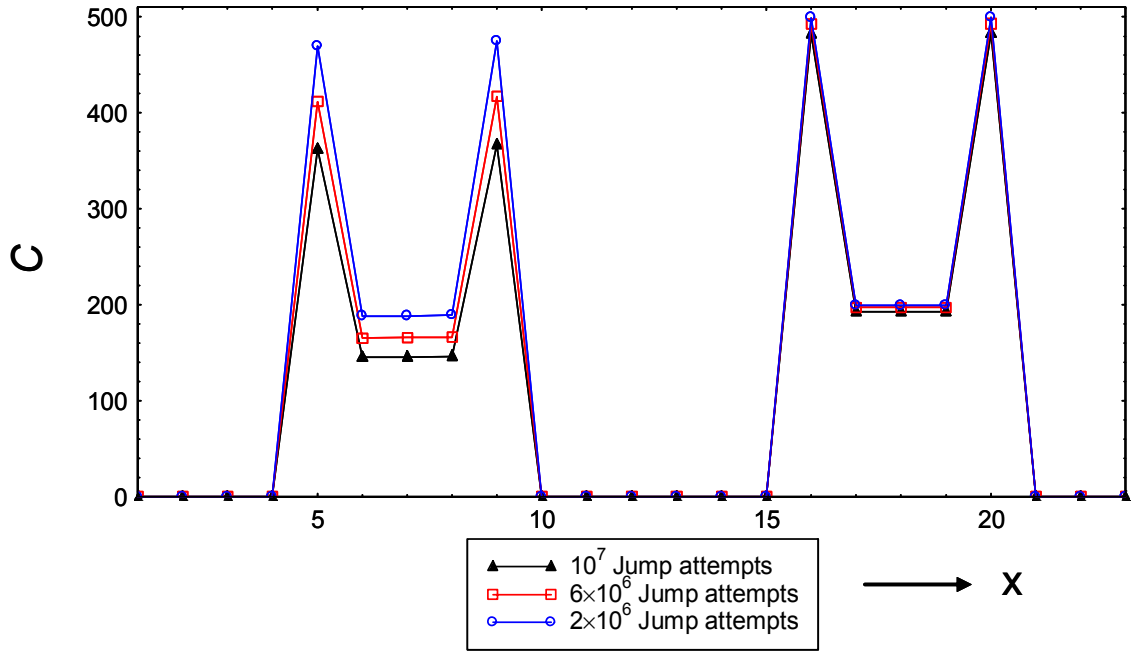

(d)

Figure 3.11 (a) Average time-dependent oxygen concentration profile of a diffusion-limited evaporation process in a semi-infinite Ag/MgO composite medium observed in the Ag matrix according to the VP strategy. Movement along the interface is restricted. Segregation factor s = 10^3, total number of jump attempts: 2×10^6, real time: 0.2217 s; 6×10^6, real time: 0.6889 s; 10^7, real time: 1.1896 s. Oxygen diffusivity in the matrix: 2.1×10^{-11} m^2s^{-1}, inclusion fraction: 0.072.

(b) Averaged oxygen concentration profile in the metal matrix taken whilst permitting particle mobility at the same conditions (c) Averaged oxygen concentration profile in inclusions at the virtual plane under same conditions. Movement along the interface is restricted. (d) Averaged oxygen concentration profile taken in inclusions at the virtual plane under same conditions. Movement along the interface is permitted.

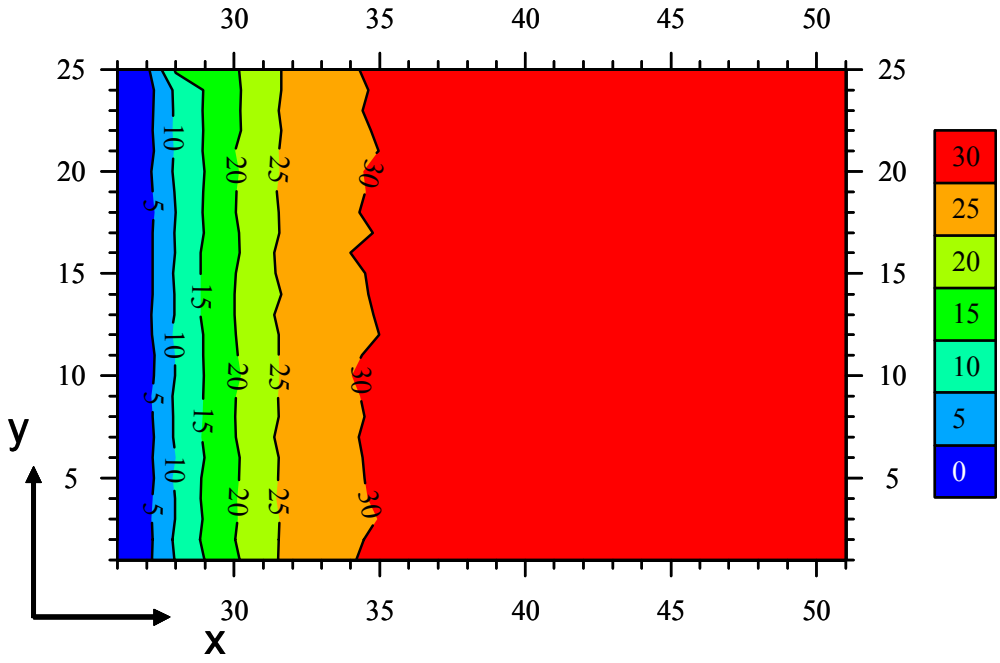

(a)

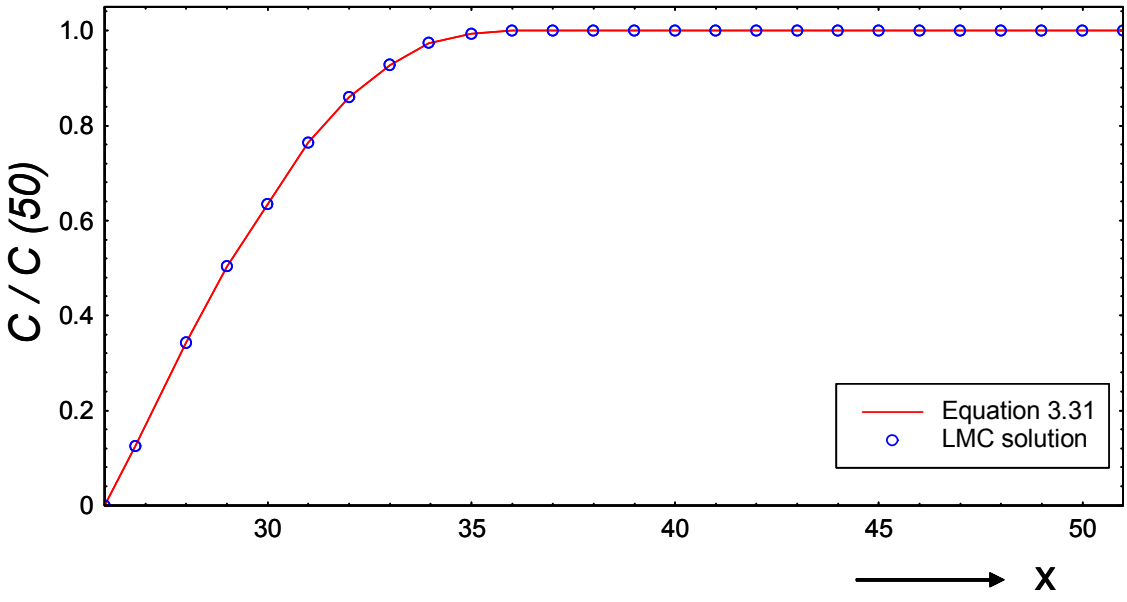

(b)

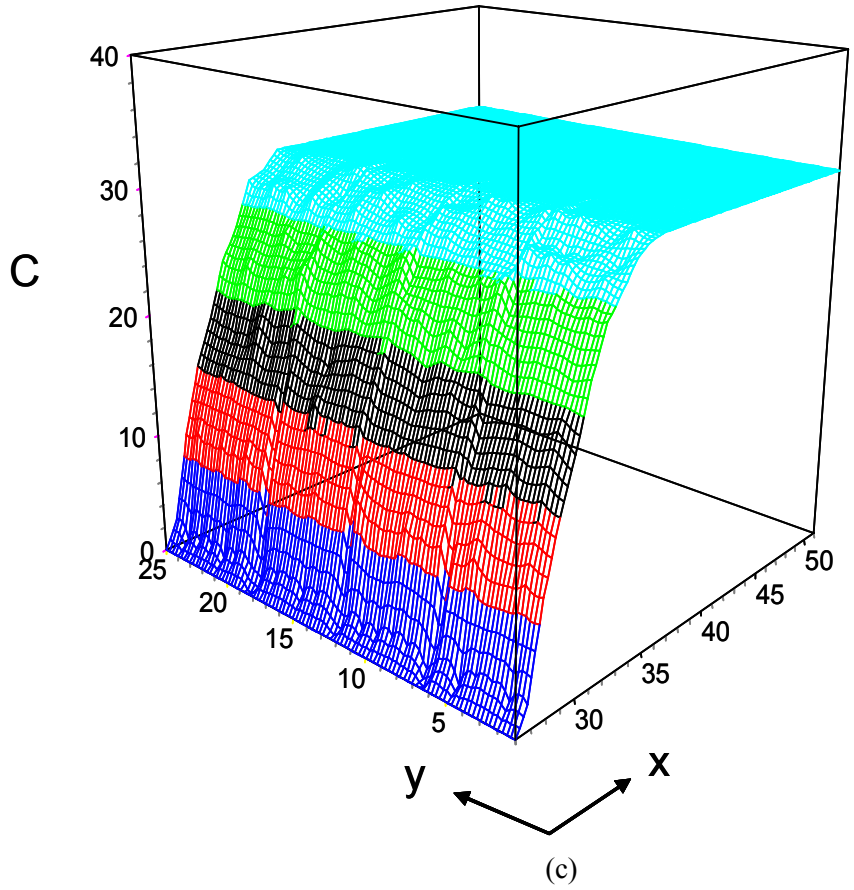

(c)

Figure 3.12 (a) A typical contour map of the averaged concentration distribution of diffusion-limited evaporation process with random MgO inclusions in Ag matrix. Segregation factor s = 10^2, total number of jump attempts: 10^8, real time: 15.69 s, oxygen diffusivity in the matrix: 2.1×10^{-11} m^2s^{-1}, inclusion fraction: 0.0303. (b) The total concentration profile averaged in the x-direction (y = 1-25, x-direction is shown as lattice plane number). (c) 2D profile of (a).

3.4 References

[1] M. Rühle , A.G. Evans, M.F. Ashby, J.P. Hirth, Metal-Ceramic Interfaces, in Acta-Scripta Metallurgica Proc. Series 4. Pergamon Press, Oxford, 1990.

[2] A. Gonis and P. Tuchi, Stability of Materials. Structure-Property Relationship of Metal-Ceramic Interfaces. Gordon & Breach, New York, 1996.

[3] A. M. Stoneham and P.W. Tasker, Surface and Near-Surface Chemistry of Oxide Materials (edited by J. Nowotny and L.-C. Dufour), Elsevier, Amsterdam, 1988.

[4] P. Jonnard, F. Vergand, C. Hombourger and C. Bonnelle, Proc. J. Automne, **SF2M 1996**, 1996, p. 191.

[5] M. Backhaus-Ricoult, S. Laurent, M. James, L. Minel, M.G. Barthes and S. Hagège, Proc. J. Automne, **SF2M 1996**, 1996, p.180.

[6] P. Lu and F. Cosanday, Ultramicroscopy, **Vol. 40**, 1992, p. 271.

[7] H.B. Groen, B.J. Kooi, W.P. Velinga and J. Th. M. De Hooson, Philos. Mag. A, **Vol. 79**, 1999, p.2083.

[8] H. Jang, D.N. Seidman and K.L. Merkle, Scripta Metal. Mater., 1992, **Vol. 26**, p. 1493.

[9] D. Imhoff, S. Laurent, C. Colliex and M. Backhaus-Ricoult, Eur. Phys. J., **AP5**, 1999, p. 9.

[10] U. Schönberger, O.K. Andersen and M. Methfessel, Acta metal. Mater., **Vol. 40**, Suppl., 1992, p. S1.

[11] M.W. Finnis, C. Kruse and U. Schönberger, Nano Struct. Mater., **Vol. 6**, 1995, p. 145.

[12] M.W. Finnis, Acta Metall. Mater., **Vol. 40**, 1992, p. S25.

[13] Y. Long, N.X. Chen and W.Q. Zhang, J. Phys.- Condens. Mat., **Vol. 17**, 2005, p. 2045.

[14] J. Gegner and G. Hörz, Interf. Sci., **Vol. 5**, 1997, p. 231.

[15] E. Pippel, J. Woltersdorf, J. Genger and R. Kirchheim, Acta Mater., **Vol. 48**, 2000, p. 2571.

[16] J.R. Rice, Z. Suo and J-S Wang, in *Metal Ceramic Interfaces*, edited by M. Rühle, A.G. Evans, M.F. Ashby and J.P. Hirth (Pergamon, Oxford, 1990), p. 269.

[17] A.G. Evans and B.J. Dalgleish, *Acta Metal. Mater.*, **Vol. 40**, 1992, p. S295.

[18] J.R. Smith, T. Hong and D.J. Srolovitch, *Phys. Rev. Lett*, **Vol. 72**, 1994, p. 402.

[19] M.P. Seah, J. Catalysis, **Vol. 57**, 1979, p. 450.

[20] A. Öchsner, M. Stasiek and J. Grácio: Defect Diffus. Forum, **Vol. 249**, 2006, p. 35.

[21] I. Kaur, Y. Mishin and W. Gust, in Fundamentals of Grain and Interphase Boundary Diffusion, Wiley; Chichester, 1995.

[22] M. Stasiek, A. Öchsner and J. Grácio: J. Phase Equilib. Diff., **Vol. 27** 2006, p. 644.

[23] P.R. Webber and D. Chadwick, Surf. Sci., **Vol. 94**, 1980, p. L151.

[24] K.K. Ziling and V. Yu. Pchelkin, Russian Metallurgy, **Vol. 3**, 1976, p. 41.

[25] D.G. Ast and D.J. Krenistsky, J. Vac. Sci. Technol., **Vol. 13**, No. 4, July/Aug. 1976, p. 969.

[26] E. Sultan, A. Boudaoud and M.B. Amar, J. Eng. Math., **Vol. 50**, 2004, p. 209.

[27] D.M. Sanders and H.A. Schaefer, J. Am. Ceram. Soc., **Vol. 59**, 1975, p. 96.

[28] J. Matousek and J. Hlavac, Glass Technol., **Vol. 12**, 1971, p. 103.

[29] J. Chen, D. Yang, X. Ma, R. Fan and D. Que, J. Appl. Phys., **Vol. 102**, 2007, p. 66102.

[30] R.A.B. Devine, D. Mathiot, J-B. Xu, I.H. Wilson, M. Gauneau, W.L. Warren, Thin Solid Films, **Vol. 286**, 1996, p. 317.

[31] C.R. Alpass, J.D. Murphy, A. Giannattasio, S. Senkader, R.J. Falster and P.R. Wilshaw, Phys. Stat. Sol. (a), **Vol. 204**, No. 7, 2007, p. 2256.

[32] A. Giese, H. Bracht, N.A. Stolwijk and D. Baither, Materials Science and Engineering, **Vol. B71**, 2000, p. 160.

[33] R.C. Miller and F.M. Smits, Phys. Rev., **Vol. 107**, No. 1, 1957.

[34] G.E. Murch, High Temp. Sci., **Vol. 20**, 1985, p. 75.

[35] G.E. Murch and I.V. Belova, Interf. Sci., **Vol. 11**, 2003, p. 91.

[36] I.V. Belova and G.E. Murch: in Cellular and Porous Materials. Thermal Properties Simulations and Prediction, Wiley – VCH; Weinheim in press.

[37] G.E. Murch and I.V. Belova, Interf. Sci., **Vol. 11**, 2003, p. 91.

[38] I.V. Belova and G.E. Murch, J. Phys. Chem. Solids, **Vol. 64**, 2003, p. 873.

[39] I.V. Belova and G.E. Murch: J. Metastable and Nanocrystalline Materials, **Vol. 19**, 2004, p. 25.

[40] T. Fiedler, A. Öchsner, N. Muthubandara, I.V. Belova and G.E. Murch, Mat. Sci. Forum, **Vol. 553**, 2007, p. 51.

[41] J. Crank, The Mathematics of Diffusion, Clarendon Press; Oxford, 1975.

[42] J.W. Haus and K.W. Kehr, Physics Reports, Vol. 150, 1987, p. 263

Chapter 4

4. Concluding Remarks

4.1 Summary

Metal/ceramic composites are widely used in thin solid films, anti-corrosion coatings, electronic packaging, gas sensors, and combustion engines. The interface between the metal and the oxide, the orientation of oxide inclusions, the geometry as a whole with the individual properties of metal material and the oxide materials determine the overall physical and mechanical properties of the composite. Predicting such properties plays a central role in designing new materials and enhancing existing materials. Not only predicting such properties as thermal resistance properties but also studying the ability to withstand oxidation and de-oxidation reactions at elevated temperatures help to obtain an overall understanding of the behaviour of new material for future applications. Our study was based on the LMC method which in turn is based on the lattice model with hopping kinetics. The LMC method is a powerful method which can be used to treat both mass and thermal diffusion problems at the phenomenological level. The aims of the study of the metal/ceramic composites were two-fold. One objective was to calculate the effective thermal conductivity of composites with different shapes, size and orientations. The other objective was to study oxygen in-diffusion, out-diffusion of metal/ceramic oxide composites and the segregation process of oxygen at the metal/ceramic interface. Historically, Monte Carlo methods of diffusion problems required a great deal of computer time and this has impeded their application. But this is now no longer a major consideration since the simulations described here were possible on a suite of high speed PCs. Comparison of the results obtained by theoretical methods and the LMC method provided an opportunity to validate the findings.

4.2 Calculation of the Effective Thermal Conductivity in Composite Materials

We considered the calculation of the effective thermal conductivity from a general point of view to determine the thermal conductivity properties of any composite material. In general, the

material can be a metal/metal, metal/ceramic and ceramic/metal composite material etc. The orientation and the geometry of inclusions were considered for analysis of the thermal conductivity properties. The thermal conductivity of the whole material was expressed in terms of an effective property, in this case the effective thermal conductivity. Effective properties are usually a result of an (unknown) average of the individual properties of the phases associated with the composite material. This also means that effective properties are affected by the individual properties of the constituent phases. Theoretical expressions to calculate effective thermal conductivity/diffusivity were considered starting from the Hart equation to the modified Maxwell-Garnett equation by Belova and Murch. Special attention was drawn towards the LMC method by addressing several possible strategies namely the Einstein equation method, Fick's first and second law methods in calculating the effective thermal conductivity/diffusivity for composite materials. The effective thermal conductivity was calculated according to the LMC method for several models of a composite. In each model, the inclusions were arranged in a periodic square planar or cubic configuration of the matrix material. The inclusions considered were square, circular, elliptical, cubic and spherical. The effective conductivity values for 2D and 3D simulations were compared separately. In some of the published papers resulting from the thesis some of the LMC results obtained were compared with results obtained by overseas collaborators using the finite element method, see the Appendix. However, in the thesis itself LMC results are compared only with the modified Maxwell-Garnett equations.

Further calculations could be made by including ellipsoid and randomly distributed inclusions. In elliptical inclusions, several orientations in the same periodic arrangement would be an interesting consideration. Similarly, this can be further extended to ellipsoid inclusions as well. The next step would be to consider two different inclusions in the same periodic cell such as circular/square, square/elliptical or elliptical/circular arrangements. This can be further extended to several different inclusions as well. The orientation of inclusions has a greater impact on effective thermal conductivity/diffusivity properties. Therefore, calculating effective properties with respect to orientation by changing the angle of tilt of some inclusions with respect to other inclusions would also be an interesting topic to consider. Not only the distributions discussed above but also a composite with randomly distributed point inclusions could relate to effectively dispersed particulate nano-composites. By analysing such situations it could be possible to predict how nano-composites might operate within certain temperature ranges. However, the square, circular, spherical, cubic, ellipse, ellipsoid and point inclusions provide reference points for real inclusions. Thus, they can never truly represent a real composite material. In general, it is very important to be able to accurately predict the properties of real materials. To simulate real material, one has to consider the shape and distribution of inclusions. This can be done by obtaining a three dimensional CT scan of an actual composite material. CT scanning would

provide a scan of the inclusions and their shape/distribution in an actual material and by digitizing the data points would help to model the real material. Incorporating such micro or nano structures into the LMC method would be a significant step forward in predicting the effective thermal and mass transport properties of real composite materials.

4.3 Modelling of Oxygen Diffusion and Segregation at Interfaces in Ag/MgO Composites

Internal interfaces play an important role in controlling the mechanical, thermal and electrical properties of many advanced composite materials. Therefore, understanding the interface reactions would help to understand and predict the behaviour of the materials at different atmospheric conditions. Oxidation and de-oxidation are such atmospheric conditions where the model Ag/MgO composite can be subjected. These processes were identified as a phenomenological diffusion problem, where diffusion of oxygen in the composite material is of primary consideration. Not only the oxygen in-diffusion and out-diffusion process, but also segregation of oxygen in the interface was the primary objects of our study. The method used was the LMC method with two types of MgO inclusions, square and randomly distributed multiple inclusions with periodic boundary conditions as discussed in Chapter 3. Initial investigations were made for oxidation and de-oxidation processes of a pure Ag metal matrix. Then segregation effects of oxygen to the metal/ceramic oxide interface were considered by making use of a virtual segregation layer around the square ceramic oxide inclusions by introducing a special virtual plane. A separate segregation layer was not considered for randomly placed inclusions each of which takes only a single site of the lattice. In that situation, the inclusions were considered themselves to be sources and sinks for the diffusant in the corresponding diffusion process. Simulation results for oxygen in-diffusion and out-diffusion processes for the metal matrix alone were compared with solutions of the diffusion equation and excellent agreement was found. In papers published from the thesis results for the composite with square inclusions were compared with results from collaborators using a Finite Element Method (see the Appendix). However, this comparison is not included in Chapter 3. For the case of random distributions of (point) inclusions a comparison was made with a theoretical expression for the effective diffusivity found in the literature. Excellent agreement was obtained.

From a general perspective, future work in the area would probably focus further on the chemistry of oxygen at the metal/ceramic oxide interface using first principles methods and, if suitable inter-atomic potentials can be obtained or developed, the method of molecular

dynamics could be used to explore the nature of oxygen mobility at and near the interface. From such studies it would be possible to describe the oxygen diffusion processes and segregation from a detailed atomic perspective. Since such studies could not possibly be done at the large length scales of a composite body, they would in effect complement the present phenomenological diffusion analysis and provide useful input parameters to it.

Since the amount of oxygen that segregates to the metal/ceramic oxide interface can be quite large and could influence the results, a useful immediate extension to the present work would make use of the McLean blocking expression for the segregation factor. Another extension of the present work would consider inclusions other than square or random point inclusions and extend the 2D simulations to 3D. Different examples for inclusions would be elliptical, spherical, cubic, ellipsoid and randomly shaped inclusions. Complex surface structures of the inclusions would make it more difficult to use the LMC method unless a very fine mesh was used that could capture the topological details of the inclusions. Analogous to what was discussed above (section 4.2) with respect to thermal conductivity in composites, in principle, CT scans of a real metal/ceramic oxide composite could be used in conjunction with the LMC method to model the oxygen in-diffusion/out-diffusion and segregation of an actual material.

Appendix

The research work presented in this thesis was conducted at the Centre for Mass and Thermal Transport for Engineering Materials, Faculty of Engineering and Built Environment at the University of Newcastle, Australia. This work was performed under the supervision of Prof. I.V. Belova and Prof. G.E. Murch from February 2006 to June 2008. During the term of candidature the following papers were published:

1. T. Fiedler, A. Öchsner, N. Muthubandara, I.V. Belova and G.E. Murch, "Calculation of the Effective Thermal Conductivity in Composites Using Finite Element and Monte Carlo Methods", Materials Science Forum, Vol. 553, 2007, p. 51-56.

2. I.V. Belova, A. Öchsner, N. Muthubandara and G.E. Murch, "Modelling of Oxygen Diffusion and Segregation at Interfaces in Ag-MgO Composites", Defect and Diffusion Vol. 266, 2007, p. 29-38.

3. I.V. Belova, G.E. Murch, N. Muthubandara and A. Öchsner, "Analysis of Oxygen Segregation at Metal-Oxide Interfaces Using a New Lattice Monte Carlo Method", Solid State Phenomena Vol. 129, 2007, p. 111-117.